Mitochondrial metabolism in cancer transformation and progression

University of Cambridge

Edoardo Gaude

Clare College

January 2018

This dissertation is submitted for the degree of Doctor of Philosophy.

Declaration

This dissertation is submitted for the degree of Doctor of Philosophy at the University of Cambridge. The research described herein was conducted under the supervision of Doctor Christian Frezza in the Medical Research Council Cancer Unit at the Hutchison/MRC Research Centre, University of Cambridge, between October 2014 and September 2017.

This dissertation is the result of my own work and includes nothing which is the outcome of work done in collaboration except as specified in the text. It is not substantially the same as any that I have submitted, or, is being concurrently submitted for a degree or diploma or other qualification at the University of Cambridge or any other University. I further state that no substantial part of my dissertation has already been submitted, or, is being concurrently submitted for any such degree, diploma or other qualification at the University of Cambridge or any other University or similar institution. It does not exceed the prescribed word limit of 60000 words.

January 2018
Edoardo Gaude

Abstract

Cancer cells undergo a multifaceted rewiring of cellular metabolism to support their biosynthetic needs. Although the major determinants of this metabolic transformation have been elucidated, their broad biological implications and clinical relevance are unclear. In this study, I systematically analysed the expression of metabolic genes across 20 different cancer types and investigated their impact on clinical outcome. I found that cancers undergo a tissue-specific metabolic rewiring, which converges towards a common metabolic landscape. Of note, downregulation of mitochondrial genes is associated with the worst clinical outcome across all cancer types and correlates with the expression of epithelial-to-mesenchymal transition (EMT) gene signature, a feature of invasive and metastatic cancers. Consistently, suppression of mitochondrial genes is identified as key metabolic signature of metastatic melanoma and renal cancer, and metastatic cell lines. This comprehensive analysis reveals unexpected facets of cancer metabolism, with important implications for cancer patients stratification, prognosis, and therapy. I then investigated how mitochondrial dysfunction could affect cell behaviour. I capitalised on a recently developed *in vitro* cell model with increasing levels of m.8993T>G mutation heteroplasmy. I found that impaired utilisation of reduced nicotinamide adenine dinucleotide (NADH) by the mitochondrial respiratory chain leads to cytosolic reductive carboxylation of glutamine as a new mechanism for cytosol-confined NADH recycling supported by malate dehydrogenase 1 (MDH1). This metabolic coupling is facilitated by the formation of a multienzymatic complex between MDH1 and GAPDH. Importantly, such metabolic coupling between glutamine metabolism and cytosolic NADH recycling is able to support increased glycolytic flux, an important hallmark of cells with dysfunctional mitochondria, as well as cancer cells. Finally, increased glycolysis in cells with mitochondrial dysfunction is associated with enhanced cell migration, in an MDH1-dependent fashion. These results describe a novel link between glycolysis and mitochondrial dysfunction, and uncover potential targets for cells that rely on aerobic glycolysis for proliferation and migration, such as cancer cells.

Contents

Abbreviations

2HG 2-hydroxyglutarate

3PG 3-phosphoglycerate

αKG α-ketoglutarate

ALL acute lymphoblastic leukemia

AMPK AMP-activated protein kinase

ATP adenosine triphosphate

BRAF v-Raf murine sarcoma viral oncogene homolog B

CAC citric acid cycle

DHAP dihydroxyacetone phosphate

DHODH dihydroorotate dehydrogenase

ECAR extracellular acidification rate

EMT epithelial-to-mesenchymal transition

$FADH_2$ reduced flavin adenine dinucleotide

FCCP carbonyl cyanide-p-trifluoromethoxyphenylhydrazone

^{18}F-FDG ^{18}F-fluorodeoxyglucose

FH fumarate hydratase

G6PD glucose 6-phosphate dehydrogenase

GAPDH glyceraldehyde 3-phosphate dehydrogenase

GC-MS gas chromatography-mass spectrometry

GFPT1 fructose 6-phospate aminotransferase 1

GLUT1 glucose transporter 1

GOT1 glutamate-oxaloacetate transaminase 1

GPD glycerol 3-phosphate dehydrogenase

GSEA gene set enrichment analysis

HK hexokinase

IDH1 isocitrate dehydrogenase 1

IDH2 isocitrate dehydrogenase 2

KEAP1 Kelch-like ECH-associated protein 1

KRAS Kirsten rat sarcoma

LC-MS liquid chromatography-mass spectrometry

LDH lactate dehydrogenase

MAS malate-aspartate shuttle

MDH1 malate dehydrogenase 1

MDH2 malate dehydrogenase 2

mFAO mitochondrial fatty acids oxidation

MILS maternally inherited Leigh's syndrome

mtDNA mitochondrial DNA

mTOR mammalian target of rapamycin

mtZFNs mitochondrially-targeted zinc-finger nucleases

NAD^+ oxidised nicotinamide adenine dinucleotide

NADH reduced nicotinamide adenine dinucleotide

NADPH reduced nicotinamide adenine dinucleotide phosphate

NARP neuropathy ataxia and retinitis pigmentosa

NDI-1 NADH dehydrogenase internal

NMR nuclear magnetic resonance

NRF2 nuclear factor erythroid 2-related factor

OCR oxygen consumption rate

OXPHOS oxidative phosphorylation

PAICS Phosphoribosylaminoimidazole carboxylase phosphoribosylaminoimidazole succinocarboxamide synthetase

PET positron emission tomography

PGC1α nuclear coactivator PPARγ coactivator-1α

PGI phosphoglucose isomerase

PGK phosphoglycerate kinase

PHGDH 3-phosphoglycerate dehydrogenase

PI3K phosphoinositide 3-kinase

PK pyruvate kinase

PPP pentose phosphate pathway

PTEN phosphate and tensin homologue

RC respiratory chain

RNAseq mRNA sequencing

ROS reactive oxygen species

SDH succinate dehydrogenase

TCGA the cancer genome atlas

List of Figures

List of Tables

to Daniela and Agostino.

CHAPTER 1

Introduction

1.1 Cancer metabolism: a historical preamble

CANCER is a highly complex disease that defies univocal definition. As for many other fields of research, cancer research followed different directions throughout history. Scientific discoveries and technological advances guided cancer research towards different fields and scientists have been trying to define cancer according to the existing leading paradigma. In this chapter I will introduce the two main historical eras of cancer research, the *biochemical* and *genetic* eras.

1.1.1 Cancer as a metabolic disease: the biochemical era

At the dawn of medical research the diagnosis and investigation of medical conditions were performed by combining information from external, phenotypical traits that were readily accessible from the patient. Among these, biofluids, such as urine and blood, were inspected for abnormalities. Indeed, in 1506 Ullrich Pilner published a guide where colour, smell, and taste of people's urine was used to distinguish different medical conditions (Nicholson and Lindon 2008). Applying a similar methodology in the 19^{th} century Johannes Müller started noticing different traces in the urine of cancer patients (Müller 1838).

Following these initial observations, scientists expanded our understanding of cancer biochemistry until the beginning of the 20^{th} century, when metabolic traits of cancer begun to play a role in the treatment of cancer patients. August von Wasserman was the pioneer of this new approach. He hypothesised that cancer cell proliferation could be supported by abnormal cell respiration and set out to treat, quite successfully, several animal models with selenium-eosin, a chemical once thought to inhibit mitochondrial metabolism (Wassermann et al. 1911). Although the initial success of Wasserman's animal experimentation, together with the first cancer patient cured with selenite by Lanciere and Thiroloix (Brigelius-Flohé and Sies 2015), further trials in human patients showed high toxicity for selenium and this approach was discontinued.

A more systematic investigation of the metabolism of cancer cells was performed only a few years later by the pioneering mind of the German biochemist Otto Heinrich Warburg. Warburg bestowed his scientific efforts towards the investigation of cell metabolism in several animal models, such as sea urchins, by developing novel experimental techniques, such as the use of thin tissue slices for *ex vivo* experiments, as well as by devising an improved manometer for the measurement of

O_2 consumption and CO_2 production (Koppenol et al. 2011). The combination of all these scientific advancements resulted in the seminal work that imprinted Warburg's name in the history of cancer. Warburg compared the metabolism of tissue slices from normal rat liver and rat liver carcinoma and observed, in the presence of glucose and oxygen, an increased production of lactic acid by liver carcinoma (Warburg 1924). This discovery led him to hypothesise that cancer cells undergo *aerobic glycolysis*, a metabolic process whereby glucose is fermented to lactate even in the presence of high levels of oxygen, as opposed to normal cells that prefer to extract energy from glucose via respiration, and undergo glycolysis mainly under anaerobic conditions. Soon after Warburg's discovery, Cori and Cori analysed the blood effusate of a Rous sarcoma tumour implanted on a chicken's wing and compared it to the blood passing through the contralateral normal wing. They observed that glucose levels were depleted and lactate was increased in the blood effusate of the tumour, thus confirming Warburg's discovery in an *in vivo* setting (Cori and Cori 1925).

Almost concurrently to Warburg's work, Sidney Farber, an American pathologist at Harvard Medical School set out to revolutionise the way we treat cancer patients. Farber spent great effort in understanding and treating children with acute lymphoblastic leukemia (ALL) and he observed that interfering with metabolism of nucleotides could limit lymphoblastic growth (Farber, Cutler, et al. 1947). Together with Y. Subbarow he developed the first chemotherapeutic agent, aminopterin, an antagonist of folic acid able to disrupt nucleotide biosynthesis and begun the first clinical trial for aminopterin on children with ALL. With this first study Farber increased the disease-free overall survival of childood ALL from 0% to 80% (Farber, Diamond, et al. 1948), a truly impressive achievement. Farber is regarded to be the father of modern chemotherapy and approaches that disrupt nucleotide biosynthesis are, 70 years later, amongst current front-line treatments for several forms of cancer.

The historical moment experienced by Warburg and Farber was extremely exciting for biochemistry. In 1929 adenosine triphosphate (ATP) was discovered and Hans Krebs unveiled the existence of the citric acid cycle (CAC) in 1937, while the formulation of the glycolytic pathway occurred soon after in 1940 (Koppenol et al. 2011). Despite the blooming of biochemistry and the strong connection between cell metabolism and cancer, another biochemical discovery was about to change the direction of cancer research.

1.1.2 Cancer as a result of mutations: the genetic era

Studies on the aetiology of cancer begun with the pioneering work of Peyton Rous, who discovered that a form of chicken sarcoma could be transferred to different chickens by a filterable agent (Rous 1910; Rous 1911). Years later such agent was unveiled to be a retrovirus (Rous sarcoma virus or RSV) (Vogt 2012) and this fostered the notion that cancer could be caused by viruses disrupting normal cells' physiology.

The discovery of DNA as the molecule carrying genetic, transferable, material in 1946 and 1952 (Avery et al. 1944; Hershey and Chase 1952), followed by the discovery of the structure of DNA by Watson and Crick (Watson and Crick 1953), inspired the scientific community to investigate the role of the "molecule of life" in cellular processes and human diseases. In addition, these discoveries fostered

technological advances that helped geneticists to further DNA research. One such advancement was performed by Bishop and Varmus during their investigation on the origin of the viral *SRC* gene, the gene delivered by the Rous sarcoma virus and responsible for chicken sarcoma. Bishop and Varmus devised a radio-labelled molecular probe that could show the presence of the *oncogene SRC* in different cells and, strikingly, they found that the probe could signal not only in cells infected with RSV, but also in normal cells from different avian species (Stehelin et al. 1976). This seminal discovery prompted the notion that cancer-causing genes are present within normal cells as *proto-oncogenes*, where they conduct important functions for cellular physiology and, if mutated, they can trigger cancer transformation (Parker et al. 1984; Iba et al. 1984).

The discovery of the first proto-oncogene inspired a wealth of research towards finding new cellular genes that could drive cancer transformation. The list of proto-oncogenes started to grow steadily, including *MYC* (Duesberg et al. 1977), *RAS* (Shih et al. 1979), *ERBB* (Bister and Duesberg 1979; Lai et al. 1979), *JUN* (Maki et al. 1987), and *PI3K* (Chang et al. 1997) and begun to include also tumour suppressor genes like *RB* (Knudson 1971) and *TP53* (Linzer and Levine 1979; Lane and Crawford 1979).

Mutations in oncogenes or tumour suppressor genes can be found in every human cancer sample and it is now an established cancer dogma that the combination of multiple genetic mutations is necessary for cancer to fully develop (Vogelstein and Kinzler 1993). Following the extensive discovery of several cancer-causing genes, scientists begun to investigate the functional consequences of those mutations, trying to understand the mechanisms by which mutated cancer genes could induce transformation. As a result of such global research efforts, cancer mutations have now been associated with abnormalities in virtually all cellular functions. Recently, the discoveries made by Warburg and his legacy have been ascribed among the effects that mutated oncogenes and tumour suppressor genes exert during transformation. After half a century, the metabolic and genetic fields of cancer research are now merging and this synergistic combination is currently offering a deeper understanding of cancer biology, as well as novel therapeutic strategies to treat cancer patients.

1.2 A unifying view of cancer: mutations drive metabolic rewiring

The first association between a common genetic event in cancer and its functional metabolic outcome occurred at the end of the 1990s. Studying the role of c-Myc-mediated regulation of transcription, the group of Chi Van Dang at John Hopkins University in Baltimore reported that lactate dehydrogenase (LDH)-A, the gene coding for the enzyme responsible for the last, and rate-limiting, step of glycolysis, could be transactivated by c-Myc (Shim et al. 1997). The authors showed that activation of LDH-A by c-Myc was associated with metabolic rewiring, resulting in increased lactate production, thus providing the first genetic explanation for Warburg's aerobic glycolysis. Most importantly, they showed that inhibition of LDH-A could inhibit c-Myc-mediated transformation of cancer cells grown in a three-dimensional matrix (Shim et al. 1997). This result proved, for the first time, that the metabolic rewiring induced by an activated oncogene was necessary for transformation and set

the stage for new avenues of cancer therapies aimed at disrupting cancer-specific metabolic traits.

The discovery of c-Myc as a potent activator of cell anabolism in cancer cells inspired the investigation of other links between mutated cancer genes and cell metabolism. Soon after Chi Van Dang's findings, activation of the phosphoinositide 3-kinase (PI3K)/Akt (or protein kinase B) axis, one of the most commonly deregulated pathways in cancer (Shaw and Cantley 2006), was found to regulate cell metabolism. Together with operating a strong activation of the glycolytic pathway (Kohn et al. 1996; Deprez et al. 1997; Gottlob et al. 2001; Rathmell et al. 2003), PI3K/Akt supports cell proliferation via the activation of lipid synthesis (Berwick et al. 2002). More recently, also phosphate and tensin homologue (PTEN), a negative regulator of the PI3K/Akt signalling frequently mutated in human cancers (Hollander et al. 2011), has been shown to limit anabolic growth via negative regulation of glycolysis and increasing oxidative metabolism (Garcia-Cao et al. 2012). In the early 2000s the most commonly altered human tumour suppressor, TP53, was found to operate a multilevel inhibition of glycolysis (Schwartzenberg-Bar-Yoseph et al. 2004; Contractor and Harris 2012; Boidot et al. 2011), as well as a profound activation of mitochondrial metabolism (Matoba et al. 2006; Stambolsky et al. 2006; Zhang, Lin, et al. 2011; Hu, Zhang, et al. 2010; Suzuki et al. 2010), thus adding to the list of genetic events impinging on cancer cells metabolism.

In the last two decades virtually all cancer-associated genetic mutations have been described to activate metabolic programs that support tumourigenesis (Cantor and Sabatini 2012; Boroughs and DeBerardinis 2015; Ward and Thompson 2012). After almost a century, Warburg's hypothesis is now supported by wide genetic evidence. Not only Warburg's hypothesis of aerobic glycolysis was confirmed by a plethora of studies, but also the concept of cancer metabolic rewiring expanded to a larger scale, comprising the concomitant regulation of several metabolic pathways supporting anabolism. Yet, despite several studies showing that such metabolic changes are required for the survival of cancer cells, the role of metabolism in tumourigenesis has been for long time perceived as collateral or epiphenomenal.

1.3 Mutated metabolic enzymes drive cancer formation

The discovery that housekeeping metabolic enzymes, if mutated, could drive tumour development shook the field. In the early 2000s the germline mutation of the mitochondrial enzyme succinate dehydrogenase (SDH) was found to cause the onset of hereditary pheochromocytoma and paraganglioma (Baysal et al. 2000). Two years later another component of the CAC, fumarate hydratase (FH), was associated with hereditary leiomyomatosis and renal cell cancer syndrome (Tomlinson et al. 2002). Mutations of the genes encoding for SDH or FH lead to partial or total loss of enzymatic activity, indicating that SDH and FH act as *bona fide* tumour suppressors.

The group of Gottlieb provided mechanistic explanation on the role of SDH mutations in supporting cell proliferation. SDH inactivation leads to accumulation of its substrate, succinate, which in turn can product-inhibit αKG-dependent prolyl hydroxylases domain (PHD) proteins (Selak et al. 2005). Given the role of PHDs in the degradation of hypoxia inducible factors (HIFs), inhibition of PHDs by succinate indirectly leads to HIFs stabilisation and induction of a pseudo-hypoxic state, which ultimately leads to the activation of anabolic programs including glycolysis (Gottlieb

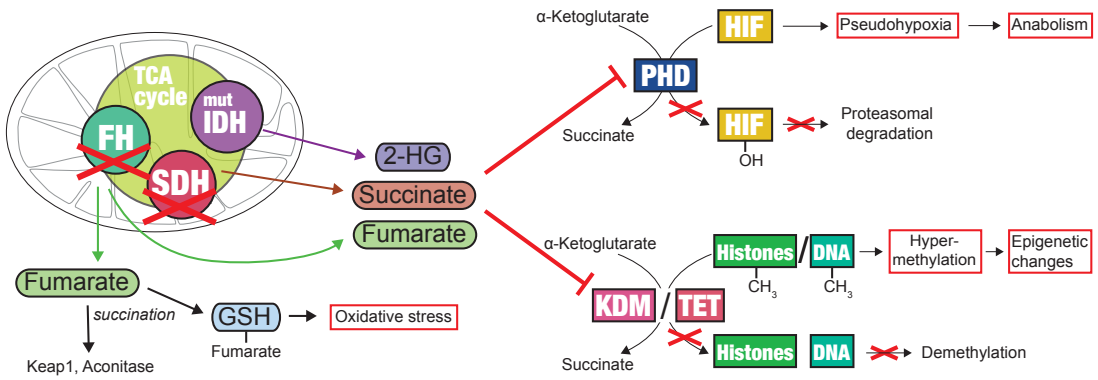

Figure 1.1: Molecular mechanisms of carcinogenesis induced by mutation of the metabolic enzymes succinate dehydrogenase (SDH), fumarate hydratase (FH) and isocitrate dehydrogenase (IDH). Accumulation of the oncometabolites succinate, fumarate and 2-hydroxyglutarate (2HG) can result in analogous effects via the inhibition of αKG-dependent enzymes, such as prolyl hydroxylases (PHD), leading to HIF stabilisation, or histone and DNA demethylases, leading to hypermethylation and epigenetic changes. In addition, accumulation of fumarate upon mutation of FH can induce protein succination and affects protein activity, as well as results in the formation of the metabolite succinic-GSH, thus affecting redox stress.

and Tomlinson 2005) (**Figure 1.1**).

Inactivation of FH causes accumulation of fumarate, with subsequent inhibition of PHDs and HIFs stabilisation, therefore leading to pseudo-hypoxia and metabolic reprogramming (Isaacs et al. 2005; Frezza, Zheng, Tennant, et al. 2011). Despite similarities between SDH and FH inactivation, accumulation of intracellular fumarate triggered by FH loss has been shown to affect the function of several proteins. Fumarate has mild electrophillic characteristics and can spontaneously bind to thiol groups of proteins or other molecules. For instance, by binding to Kelch-like ECH-associated protein 1 (KEAP1), fumarate can inhibit the interaction between KEAP1 and nuclear factor erythroid 2-related factor (NRF2), thus eliciting a potent antioxidant response (Adam et al. 2011; Ooi et al. 2011). Fumarate has also been shown to bind and inhibit the activity of the CAC enzyme aconitase (Ternette et al. 2013), thus further impinging on the activity of the CAC and inhibiting mitochondrial metabolism. Finally, fumarate can covalently bind the reduced form of the antioxidant metabolite glutathione, thus scavenging its reducing moiety and increasing reactive oxygen species (ROS) levels in the cell (Sullivan, Martinez-Garcia, et al. 2013; Zheng, Cardaci, et al. 2015) (**Figure 1.1**).

Finally, the role of succinate and fumarate accumulation has been shown to go beyond dysregulation of cell metabolism. Accumulation of these metabolites can inhibit the activity of the αKG-dependent dioxygenases responsible for histone and DNA demethylation, inidicating the ability of small molecules to induce epigenetic changes. Importantly, metabolite-induced epigenetic modifications can have global genomic effects and have been shown to affect the expression of genes involved in tumourigenesis (Letouzé et al. 2013; Xiao et al. 2012; Sciacovelli, Gonçalves, et al. 2016) (**Figure 1.1**).

More recently the mutation of another enzyme of the CAC, isocitrate dehydrogenase 1 and 2 (IDH1-2) was observed in gliomas, leukemia and chondrosarcomas

(Parsons et al. 2008; Mardis et al. 2009; Amary et al. 2011). In contrast with mutations in SDH and FH that act as tumour suppressors, mutation of IDHs leads to the acquisition of a neomorphic activity, thus regarding IDHs as *bona fide* proto-oncogene. Instead of converting isocitrate to αKG, mutated IDH produces high levels of the R enantiomer of 2-hydroxyglutarate (2HG) (Dang et al. 2009). Similar to succinate and fumarate, the oncogenic effect of accumulated 2HG has been shown to relate to inhibition of αKG-dependent histone and DNA demethylases (Chowdhury et al. 2011; Lu, Ward, et al. 2012; Figueroa et al. 2010; Turcan et al. 2012). Interestingly, the epigenetic effect of accumulated 2HG has been associated with a block of cell differentiation and target inhibition of mutant IDH is able to induce differentiation and inhibit formation of leukemia and glioblastoma (Wang et al. 2013; Rohle et al. 2013) (**Figure 1.1**).

Together, these findings ultimately regarded altered metabolism as a central process during tumour transformation. Importantly, these studies shed light on the role of accumulated metabolites in affecting cellular functions beyond the reign of metabolism. Following these discoveries scientists gave birth to the term *oncometabolite*, referring to the independent ability of accumulated metabolites to trigger signals for oncogenic growth.

1.4 Hallmarks of altered metabolism in cancer

In the last two decades numerous research efforts have gathered extensive evidence on the molecular underpinnings of cancer metabolism. A new understanding of the field has recently appeared, whereby the vast heterogeneity of cancer-associated genetic alterations converge at the functional level by altering common metabolic pathways to support cancer cell proliferation and survival. In this section, I will describe the metabolic pathways that have been found, in the last two decades, to be commonly targeted by cancer mutations, and that can support anabolism in different cancer settings.

1.4.1 Deregulated uptake of nutrients

To satisfy the high anabolic demands of uncontrolled cell proliferation, cancer cells devise several strategies to gain unrestrained access to energetic sources. Among most abundant energy sources in the human body, glucose and glutamine play a prominent role in supporting anabolic growth in physiological conditions (Pearce and Pearce 2013). Mutations of oncogenes and tumour suppressor genes result in the activation of mechanisms that allow cancer cells to snatch extracellular glucose and glutamine *ad libitum*.

While normal cells couple nutrient uptake with signalling from growth factors, cancer cells show a reduced dependence on growth factor signalling (Thompson 2011). Indeed, a vast number of mutations found in human cancers target components of growth factor signalling cascades, such as PI3K/Akt and PTEN, or their downstream effectors, such as mammalian target of rapamycin (mTOR) and Myc. One of the reasons of this high convergence is that PI3K/Akt signalling cascade regulates the mRNA expression of the glucose transporter 1 (GLUT1) and its delivery to the plasma membrane (Barthel et al. 1999; Wieman et al. 2007). In fact, glucose uptake strictly correlates with the levels of activation of PI3K/Akt activity and is

restrained by inhibitors of this signalling cascade (Benz et al. 2011; Lheureux et al. 2013).

Increased expression of GLUT1 and glucose uptake appear to be a metabolic bottleneck operated by several genetic mutations to unleash proliferation of cancer cells. The seminal work of Yun and colleagues has been enlightening in this regard. The authors found that cancer cells harboring *Kirsten rat sarcoma (KRAS)* or *v-Raf murine sarcoma viral oncogene homolog B (BRAF)* mutations display increased levels of GLUT1 expression and activity (Yun et al. 2009). Moreover, they investigated the environmental conditions that play a role in the selection of cancer genetic mutations and observed that growing cells in low concentrations of glucose selected for high membrane expression of GLUT1 and increased glycolysis (Yun et al. 2009). Intriguingly, only 4% of the surviving cells had acquired *KRAS* or *BRAF* mutations during this process of selection, suggesting that other genetic alterations occurred in order to support GLUT1 expression and cell survival. Together with the previous finding that exogenous expression of GLUT1 can support proliferation of cells in growth factors-free conditions (Rathmell et al. 2003), this evidence supports the role of increased glucose uptake as a metabolic requirement of cancer transformation. Indeed, the uptake of the glucose analogue ^{18}F-fluorodeoxyglucose (^{18}F-FDG) is currently measured via positron emission tomography (PET)-based imaging for the diagnosis and staging of tumours, as well as for monitoring patient response to treatment (Almuhaideb et al. 2011).

Similar to glucose, glutamine uptake is increased in actively proliferating cells both in physiological conditions and in cancer. Oncogenic activation of c-Myc has been shown to upregulate the expression of glutamine transporters ASCT2 and SN2 and to activate several enzymes for the intracellular utilisation of glutamine (Eberhardy and Farnham 2001; Gao et al. 2009; Mannava et al. 2008). On the contrary, the tumour suppressor Rb inhibits glutamine uptake and metabolism by limiting the expression of ASCT2 and glutaminase 1 (GLS1) (Reynolds et al. 2014). These studies suggest that uptake of glutamine is tightly regulated by both mutated oncogenes or tumour suppressors and is an important feature of cancer cells proliferation. In line with this evidence, cells harboring several other cancer-driving mutations, such as *KRAS* (Son et al. 2013), display high susceptibility to glutamine deprivation compared to their normal counterparts.

Perhaps one of the reasons for the convergence of oncogenic signalling on increased glutamine uptake is the role of glutamine in the uptake of essential amino acids. Essential amino acids cannot be synthesised by the cell and have to be acquired from the extracellular space. Notably, export of glutamine is coupled to the simultaneous influx of the essential amino acid leucine by the antiporter LAT1 (Nicklin et al. 2009). This evidence links glutamine uptake to the uptake of other substrates of the LAT1 transporter, including isoleucine, valine, methionine, tyrosine, tryptophan, and phenylalanine (Yanagida et al. 2001).

1.4.2 Rewiring of glucose metabolism

Deregulation of nutrient uptake by cancer cells is coupled with alternative ways of nutrient distribution and utilisation in the cell. The glycolytic pathway is fed by extracellular glucose and it is a central player in satisfying the energetic and biosynthetic demands of actively proliferating cells.

Terminally differentiated cells have restricted access to extracellular glucose and tend to maximise the amount of energy that can be extracted from each molecule of glucose by full oxidation in the mitochondria (Vander Heiden et al. 2009). This process is initiated in the cytosol, by oxidising one molecule of glucose into two molecules of pyruvate through the glycolytic pathway, thus producing 2 net molecules of ATP. Subsequent conversion of pyruvate to acetyl-CoA in the mitochondria feeds the CAC and allows for extraction of reducing equivalents from glucose carbons to produce reduced nicotinamide adenine dinucleotide (NADH) and reduced flavin adenine dinucleotide ($FADH_2$). These latter co-factors are harnessed by the mitochondrial respiratory chain (RC) to achieve a final total yield of 36 molecules of ATP from one molecule of glucose.

In contrast to this model of efficiency, cancer cells maximise the cytosolic fermentation of pyruvate into lactate and reduce oxidation of glucose in the mitochondria, thus diminishing ATP yield from each molecule of glucose. Despite this rewiring of metabolism seeming counter-intuitive for a cell with high energetic demands, what tips the balance towards glycolysis in the equation of cancer metabolism is the spectrum of biosynthetic molecules that are associated with the cytosolic metabolism of glucose. In fact, important molecules for nucleotide and amino acid synthesis, as well as reducing equivalents and co-factors, can be produced from glycolytic intermediates that spin from glycolysis and feed other biosynthetic pathways.

Pentose phosphate pathway. Upon entry into the cell, glucose is phosphorylated to glucose 6-phosphate by the enzyme hexokinase (HK), thus avoiding glucose to exit the cell. Glucose 6-phosphate can then be destined towards glycolysis via phosphoglucose isomerase (PGI) or can be shunted to the pentose phosphate pathway (PPP) by glucose 6-phosphate dehydrogenase (G6PD). Shunting of glucose into the PPP is associated with the production of ribose 5-phosphate (non-oxidative arm), the backbone sugar for RNA and DNA nucleotide synthesis, as well as with the production of the reducing molecule reduced nicotinamide adenine dinucleotide phosphate (NADPH) (oxidative arm) (**Figure 1.2**). Several mutated oncogenes and tumour suppressors have been shown to regulate this pathway in cancer cells (Patra and Hay 2014). For instance, KRAS is able to increase production of ribose 5-phosphate by increasing the activity of the non-oxidative arm of the PPP (Ying et al. 2012), while TP53 can directly bind to the first and rate-limiting enzyme G6PD, negatively regulating the entry of glucose carbons into the PPP (Jiang, Du, et al. 2011). The contribution of this pathway to cancer growth is highlighted by the finding that inhibition of distinct PPP enzymes can inhibit KRAS-driven tumourigenesis *in vivo* (Ying et al. 2012), suggesting that targeting of the PPP could be exploited for cancer therapy.

Hexosamine pathway. The product of PGI, fructose 6-phosphate, can leave glycolysis and take part into the hexosamine biosynthesis pathway. The first enzymatic step is the nitrogen transfer from glutamine to fructose 6-phosphate by fructose 6-phospate aminotransferase 1 (GFPT1), generating glucosamine 6-phosphate. Subsequent steps lead to the production of *N*-acetyl glucosamine (**Figure 1.2**), the substrate of N- and O-linked glycosylation, enabling full protein maturation (Itkonen et al. 2013). Together with providing an explanation for the combined increase in the uptake of glucose and glutamine in cancer (Wellen et al. 2010), activation of the hexosamine pathway in cancer cells could explain the important role of glyco-

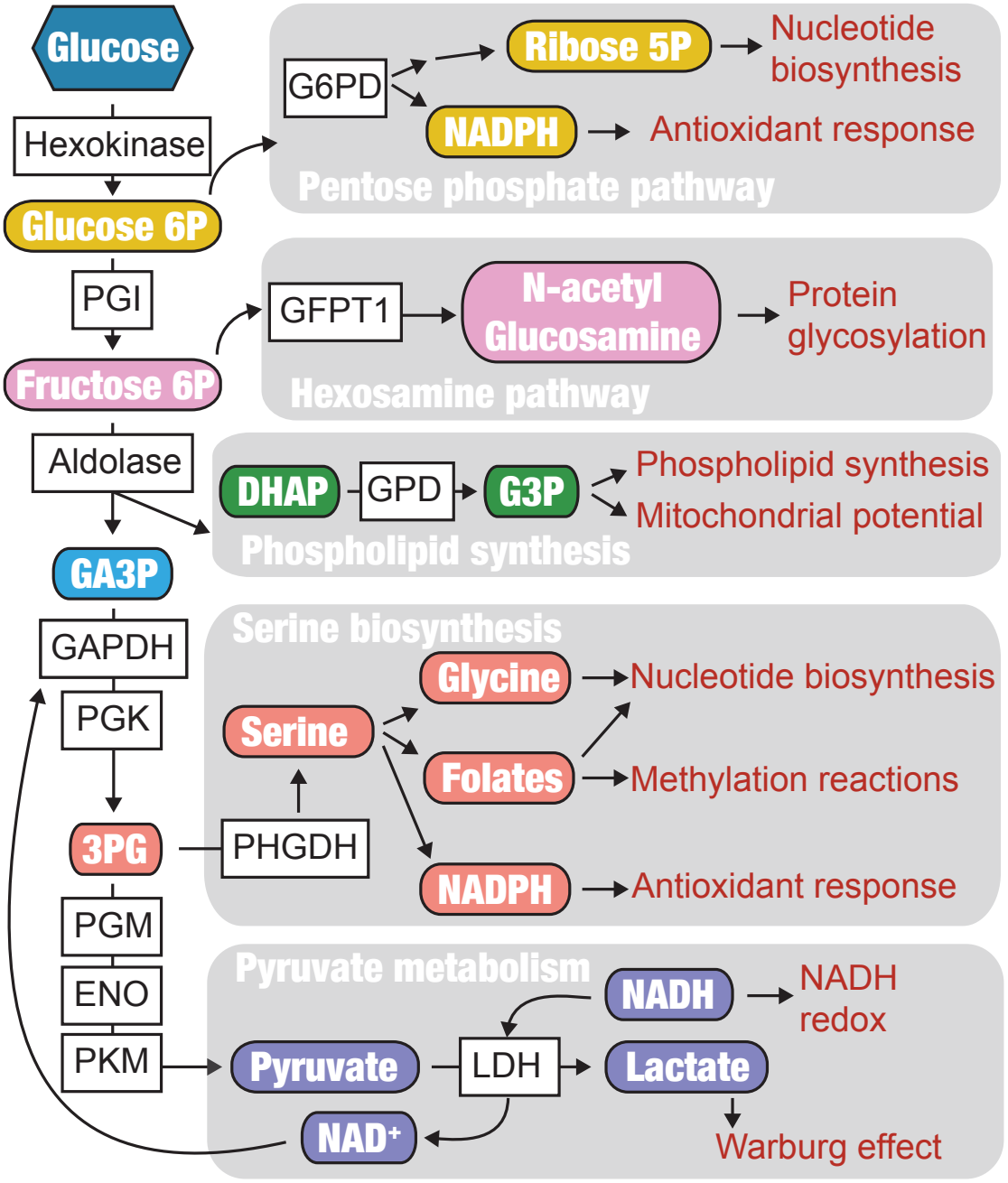

Figure 1.2: Biosynthetic pathways associated with glycolytic intermediates. Glucose-derived metabolites can be destined to several pathways for the synthesis of anabolic intermediates, such as nucleotides and phospholipids, as well as for providing molecules for antioxidant response or protein glycosylation. Aberrant uptake of glucose and activation of glycolysis can support anabolism by fueling biosynthesic pathways that stem from glycolytic intermediates.

sylation in cancer development (Pinho and Reis 2015), metastasis (Oliveira-Ferrer et al. 2017) and response to chemotherapy (Baudot et al. 2016).

Phospholipid synthesis. One of the two products of the glycolytic enzyme aldolase is dihydroxyacetone phosphate (DHAP), which can be converted to glycerol 3-phosphate by glycerol 3-phosphate dehydrogenase (GPD). Glycerol 3-phosphate is a precursor in the biosynthesis of phospholipids, fundamental components of cell

membranes (**Figure 1.2**). Moreover, glycerol 3-phosphate is a component of the glycerol phosphate shunt, an alternative pathway for the maintenance of mitochondrial membrane potential and target of the potent anticancer drug metformin (Madiraju et al. 2014).

Serine and glycine biosynthesis. The product of phosphoglycerate kinase (PGK), 3-phosphoglycerate (3PG) is the metabolic precursor of one of the most important shunts of glycolysis. Metabolism of 3PG not only gives rise to the amino acid serine, but also to amino acid glycine and reducing equivalent NADPH, as well as provides folate species for nucleotide biosynthesis and DNA methylation (Yang and Vousden 2016) (**Figure 1.2**). Notably, the first and rate-limiting step of this pathway, 3-phosphoglycerate dehydrogenase (PHGDH), has been found frequently amplified in breast cancer and melanoma, and inhibition of PHGDH has been shown to be detrimental for cancer cells (Possemato et al. 2011; Locasale et al. 2011). Serine-derived folates synthesis arises from the mitochondrial metabolism of serine by the enzymes serine hydroxylmethyltransferase 2 (SHMT2) and methylene tetrahydrofolate dehydrogenase 2 (MTHFD2). SHMT2 has been shown to protect from oxidative stress that occur during hypoxia (Ye et al. 2014) and MTHFD2 has been found among the top three most commonly amplified metabolic enzymes in cancer (Nilsson et al. 2014). Notably, overexpression of SHMT2 can rescue proliferation of cancer cells upon suppression of oncogenic c-Myc (Nikiforov et al. 2002), indicating the importance of serine biosynthesis for cancer growth. Together with the long-established role of folates in anti-cancer therapy (Farber, Diamond, et al. 1948), these findings indicate that serine biosynthesis pathway is a commonly altered metabolic pathway during cancer transformation.

Pyruvate metabolism. Pyruvate metabolism is a key point of convergence for several mutated oncogenes and tumour suppressors. Activation of the Warburg effect, or aerobic glycolysis, is achieved via the aberrant increase of pyruvate reduction to lactate via LDH. Activation of anabolic programs by several mutated oncogenes leads to enhanced expression and activity of LDH (Sciacovelli, Gaude, et al. 2014). The coupling of pyruvate reduction with NADH oxidation further enhances glycolytic flux by providing the cofactor oxidised nicotinamide adenine dinucleotide (NAD^+) for the rate-limiting enzyme glyceraldehyde 3-phosphate dehydrogenase (GAPDH) (**Figure 1.2**). Moreover, pyruvate conversion to lactate limits entry of pyruvate in the mitochondria, allowing the maintenance of low ATP levels and stimulating activation of glycolysis by low-energy sensors such as AMP-activated protein kinase (AMPK) (Cantó and Auwerx 2010). The paramount importance of convergent activation of LDH in several types of cancer is highlighted by the development of various therapeutic strategies aimed at disrupting LDH activity to inhibit cancer cells growth (Tennant et al. 2010; Martinez-Outschoorn et al. 2016).

1.4.3 Activation of nucleotide metabolism

Together with the activation of biosynthetic pathways that generate metabolic precursors for nucleotide synthesis, oncogenic signalling can directly activate enzymes involved in the production of nucleotides. For instance c-Myc can activate the first enzymatic steps of both purine and pyrimidine biosynthesis pathways, phosphoribosyl pyrophosphate synthetase 2 (PRPS2), carbamoyl phosphate synthetase (CAD) and inosine monophosphate dehydrogenase 2 (IMPDH2) (Cunningham et al. 2014;

Eberhardy and Farnham 2001; Mannava et al. 2008). Importantly, when expression of c-Myc is inhibited, proliferation of cancer cells can be rescued by ectopic expression of Myc's metabolic effectors such as the nucleotide biosynthesis enzymes IMPDH2 and PRPS2 (Mannava et al. 2008). Mutant p53 alleles have been shown to increase the expression of several enzymes for nucleotide biosynthesis, including IMPDH-1 and -2, GMP synthetase (GMPS), and nucleoside salvage enzymes deoxycytidine kinase (DCK) and thymidine kinase (TK1) (Kollareddy et al. 2015). Furthermore, phosphorylation of S6K by mTORC1, as well as MAPK activity can induce the enzyme CAD, suggesting that pyrimidine biosynthesis might be a convergent point for multiple oncogenic signals.

Activation of nucleotide synthesis is not only achieved by cancer cells through the direct activation of biosynthetic enzymes, but also via increased uptake of nutrients that provide building blocks for the construction of nucleotides' backbone. The pathway leading to the glucose-derived nucleotide precursor ribose 5-phosphate has been described above. In addition to glucose, glutamine is the fundamental source for reduced nitrogen needed in the biosynthesis of nucleotides. Synthesis of uracil and thymine require one molecule of glutamine, while for adenosine and cytosine two molecules of glutamine are needed. Moreover, metabolism of glutamine via the CAC supports the generation of the non-essential amino acid aspartate, a fundamental building block in the production of pyrimidine and purine nucleotides. It is not surprising that mutation of several oncogenes and tumour suppressor genes lead to enhanced glutamine uptake (Eberhardy and Farnham 2001; Gao et al. 2009; Mannava et al. 2008; Reynolds et al. 2014; Son et al. 2013).

Importantly, nucleotides deficiency has been suggested as a prelude to cancer transformation. Investigating the role of genome instability in the early phases of cancer development, Bester and colleagues observed that ectopic expression of the oncogenes HPV-16 E6/E7 or cyclin E oncogenes caused depletion of nucleotides and DNA damage (Bester et al. 2011). These effects were rescued by exogenous addition of nucleosides or by over-expression of c-Myc, which led to increased nucleotide synthesis. This finding suggested that aberrant activation of nucleotides biosynthesis observed in several types of cancer might be a fundamental compensatory mechanism to overcome cell death in the initial phases of tumourigenesis (Bester et al. 2011).

Finally, consumption of glycine was found to correlate with cancer cell proliferation in a large metabolic screening comprising 60 cancer cell lines (Jain et al. 2012). This association was explained by the role of glycine in providing carbons for nucleotide biosynthesis, thus indicating that a wide spectrum of oncogenic mutations converge on the activation of nucleotide biosynthesis to support cancer cell proliferation. In line with this evidence, a recent *in silico* investigation based on 23 different cancer types found that purine and pyrimidine biosynthesis are the most commonly altered metabolic pathways in human cancers (Hu, Locasale, et al. 2013), further indicating the importance of these biosynthetic pathways in tumourigenesis.

1.4.4 Induction of *de novo* lipid synthesis

Cell proliferation is supported by the production of cellular membranes. The main components of biological membrane are lipids and *de novo* lipid synthesis is a prominent pathway providing various species of membrane precursors in proliferating cells (Menendez and Lupu 2007). Biosynthesis of lipids begins with the cytosolic

carboxylation of acetyl-CoA operated by acetyl-CoA carboxylase (ACC), generating malonyl-CoA which is further assembled into long fatty acid chains by fatty acid synthase (FASN). Synthesis of cytosolic acetyl-CoA is operated by ATP-citrate lyase (ACLY) which produces oxaloacetate and acetyl-CoA from the mitochondrial metabolite citrate (**Figure 1.3**). Several enzymes for lipogenesis are activated by a wide spectrum of mutated oncogenes and tumour suppressor genes, including mutations targeting the PI3K/Akt axis (Berwick et al. 2002; Bauer et al. 2005), *BRCA1* (Chajès et al. 2006), and *MYC* (Priolo et al. 2014; Morrish et al. 2010; Edmunds et al. 2014) and are inhibited by wild type p53 (Yahagi et al. 2003). Importantly, cancer proliferation appears to be dependent on activated lipid synthesis, as genetic or pharmacological inhibition of ACLY can inhibit the growth of cancer cells *in vitro* (Hatzivassiliou et al. 2005).

Finally, acetate has been shown to support *de novo* lipid synthesis in some cancers, including glioblastoma and brain metastases (Mashimo et al. 2014). Once internalised, acetate can be converted into acetyl-CoA by acetyl-CoA synthetase 2 (ACSS2), an enzyme that has been found amplified in breast cancer (Schug et al. 2015). These findings not only demonstrate the importance of lipid synthesis - cancer cells find alternative carbon sources to feed into lipids - but also that dependence of cancer cells on extracellular acetate could be harnessed for anti-cancer therapies (Comerford et al. 2014).

1.5 Tissue environment dictates metabolic phenotype

It is now established that distinct oncogenic lesions lead to the regulation of different sets of metabolic enzymes and that cancer metabolic reprogramming functionally converges to the activation of anabolic programs for cell proliferation. In addition to the genetic regulation of metabolism, the site of tumour lesions has been recently shown to affect metabolic phenotype. Yuneva and colleagues investigated the role of different tissues in determining metabolic changes in c-Myc-transformed cancer cells (Yuneva et al. 2012). They systematically analysed the metabolic flux following c-Myc activation in the mouse liver, as opposed to the lung, and observed that, despite similar activating effects on glycolytic enzymes, glutamine metabolism was different in the two tissues analysed. While c-Myc led to the activation of GLS1 in the liver and subsequent induction of glutamine catabolism, the effect of c-Myc in lung tumours resulted in activation of glutamine synthetase (Glul), thus leading to accumulation of glutamine (Yuneva et al. 2012).

More recently this concept has been confirmed and expanded by the group of Matthew Vander Heiden. They compared the metabolic phenotype arising from two genetic lesions, mutant KRAS and loss of p53, in the pancreas and in the lung (Mayers et al. 2016). The combination of these genetic events causes pancreatic adenocarcinoma (PDAC) and non-small cell lung cancer (NSCLC) in humans, respectively. They found that, while NSCLC cells consumed high amounts of branched chain amino acids (BCAAs) for protein synthesis, PDAC cells displayed low BCAAs consumption. This effect was due to the activation of the enzymes for BCAAs metabolism BCAT1 and 2 specifically in the lung, but not in the pancreas (Mayers et al. 2016). Importantly, suppression of BCAT1 and 2 could inhibit the growth of lung tumours in mice, while it had no major effects on pancreatic tumours.

Together with affecting the metabolic phenotype of primary tumours, tissue

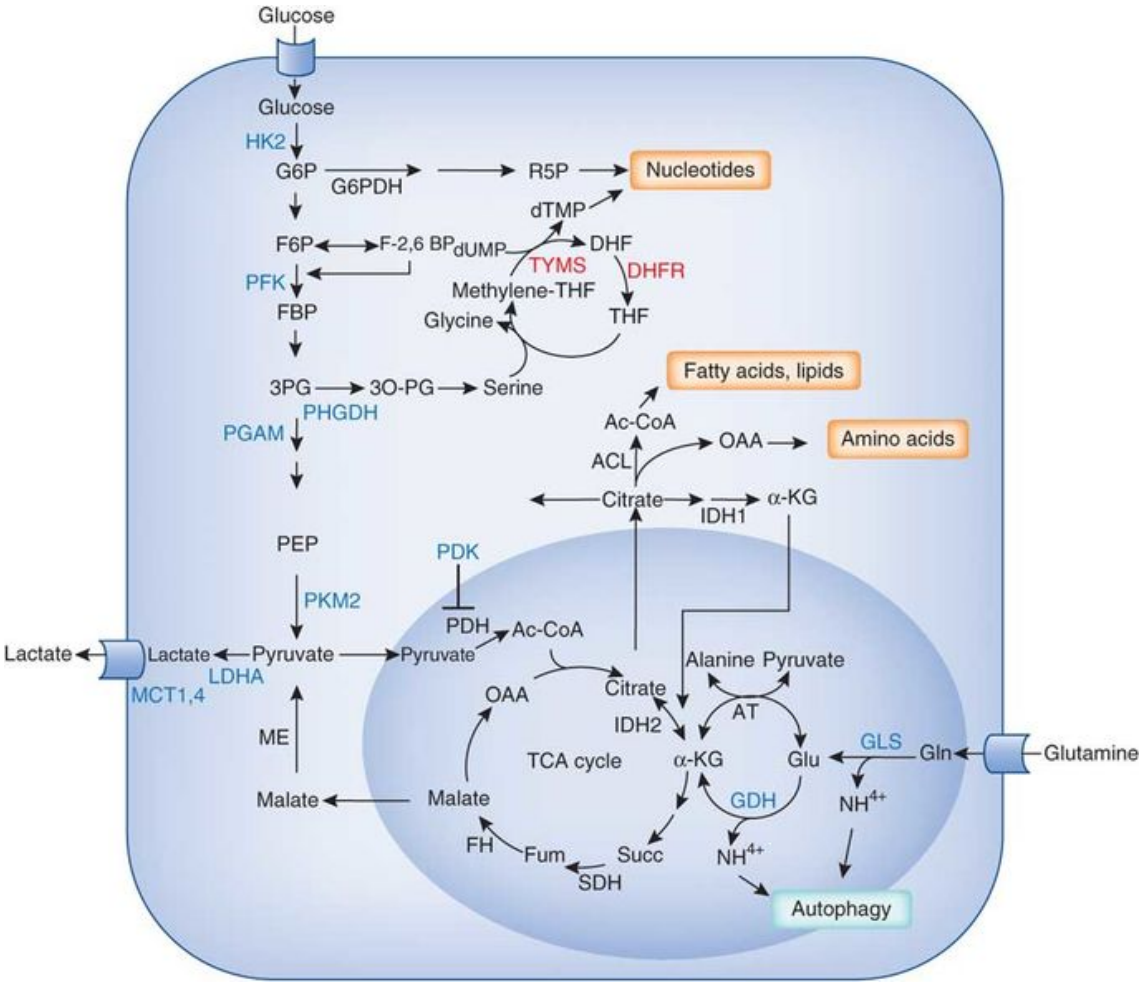

Figure 1.3: Map of altered metabolism in cancer. Altered metabolic reactions commonly found in cancer cells. The map highlights that glucose and glutamine metabolism can support induction of nucleotide and lipid biosynthesis to support proliferation of cancer cells. Adapted from Cheong et al. 2012.

environment can also regulate metabolism of cancer metastases. A recent study observed that liver metastases originated from primary mouse breast cancer had different metabolic state compared to bone and lung metastases originating from the same primary tumour (Dupuy et al. 2015). Liver metastatic cells displayed HIF1α-mediated activation of glycolytic metabolism. Such an effect was mediated by blocking pyruvate entry in the mitochondria via induction of pyruvate dehydrogenase kinase 1 (*PDK1*). In contrast with this metabolic state, bone and lung metastatic cells displayed increased consumption of glutamine and accumulation of CAC intermediates, indicating enhanced oxidative metabolism in the mitochondria (Dupuy et al. 2015). This study prompted the notion that different metabolic states give cancer cells the ability to metastasise to different tissues (Döppler and Storz 2015) and suggested that metabolism could drive formation of cancer metastases throughout the body.

Together, this evidence suggests that the site of tumour formation or cancer metastasis can profoundly affect the phenotype and growth abilities of cancer cells. Tissue-specific factors such as nutrient availability, hypoxia and cell-to-cell communication are likely to play an important role in the determination of the resulting

metabolic phenotype of cancer cells (Anastasiou 2017).

1.6 Reprogramming of mitochondrial metabolism in cancer

The mitochondrion has been the symbiotic companion of eukaryotic cells for two billion years (Wallace 2007). This partnership is thought to have begun with the endocytosis of a protobacterium by a eukaryotic ancestor and coincided with the increase of oxygen levels in the earth's atmosphere. Mitochondria could offer the ability to couple detoxification from molecular oxygen with energy production and the endosymbiosis profoundly changed not only the bioenergetics of the eukaryotic ancestor, but also its genetic organisation. Mitochondria transferred part of their genome into the nucleus and provided sufficient energy for the large expansion of the nuclear genome experienced by eukaryotic cells during evolution (Lane and Martin 2010). In addition, mitochondria are responsible for the survival of the cell by regulating programmed cell death (Koonin and Aravind 2002) and can communicate with the nucleus by signalling through ROS or by regulating the intracellular levels of calcium (Rizzuto et al. 2012) and small molecules (Frezza 2014).

Mitochondria are the major site of oxygen consumption in the cell and they are responsible for the optimised production of energy and biosynthetic molecules. They are composed of a double lipid bilayer, likely the remnant of its endocytic origin, where the internal membrane is convoluted into membranous folds named *cristae* and the external membrane is a highly permeable lipid layer that creates an intermembrane space between the two mitochondrial membranes.

Each mitochondrion contains multiple copies of the mitochondrial DNA (mtDNA), a circularly structured genome encoding for 13 mitochondrial proteins. Among these there are the proteins of the mitochondrial respiratory chain (RC), which is responsible for coupling the creation of a proton-based electrochemical gradient in the intermembrane space with the production of ATP, while reducing molecular oxygen to water. As opposed to nuclear DNA, which is present with two copies within the cell, mtDNA is present in tens to thousands of copies. For this reason, mutations of the mitochondrial genome can affect a number of copies of mtDNA, while co-existing with other copies of normal mtDNA. Thus, mtDNA mutations can be found in different proportions among different cells, generating heterogenous mixtures of normal and mutated mtDNA, a phenomenon also known as *heteroplasmy*. Varying degrees of mtDNA heteroplasmy can give rise to a spectrum of defects, ranging from mild to severe bioenergetic dysfunction that can eventually lead to cell death (Wallace and Fan 2010).

1.6.1 mtDNA mutations in cancer

Mutations of the mitochondrial genome have been found in a wide array of cancer types, including colon, breast, lung, prostate, liver, pancreas, kidney, thyroid, brain, gastric carcinoma and ovarian cancer (Chatterjee et al. 2006) and they are associated with a spectrum of bioenergetic defects. In line with this evidence, when comparing the abundance of mtDNA between normal and cancer samples, Reznik and colleagues found that mtDNA is widely depleted in several types of human

cancer (Reznik, Miller, et al. 2016). These findings suggest that some extent of mitochondrial dysfunction might be selected for during tumour development and that mutations of mtDNA, together with loss of mitochondria, could provide cancer with a proliferative advantage. Despite positive selection of mtDNA mutations in cancer has been debated (Ju et al. 2014), a recent comprehensive study found similar mutational signatures in ∼40 different types of cancer, with gene truncating mutations being enriched in kidney, colorectal and thyroid cancers (Yuan et al. 2017). Interestingly, the authors also found that transfer of mitochondrial genes into the nucleus of cancer cells induced disruption of critical genes for cancer development, such as ErbB2. This finding suggests that instability of mtDNA could have important effects on cancer development beyond the modulation of cellular bioenergetics (Wallace 2012). Finally, a recent study found that mitochondrial single nucleotide variants (mtSNVs) accumulate in mutational hot-spots in the mtDNA of patients with prostate cancer (Hopkins et al. 2017), suggesting positive selection of specific mutations in the mitochondrial genome. Notably, mtSNVs were associated with copy number alterations of the nuclear oncogene *MYC* and specific mtSNVs were linked to patient survival (Hopkins et al. 2017), indicating that mtDNA mutations can affect cancer aggressiveness and have important clinical implications.

Mutations of Complex I. Complex I (CI) is a NADH:ubiquinone oxidoreductase that catalyses the transfer of two electrons from NADH to ubiquinone via flavin mononucleotides, producing NAD^+ and four protons, which are pumped in the intermembrane space (Salway 2016). CI is the first site of the electron transport chain and active site of ROS production. Mutations in mitochondrial genes encoding for CI have been linked to the development of colon, thyroid, pancreas, breast, bladder, and prostate cancer as well as of head and neck tumors and medulloblastoma (Chatterjee et al. 2006) (**Figure 1.4**). Furthermore, mutations of CI have been linked to increased ROS-dependent metastatic potential in Lewis lung carcinoma and breast cancer cells (Ishikawa et al. 2008; He et al. 2013). The extent of CI dysfunction caused by the mtDNA mutation is critical for promoting or inhibiting cancer proliferation. Profound CI dysfunction leads to diminished growth of cancer cells both *in vitro* and *in vivo* (Iommarini et al. 2013), but some extent of CI activity is required to support glycolytic rates associated with anabolism (Calabrese et al. 2013), indicating that modulation of CI activity is critical for cancer cells' growth.

Mutations of Complex III. Complex III (CIII) is also known as coenzyme Q:cytochrome *c* oxidoreductase, or cytochrome b*c*1, and catalyses the electron transfer from reduced ubiquinone to cytochrome *c*. The electron transfer is coupled with the pumping of four protons into the intermembrane space. Mutations affecting mtDNA genes encoding for CIII have been found in several cancers, including colorectal, ovarian, thyroid, breast and bladder cancers (Polyak et al. 1998; Liu, Shi, et al. 2001; Máximo et al. 2002; Owens et al. 2011; Fliss et al. 2000) (**Figure 1.4**). Investigation of the effects of CIII dysfunction on cell metabolism and cancer cell proliferation has been investigated by the expression of a truncated form of a CIII subunit (Dasgupta et al. 2008). This CIII mutation was associated with increased lactate and ROS production, together with enhanced proliferative ability and invasion *in vitro* and *in vivo* (Dasgupta et al. 2008).

Mutations of Complex IV. Complex IV (CIV) or cytochrome *c* oxidase is the final complex of the electron transport chain. Electrons received from cytochrome *c* are used by CIV to reduce molecular oxygen into water and pump four protons

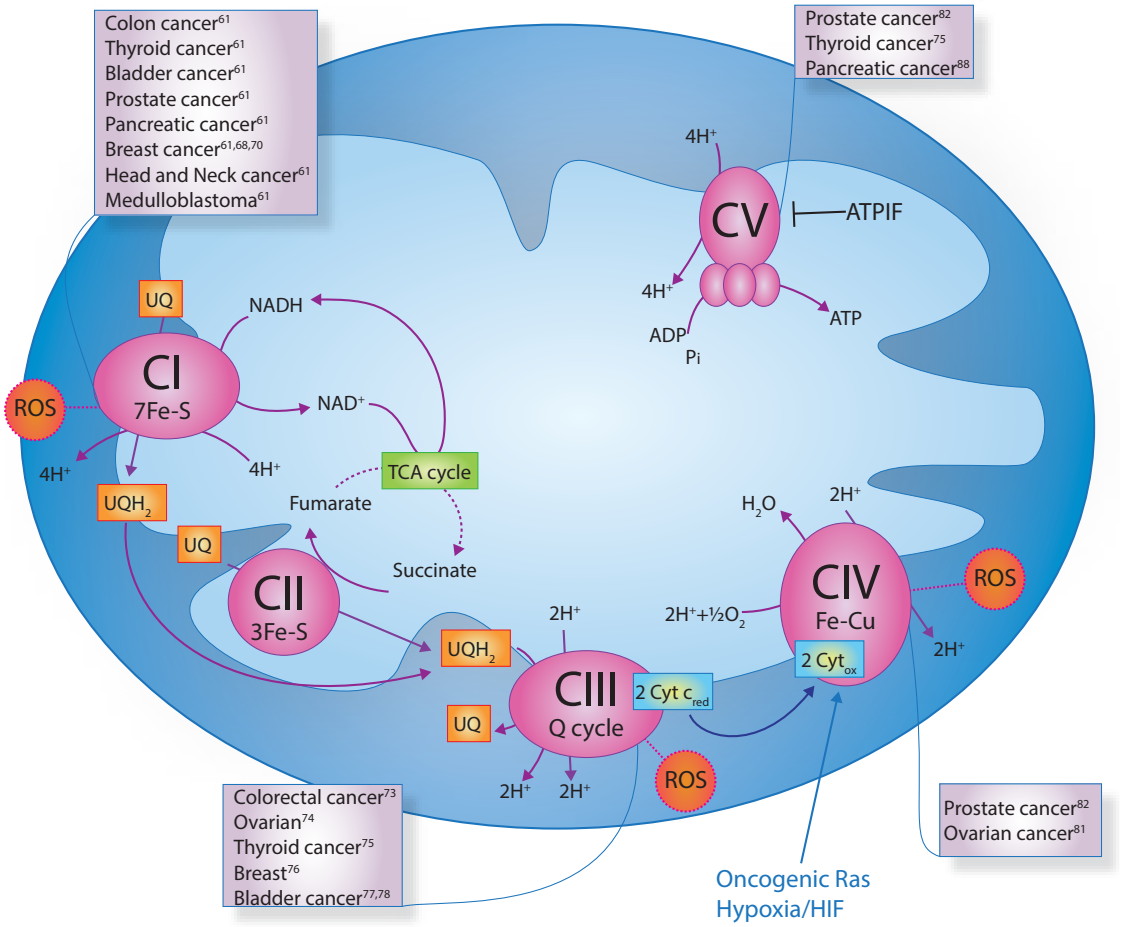

Figure 1.4: Representation of the mitochondrial respiratory chain complexes and associated cancer types. Adapted from Gaude and Frezza 2014.

in the intermembrane space. Mutations of the mtDNA-encoded CIV subunit 1 (COX1) have been associated with CIV dysfunction and various cancer types, including ovarian and prostate cancer (Permuth-Wey et al. 2011; Petros et al. 2005) (**Figure 1.4**). Nevertheless, some subunits of CIV are encoded by the nuclear DNA, and the role of mutations affecting the nuclear genes in supporting tumourigenesis is not trivial. For instance, increased expression of nuclear CIV subunits is associated with enhanced respiration and ROS production in Bcl2-transformed leukemia cells (Chen and Pervaiz 2010) and expression of the oncogene *KRAS* is associated with increased CIV activity in A549 lung adenocarcinoma cells (Telang et al. 2012). These results indicate that regulation of CIV function can support cancer proliferation and that combination of different oncogenic signals converge on increasing CIV activity. A possible explanation for this latter effect could be offered by CIV being a site of ROS production (Kadenbach et al. 2013), which are known to contribute to the proliferation of some cancer cells (Reczek and Chandel 2017). Alternatively, increased activity of CIV might support cancer cell growth by enhancing mitochondrial metabolism and its associated biosynthetic pathways.

Mutations of Complex V. Complex V (CV) or ATP synthase, is the final enzyme of oxidative phosphorylation. CV exploits the electrochemical potential gradient across the inner mitochondrial membrane to generate ATP from ADP and inorganic phosphate. Mutations of mtDNA encoding for CV subunits have been

found in thyroid (Máximo et al. 2002), pancreatic (Jones et al. 2001), prostate (Petros et al. 2005) and breast (Tan, Bai, et al. 2002) cancer (**Figure 1.4**). The mechanisms linked between CV mutations and cancer have been investigated by Shidara and colleagues (Shidara et al. 2005). By expressing two mutants of the mtDNA gene encoding for subunit 6 of CV (*MT-ATP6*), they observed increased *in vitro* cell proliferation, as well as enhanced tumourigenesis in *in vivo* xenografts (Shidara et al. 2005). Importantly, mutant cells were associated with decreased apoptosis and increased ROS production. This suggests that dysfunction of CV can not only interfere with mechanisms of programmed cell death, but also can inhibit the function of the whole electron transport chain. This observation is in line with the finding that different mutants of MT-ATP6 display marked reduction of oxygen consumption and increased lactate secretion (Pallotti et al. 2004). Importantly, point mutations of another gene encoding for CV, *MT-ATP8*, have been recently associated to human prostate cancer aggressiveness and *MT-ATP8* mutational status was associated to cancer patient survival (Hopkins et al. 2017). On the other hand, when a profound dysfunction of the respiratory chain is induced by depletion of mtDNA, intact ATP synthase is required for cell survival (Chen, Birsoy, et al. 2014; Martnez-Reyes et al. 2016). In this context CV is able to reverse its activity, consuming glycolytic ATP and pumping protons in the intermembrane space, in order to maintain mitochondrial membrane potential and ensure cell survival. Together, these findings indicate the high flexibility of CV in compensating for bioenergetic defects and suggest CV as a central player in mitochondrial metabolism.

1.6.2 Complete mitochondrial dysfunction is detrimental to tumourigenesis

The initial observation made by Warburg led him to hypothesise that activation of aerobic glycolysis was a consequence of irreversible damage to cellular respiration (Warburg 1956). Even though this phenomenon is partially observed in several types of cancer (Wallace 2012), it is now well established that complete mitochondrial dysfunction is detrimental for the survival of cancer cells. In fact, complete ablation of mtDNA by treatment with ethydium bromide (ρ^0 cells) (Desjardins et al. 1985) inhibits growth rate, proliferation in soft agar and tumour growth in nude mice (Magda et al. 2008; Morais et al. 1994; Cavalli et al. 1997; Weinberg et al. 2010). Moreover, breast cancer cell lines (Tan, Baty, et al. 2015) or melanoma cells (Dong et al. 2017) devoid of mtDNA require the acquisition of intact mitochondria from the host in order to form tumours *in vivo*. In both scenarios acquisition of healthy mitochondria was associated with rescue of respiratory abilities (Tan, Baty, et al. 2015; Dong et al. 2017) and dissemination of primary tumour cells to form metastases was dependent on the degree of mitochondrial function (Tan, Baty, et al. 2015). This evidence suggests that the role of mitochondrial (dys)function in tumourigenesis is far from trivial and that a combination of mitochondrial defects and metabolic reprogramming is likely to be required to allow proliferation of cancer cells.

1.6.3 Reprogramming of the CAC cycle by cancer cells

First described by Hans Krebs in 1937 (Krebs and Johnson 1937), the CAC is a series of enzymatic reactions that begins by generating citrate via condensation of

the acetyl group from acetyl-CoA with oxaloacetate, and proceeds through decarboxylating and oxidising reactions, ultimately leading to the generation of a new molecule of oxaloacetate. While this process is mainly thought to provide precursors for ATP generation in the mitochondria, the CAC provides intermediates for the biosynthesis of lipids, non-essential amino acids and iron-sulfur-containing compounds (Owen et al. 2002). The full cycle leads to the production of two molecules of CO_2, one molecule of ATP/GTP and, fundamental for connecting the CAC with oxidative phosphorylation, three molecules of NADH.

Despite the CAC is generally represented via a closed, circular topography, nutrients and products can join or leave the cycle at many different sites. Together with glucose, that mainly provides carbons in the form of acetyl-CoA, other *anaplerotic* substrates can contribute to the flux of the CAC, such as glutamine, which feeds into αKG, and fatty acids, which serve as carbon sources for acetyl-CoA and succinyl-CoA. Similarly, carbons can depart from the CAC via *cataplerotic* mechanisms, such as the export of citrate for lipid synthesis or αKG for generation of glutamate, as well as the use of succinyl-CoA for heme biosynthesis and oxaloacetate for the generation of aspartate (Owen et al. 2002). Such dynamic organisation shows the flexibility of this metabolic pathway which can be adapted for the production of specific precursor molecules. Distinct oncogenic events preferentially activate segments of the CAC and exploit different reactions to meet the biosynthetic needs of cell proliferation.

As mentioned above, mutations of the CAC enzymes isocitrate dehydrogenase 1 (IDH1) and isocitrate dehydrogenase 2 (IDH2) confer a neomorphic activity which, instead of converting isocitrate in αKG, reduce αKG into the R-enantiomer of 2HG, which accumulates up to millimolar levels in cancer cells (Dang et al. 2009; Ward, Patel, et al. 2010. Oncogenic mutations of IDHs have been found in various human cancers, including colon cancer (Sjöblom et al. 2006), glioblastoma Parsons et al. 2008), glioma Yan et al. 2009), acute myeloid leukemia (Mardis et al. 2009), prostate cancer (Kang et al. 2009), B-acute lymphoblastic leukemia (Kang et al. 2009), osteosarcoma (Liu, Kato, et al. 2013), and intrahepatic cholangiocarcinoma (Borger et al. 2014). Accumulation of 2HG is considered a major contributor to the oncogenic activity of mutated IDHs. The tumourigenic activity of 2HG has been attributed to its inhibitory effect on various αKG-dependent dioxygenases, including the hypoxia-inducible factors (HIFs) prolyl hydroxylases (PHDs), histone demethylases, and the ten-eleven translocation (TET) family of DNA demethylases (Chowdhury et al. 2011; Xu et al. 2011). The first evidence that 2HG acted upon DNA methylation arose in 2010 when a large-scale DNA methylation analysis of human leukemia found that the expression of mutated IDH, by increasing 2HG levels, led to DNA hyper-methylation, a broad epigenetic change associated with poor hematopoietic differentiation. Of note, such a peculiar change in DNA methylation was dependent on the inhibition of TET2 caused by 2HG (Figueroa et al. 2010). A similar epigenetic fingerprint has also been observed in a subset of breast tumors where 2HG was found to accumulate to millimolar levels. Interestingly, however, in these tumors, the accumulation of 2HG was not caused by overt IDH mutations but, rather, by a particular metabolic rewiring instigated by Myc overexpression (Terunuma et al. 2014). These results suggest that 2HG has an important role in tumorigenesis and that it can accumulate in cancer cells not only upon IDH mutations but also as a consequence of metabolic derangements, including hypoxia (Wise

et al. 2011). More recent results revealed that, besides inhibiting DNA demethylases, 2HG accumulation also causes profound changes in histone methylation (Lu, Ward, et al. 2012), indicating that this metabolite has multiple and well-defined epigenetic roles.

Similarly to mutant IDHs, most of the oncogenic activity of another mutated enzyme of the CAC, SDH, has been attributed to a metabolite, succinate, which accumulates in SDH-deficient cells. The oncogenic role of succinate was initially linked to the inhibition of PHDs and the subsequent stabilization of HIF (Selak et al. 2005). More recently, succinate was found to be a prototypical epigenetic hacker (Yang and Pollard 2013), capable of inhibiting both DNA (Xiao et al. 2012; Killian et al. 2013) and histone demethylases (Cervera et al. 2009), leading to epigenetic changes that overlap with those observed in mutant IDH cancers (Letouzé et al. 2013). Beyond the epigenetic effects exerted by succinate as an oncometabolite, loss of enzymatic activity due to mutation of SDH leads to interruption of the carbon flow through the CAC. Together with accumulation of succinate, interruption of CAC also leads to depletion of downstream metabolites, such as malate and oxaloacetate, two important intermediaries in the malate-aspartate shuttle, leading to depletion of the non-essential amino acid aspartate (Cardaci et al. 2015), whose role in supporting proliferation of cancer cells has recently emerged (Sullivan, Gui, et al. 2015; Birsoy et al. 2015). In order to replenish oxaloacetate levels and support aspartate biosynthesis, SDH-deficient cells activate flux through pyruvate carboxylase, an alternative anaplerotic reaction which can generate oxaloacetate directly through carboxylation of pyruvate (Cardaci et al. 2015). In this scenario, rewiring of the CAC is fundamental to supply carbons for aspartate biosynthesis and support proliferation of SDH-deficient cancer cells.

As discussed above, FH deficiency leads to a disruption of the carbon flux through the cycle and accumulation of its substrate fumarate, which subsequently induces accumulation of the CAC intermediates succinate and succinyl-CoA (Frezza, Zheng, Folger, et al. 2011). To overcome this defect, FH-deficient cells activate a detoxifying strategy whereby glutamine carbons enter the CAC and support cataplerosis of succinyl-CoA towards the heme biosynthetic pathway. Such adaptation of the normal flow of the CAC is important for the generation of NADH to maintain mitochondrial function and leads to secretion of bilirubin. Importantly, inhibition of the heme biosynthetic pathway leads to mitochondrial dysfunction and death of FH-deficient cells (Frezza, Zheng, Folger, et al. 2011), indicating the importance of such rewiring for survival of FH-deficient cancer cells.

In addition, other oncogenic events can affect the activity of CAC reactions. Most oncogenes activate a metabolic switch towards aerobic glycolysis and reduction of pyruvate through LDH limits pyruvate entry into the CAC. Inhibition of pyruvate dehydrogenase (PDH), the entry step of pyruvate in the CAC, is achieved by activation of its negative regulator pyruvate dehydrogenase kinase (PDK). This regulatory mechanism is operated by oncogeninc activation of Myc, β-catenin/TCF or HIF (Pate et al. 2014; Kim et al. 2006; Papandreou et al. 2006) and leads to reduced glucose carbons feeding into the CAC.

Despite this, entry of pyruvate into the CAC is increased in other oncogenic settings. For instance, acquisition of homozygous copies of mutant *KRAS* in mouse lung tumours facilitates the generation of the first CAC intermediate citrate, but citrate carbons subsequently depart from the CAC to generate glutamate and support

glutathione biosynthesis (Kerr et al. 2016). Mutations of *KRAS* in a pancreatic cancer setting elicit a different rewiring of the CAC. A recent study showed that KRAS induced dependency on extracellular glutamine, and this glutamine was metabolised through the CAC in order to produce aspartate (Son et al. 2013). Aspartate was then transported into the cytosol, and converted into pyruvate and NADPH by a series of reactions involving glutamate-oxaloacetate transaminase 1 (GOT1), malate dehydrogenase 1 (MDH1) and malic enzyme 1 (ME1), thus supporting cytosolic redox balance and ROS scavenging (Son et al. 2013). Suppression of the enzymes GOT1, MDH1 or ME1 led to impaired tumour formation in nude mice, indicating that this KRAS-mediated metabolic reprogramming was instrumental for cancer growth.

This evidence suggests that, even though flux through the CAC can be impaired or suboptimal in cancer cells, *ad hoc* rewiring of specific anaplerotic and cataplerotic reactions can support the biosynthetic needs of anabolism under the proliferative conditions imposed by distinct cancer-initiating events.

1.7 Metabolic alterations induced by mitochondrial dysfunction

The evidence reported above indicates that different oncogenic events harness the ability of mitochondria to provide biosynthetic precursors by altering the normal function of mitochondrial metabolism. Mutations of components of the mitochondrial RC or of the CAC, as well as activation of other oncogenic programs can lead to various degrees of mitochondrial dysfunction. Given the role of mitochondria as the central metabolic hub of the cell, regulation of mitochondrial function can have profound effects on several other metabolic pathways.

Effects on glycolysis. Flow of glucose carbons through the glycolytic pathway in the cytosol is associated with production of ATP and NADH. While ATP can be readily used in the cytosol, NADH is shuttled into the mitochondria to support oxidative phosphorylation (Blacker and Duchen 2016). Importantly, NADH consumption by the mitochondrial RC not only supports mitochondrial homeostasis and ATP production, but it is also fundamental for maintaining glycolytic flux. In fact, the rate-limiting glycolytic enzyme GAPDH is dependent on the conversion of NADH into NAD^+, and NAD^+ availability is thought to be a major regulator of glycolysis (Stanley et al. 1997). Regulation of the cytosolic NAD^+/NADH ratio is achieved via two mechanisms, the first entailing conversion of pyruvate into lactate via LDH with concomitant recycling of NADH into NAD^+, while the second being the malate-aspartate shuttle (MAS). The MAS is a six-step enzymatic mechanism that involves passing a hydrogen atom from NADH to oxaloacetate via the enzyme malate dehydrogenase 1 (MDH1) thus forming malate. Shuttling of malate into the mitochondria, followed by oxidation to oxaloacetate by malate dehydrogenase 2 (MDH2), ensures supply of NADH to the mitochondrial RC.

Decreased demand for mitochondrial NADH induced by defects of respiration inhibits flux through the MAS (Lu, Zhou, et al. 2008) and is associated with imbalance of cellular NAD^+/NADH ratio (Fendt et al. 2013). In order to maintain flux through glycolysis, additional recycling of NADH via LDH is required, and this is known to support energy production during hypoxia or anaerobic exercise (Spriet

et al. 2000), as well as being the molecular determinant of the Warburg effect. Mutations of mtDNA affecting respiratory complexes, or mutations of CAC enzymes have been shown to cause impairment of mitochondrial respiration and increase lactate secretion. The switch towards Warburg's aerobic glycolysis, initiated by NAD^+/NADH imbalance, can lead to the activation of glycolysis and accumulation of glycolytic intermediates. This metabolic state can subsequently lead to increased flux through the biosynthetic pathways associated with high glycolysis (see above) and support anabolism.

Glutamine metabolism. Mitochondrial dysfunction can affect the metabolism of another important energy source, glutamine. Metallo and colleagues recently showed that diversion of glucose carbons away from the CAC in cells exposed to hypoxia is associated with increased conversion of glutamine to αKG. Moreover, instead of undergoing oxidation via αKG dehydrogenase (KGDH), αKG was reduced

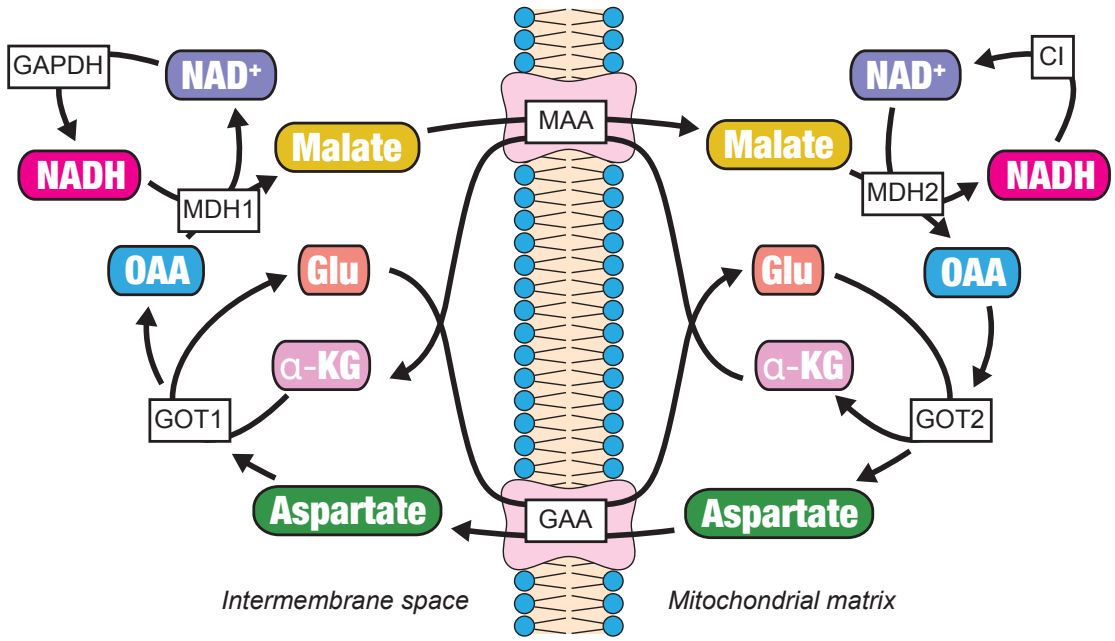

Figure 1.5: The malate-aspartate shuttle transports reducing equivalents between cytosolic and mitochondrial compartments. Cytosolic NADH diffuses to the mitochondrial intermembrane space and donates two reducing equivalents to oxaloacetate (OAA) via malate dehydrogenase 1 (MDH1), producing malate and NAD^+. NAD^+ can be used by the glycolytic, rate-limiting enzyme glyceraldehyde 3-phosphate dehydrogenase (GAPDH). Malate is transported into the mitochondrial matrix by the malate-α-ketoglutarate antiporter (MAA), with concomitant exchange of α-ketoglutarate (α-KG). Mitochondrial malate is then oxidised by MDH2 to OAA with reduction of NAD^+ to NADH. In this way, cytosolic reducing equivalents are transported, via NADH, into the mitochondria, and can be used by respiratory complex I (CI). In the mitochondria, the amino group from glutamate is then transferred to OAA by glutamate-oxaloacetate transaminase (GOT)-2, generating α-KG and aspartate. In this way, regeneration of α-KG allows the transport of a new molecule of malate into the mitochondrial matrix, while transport of aspartate to the cytosol via glutamate-aspartate antiporter (GAA) ensures glutamate availability for a further reaction via GOT2. Finally, aspartate is transaminated by GOT1 in the intermembrane space, regenerating OAA and allowing for a new cycle to begin.

to citrate by reversal of IDH1 in the cytosol (Metallo et al. 2012). This glutamine-supported reductive carboxylation of αKG was able to provide carbons for *de novo* lipogenesis through production of acetyl-CoA from citrate, identifying a role for oxygen availability in redirecting carbon utilisation and meeting anabolic needs under stress conditions (Metallo et al. 2012). In line with this evidence, the group of Ralph DeBerardinis showed that mutations of complex I or complex III of the mitochondrial RC disrupt oxidative metabolism of glutamine and induce glutamine reductive carboxylation (Mullen et al. 2012). Notably, this metabolic rewiring was observed also in patient-derived cancer cells with mutations of the CAC enzyme FH or upon pharmacological inhibition of the RC, where reductive carboxylation was the main carbon source for lipid synthesis (Mullen et al. 2012). A recent study also showed that pharmacological inhibition of the mitochondrial RC inhibits pyruvate entry into the mitochondria and leads to decreased levels of citrate (Fendt et al. 2013). In this scenario, reductive carboxylation of glutamine is induced in order to re-establish the citrate:αKG levels and support cancer cells proliferation. Intriguingly, induction of reductive carboxylation is associated with production of the oncometabolite 2HG, even in the presence of wild type IDH2 (Wise et al. 2011; Smolková et al. 2015). This evidence suggests that reversal of IDHs could support tumour growth not only by providing precursors for lipid synthesis, but also by reinforcing aerobic glycolysis via 2HG-mediated HIF stabilisation (Zhao et al. 2009), as well as via 2HG-mediated epigenetic effects (Chowdhury et al. 2011).

Nucleotide biosynthesis. Together with supplying substrates for nucleotide biosynthesis, mitochondrial function is intimately linked with pyrimidine biosynthesis via the enzyme dihydroorotate dehydrogenase (DHODH). An integral component of the mitochondrial RC, DHODH couples the conversion of dihydroorotate to orotate with the reduction of ubiquinone to ubiquinol (Ahn and Metallo 2015). Importantly, oxidation of ubiquinol by a functional RC is fundamental for DHODH activity and cell lines with mitochondrial defects require supplementation of the pyrimidine precursor uridine in order to be cultured *in vitro* (Ditta et al. 1976; King and Attardi 1989).

Together with dependence on uridine, mitochondrial dysfunction can lead to auxotrophy also for aspartate, another precursor in the pyrimidine biosynthesis pathway. In an attempt to understand the dependence of cells with dysfunctional mitochondria on the extracellular supply of pyruvate, the group of Vander Heiden discovered that pyruvate is utilised to support the production of aspartate, an important precursor of pyrimidine and purine synthesis (Sullivan, Gui, et al. 2015). The authors showed that generation of NAD^+ via pyruvate-mediated flux through LDH was used to support MDH1 activity and generation of oxaloacetate in the cytosol. Subsequent production of aspartate via transamination of oxaloacetate by glutamate-oxaloacetate transaminase 1 (GOT1) was then able to support nucleotide synthesis. In support of this study, the group of Sabatini showed that chemical inhibition of the mitochondrial RC induced essentiality for GOT1, identifying the production of aspartate as one of the main functions of the RC in proliferating cells (Birsoy et al. 2015). Importantly, in the absence of extracellular pyruvate, supplementation of aspartate rescued the growth of mitochondria-defective cells by supporting nucleotide synthesis (Sullivan, Gui, et al. 2015; Birsoy et al. 2015).

This evidence indicates that mitochondrial function can have profound ef-

fects on several metabolic pathways inside the cell. Regulation of mitochondrial activity by cancer cells allows parallel modulation of biosynthetic pathways connected to mitochondrial function, and offers important mechanisms of metabolic flexibility to meet anabolic needs of cancer proliferation.

1.8 Association between metabolism and cancer progression

Following the establishment of an initial tumour mass, cancer cells constantly face new challenges and cancer is far from being a static entity. Environmental cues, such as nutrient availability or treatment with anti-cancer therapies, force cancer cells to adapt their metabolism for survival. Indeed, metabolic changes have been identified at different disease stages of prostate (Pertega-Gomes et al. 2015; Torrano et al. 2016), breast (Denkert et al. 2012), renal (Hakimi et al. 2016) and lung (Kerr et al. 2016) cancers.

The metabolic flexibility displayed by cancer cells allow them to thrive in different conditions. Detachment from the initial tumour mass and survival in circulation are among most critical challenges faced by cancer cells. To overcome anoikis, the process of cell death induced by matrix detachment, and survive in the blood stream, cancer cells undergo metabolic changes (Schafer et al. 2009). Metastatic cells from mouse melanoma activate antioxidant pathways in order to survive in suspension (Jeon et al. 2012) and matrix-detached cells exploit cytosolic reductive carboxylation in order to feed NADPH-producing mitochondrial reactions of the CAC (Jiang, Shestov, et al. 2016). Moreover, melanoma cells that are intravenously injected into nude mice face high levels of oxidative stress and form only minor metastases (Piskounova et al. 2015). In this scenario, inhibition of antioxidant NADPH-producing enzymes can ablate metastatic potential entirely (Piskounova et al. 2015), suggesting that metabolic pathways counteracting oxidative stress are crucial for metastatic cells. Together with other studies showing that activation of antioxidant pathways, such as heme biosynthesis (Dey et al. 2015) and superoxide dismutase (Kamarajugadda et al. 2013), can support tumour metastasis, this evidence indicates that rewiring of cell metabolism is triggered in metastatic cancer cells to survive in the blood-stream and colonise distant tissues.

In addition to antioxidant mechanisms, mitochondrial metabolism plays an important role in cancer metastasis. Mutations of the CAC enzymes SDH in pheochromocytoma and paraganglioma, as well as of FH in renal cancer, are linked to the activation of epithelial-to-mesenchymal transition (EMT) (Loriot et al. 2012; Sciacovelli, Gonçalves, et al. 2016), a gene signature associated with invasion and metastasis (Tsai and Yang 2013) and resistance to anti-cancer therapies (Zheng, Carstens, et al. 2015). Moreover, downregulation of the master regulator of mitochondrial biogenesis nuclear coactivator PPARγ coactivator-1α (PGC1α) is observed in human samples of metastatic prostate cancer, and deletion of PGC1α in the mouse prostate triggers cancer progression and metastasis (Torrano et al. 2016). In line with this evidence, partial inhibition of the mitochondrial RC was shown to enhance migratory abilities of cancer cells *in vitro* and to promote lung metastases *in vivo* (Porporato et al. 2014). Finally, mtDNA mutations targeting the activity of complex I were recently shown to induce breast cancer metastasis *in vivo*, and

rescue of complex I was sufficient to abolish metastatic properties (Santidrian et al. 2013).

The evidence mentioned above indicates a role for mitochondrial defects in supporting cancer metastasis. Nonetheless, other studies have shown that intact mitochondrial metabolism might be preferred for cancer cells to achieve colonisation of distant tissues. For instance, increased transcriptional activation of oxidative phosphorylation (OXPHOS) genes has been detected in circulating tumour cells after implantation of breast cancer cells in mice (LeBleu et al. 2014).

Since cancer metastasis is one of the principal causes of cancer deaths across different cancer types (Tsai and Yang 2013), regulation of mitochondrial metabolism in cancer cells might have important implications for survival of cancer patients. In line with this hypothesis, a recent study conducted on several types of human cancer found that depletion of mtDNA correlated with poor prognosis of cancer patients (Reznik, Miller, et al. 2016).

Another important determinant of survival for cancer patients is the resistance of cancer cells to anti-cancer therapies. In this regard, metabolic adaptation has been shown to play an important role. Survival of cancer cells upon treatment with the chemotherapeutic drug cisplatin is achieved via the activation of antioxidant mechanisms, entailing the production of NADPH by PPP (Catanzaro et al. 2015). Pharmacological inhibition of the PPP enzyme G6PD was shown to abrogate resistance to cisplatin (Catanzaro et al. 2015), suggesting that combination therapies targeting metabolic enzymes might limit therapy resistance and increase the success of chemotherapy. A study conducted by Viale and colleagues supports this hypothesis. The authors investigated the mechanisms related to oncogene addiction by inducing expression of oncogenic *KRAS* in mouse pancreas and by allowing tumours to form *in vivo*. Subsequent ablation of oncogenic *KRAS* revealed that surviving cancer cells were dependent on OXPHOS metabolism, and treatment with mitochondrial inhibitors could block tumour recurrence (Viale et al. 2014). Similarly, inhibition of oncogenic BRAF in melanoma cells induces activation of a PGC1α transcriptional program that allows cell survival via the activation of antioxidant mechanisms (Vazquez et al. 2013; Haq et al. 2013). This evidence indicates that metabolic adaptation is an important mechanism operated by different cancer types when challenged by treatment with cancer therapies. Inhibition of the metabolic strategies adopted by cancer cells upon treatment might help in designing more successful combination therapies.

1.9 Analytical techniques for the investigation of metabolism

1.9.1 Enzymatic assays

Investigation of metabolism entails the assessment of enzymatic (metabolic) reaction(s) by measuring the production or consumption of specific metabolites or small molecules. Traditionally, measurements of metabolites have been possible through the design and application of *enzymatic assays*, whereby an external, purified enzyme is introduced into the system under investigation (cell suspension, biological fluid, etc) and assessment of its enzymatic activity can indicate the presence and

abundance of a specific metabolite. Different enzymes will preferentially react with different metabolites, and application of an array of metabolic enzymes will provide information on the levels of different metabolic species in the system under investigation. An example of enzymatic assay is the measurement of the metabolite lactate via the activity of lactate dehydrogenases. In the presence of lactate and NAD^+, the enzymes will produce pyruvate and NADH. Production rates of NADH over time indicate enzymatic activity and are used to interpolate initial lactate concentrations. Although enzymatic assays have been widely used to assess specific metabolic reactions or the levels of specific metabolites, they allow the investigation of one or few metabolites at a time, thus providing a narrow view of metabolism.

1.9.2 Metabolomics techniques

"Omics" techniques have emerged that allow measurement of several metabolites simultaneously, thus providing more comprehensive information on metabolism compared to enzymatic assays. Due to their ability to provide a holistic view of metabolism, these techniques are regarded as *metabolomics* techniques and they include, among others, nuclear magnetic resonance (NMR) spectroscopy, gas chromatography-mass spectrometry (GC-MS) and liquid chromatography-mass spectrometry (LC-MS).

NMR spectroscopy exploits the magnetic properties of certain atomic nuclei and can identify different small molecules based on their different atomic composition. When exposed to high magnetic fields, different atoms respond differently based on intrinsic magnetic properties and based on other surrounding atoms. Due to these properties, different molecules will respond differently when subjected to a magnetic field. NMR can uniquely identify and simultaneously quantify a range of metabolites in the micromolar range of concentration. NMR is largely automated and is non destructive, thus reducing sample preparation and manipulation to the minimum and allowing for further analysis of biological samples. The main disadvantage of NMR, compared to MS-based techniques, is its low sensitivity and reduced range of metabolites that can be measured.

MS-based techniques can identify different molecules based on their mass: different atomic compositions lead to different molecular weights. When measured with sufficient accuracy molecular mass can uniquely identify different molecules. Together with identification through molecular mass, MS-based techniques are usually preceded by other separation techniques, such as gas or liquid chromatography, that separate molecules based on chemico-physical properties (such as polarity and hydrophilicity). These techniques allow different molecules to reach the mass spectrometer at different times (retention time) and the combination of both retention time and measured mass lead to the identification of a wide range metabolites.

GC-MS requires a derivatisation reaction to generate volatile compounds that are subsequently separated through gas chromatography and analysed by a mass spectrometer. The derivatisation process is the main limitation of this technique due to the fact that only a subset of metabolites will derivatise and due to potential artifacts arising from the derivatisation reaction. Despite these limitations GC-MS has been widely applied for untargeted metabolomics screenings because of the wide range of metabolites that can be simultaneously detected and quantified (Tsugawa et al. 2011). An advantage of the derivatisation reaction is the possibility

to analyse very low molecular weight molecules (below 50 Da) that would otherwise be under the limit of detection for other MS-based techniques (Meiser et al. 2016).

With LC-MS there is no need to derivatise compounds prior to analysis, thus allowing reliable measurement of labile and nonvolatile polar and non-polar compounds in their native form. Combination of different liquid chromatographic techniques allow separation of different metabolic species and can provide a powerful tool to expand the array of molecules that can be identified and quantified in a biological sample. Due to its reproducibility and minimal sample preparation procedure LC-MS has been successfully applied in a high number of untargeted and targeted metabolomics studies (Zhang, Sun, et al. 2012).

Finally, each technique has associated advantages and disadvantages, and no single analytical method is ideal for analysing the several thousands of metabolites in a biological system. Combination of different techniques is likely to offer the ability of measuring a wide range of metabolites with different polarity, functional groups and molecular weight, thus allowing a comprehensive profile of the metabolome.

1.9.3 Isotope tracing

Measurement of metabolites in a biological sample can give information on steady-state levels of metabolites that derive from homeostatic metabolic reactions, but it neither provides information on the specific reactions that generated those metabolites, nor it allows comparison of the rate of specific metabolic reactions. Due to recent advancement in analytical techniques, isotope tracing has become a widely used technique to assess the activity of specific metabolic reactions or selective activation of metabolic pathways. Isotope tracing is performed through the introduction of an external compound that can be metabolised by the biological system under investigation (e.g. cell culture) and that is composed of isotope atoms different from the ones normally present in nature. An example of isotope tracer is a form of glucose composed of ^{13}C instead of the naturally-occurring ^{12}C. When metabolised by the cells, ^{13}C-glucose will give rise to ^{13}C-labelled metabolites, allowing for the identification of specific metabolites that can be obtained via glucose metabolism. Moreover, interpretation of the labelling patterns obtained by isotope tracing can provide information on the activation of specific metabolic reactions. For instance, in the case of ^{13}C-glucose been provided to mammalian cells, detection of citrate bearing 2 labelled carbons (citrate m+2) will indicate metabolism of pyruvate through pyruvate dehydrogenase, whereas detection of citrate m+3 will signify metabolism of pyruvate through the pyruvate carboxylase reaction (Cardaci et al. 2015). Design of different tracing strategies by using different labelled compounds can provide information on specific metabolic reactions inside the cell and has proven a very useful technique to investigate metabolism (Metallo et al. 2012; Lewis et al. 2014).

Aims of the study

DEVELOPMENT and progression of cancer depend upon changes of cell metabolism. Mutation of different oncogenes and tumour suppressor genes elicits specific metabolic changes aimed at supporting the bioenergetic and biosynthetic needs of cancer proliferation and survival. Cancer cells are dependent on the induced metabolic changes and identifying the key regulators of cancer metabolic rewiring is important for the design of efficacious anti-cancer therapies. Despite the general landscape of cancer metabolic transformation has recently emerged (Hu, Locasale, et al. 2013; Pavlova and Thompson 2016), the association between metabolic rewiring and survival of cancer patients is not well understood.

My study will be aimed at:

1) Exploring the metabolic landscape of human cancers, as opposed to the metabolic phenotype of normal human tissues. This investigation will be performed with the use of bioinformatic tools and will add onto previously known metabolic alterations by including a larger number of patient samples and by improving current methodology.

2) Investigating the association between metabolic changes and survival of cancer patients. This part will combine gene expression data with overall survival of cancer patients and will aim at identifying metabolic pathways that are commonly linked with poor patient prognosis.

3) Investigating the molecular determinants of important metabolic pathways arising from aim (2). This part of the study will require an appropriate *in vitro* system for understanding the link between altered metabolic pathways and other cellular functions potentially linked with cancer aggressiveness.

CHAPTER 2

Materials and methods

2.1 Selection of normal and cancer samples for bioinformatic analysis

Samples from 20 different solid cancer types were downloaded from the cancer genome atlas (TCGA) data portal (https://tcga-data.nci.nih.gov/tcga/dataAccessMatrix.htm). For each cancer type, mRNA expression data of cancer and normal samples were downloaded. More in detail, level 3 (open access) Read Counts of genes obtained from the platform RNAseqV2 were considered. Although TCGA regards as "normal sample" both samples originated from blood and solid tissues adjacent to tumour site, I included in my analysis only normal samples originated from solid normal adjacent tissue.

2.2 Differential gene expression and pathway enrichment analysis

2.2.1 Data download

Raw counts of RNAseq data were obtained from TCGA database for each cancer dataset considered and analysed with the R package DESeq2 (version 1.6.3), which assesses differential gene expression by use of negative binomial generalized linear model (Love et al. 2014). Default parameters of DESeq2 function were used based on the package vignette (https://bioconductor.org/packages/release/bioc/vignettes/DESeq2/inst/doc/DESeq2.html). The outcome of the DESeq analysis (i.e. Wald test statistics of cancer tissue vs normal tissue) was used as an estimate of differential gene expression in the subsequent pathway enrichment analysis.

2.2.2 Manual curation of metabolic gene signature

Every gene was associated to one or more metabolic pathways, according to the genome scale metabolic model Recon1 (Duarte et al. 2007). This metabolic gene signature was use as the starting point for compiling a more comprehensive and curated association of metabolic genes to corresponding pathways. To this aim, I manually integrated information from several online databases, including the Human Metabolome Database (HMDB, http://www.hmdb.ca), the Kyoto Encyclopedia of Genes and Genomes (KEGG, http://www.genome.jp/kegg/pathway.html#metabolism)

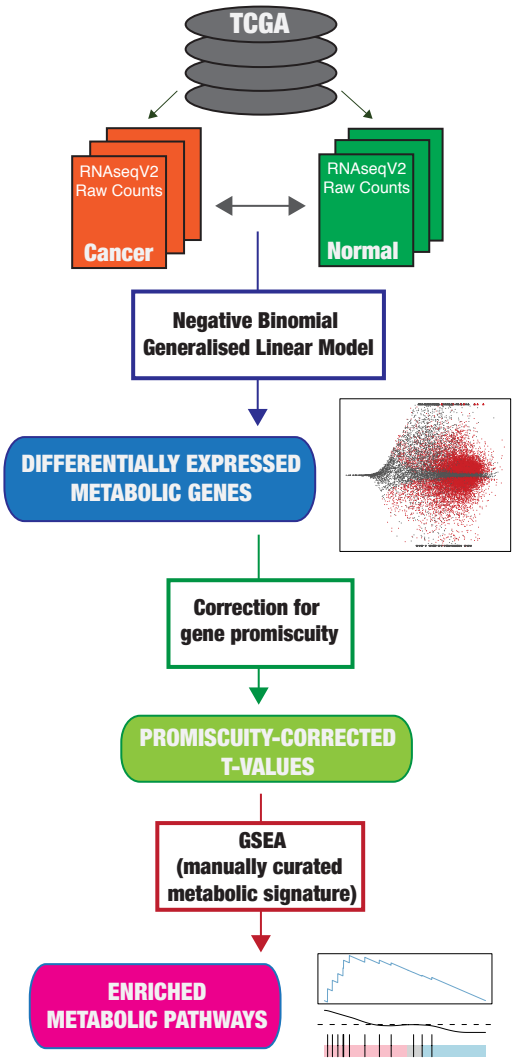

Figure 2.1: Analysis pipeline for differential gene expression and metabolic GSEA between cancer and normal samples.

and the Online Mendelian Inheritance in Man (OMIM, https://www.omim.org) and expanded the information included in Recon1 gene signature in order to comprehend missing genes or function, as well as to include correct association of genes to metabolic pathways. Full details of the metabolic gene signature can be found in Gaude and Frezza 2016.

2.2.3 Differential expression analysis

Differential gene expression was corrected for promiscuity across metabolic pathways by dividing the Wald t-value statistics obtained from DESeq2 analysis by the number of associated pathways (promiscuity). To assess the effect of promiscuity correction the median t-value, per each gene, across all cancers was calculated and plotted against promiscuity (see Chapter 3). Corrected t-values were then used as input for gene set enrichment analysis (GSEA). GSEA was performed by applying the manually curated metabolic gene signature to promiscuity-corrected t-values according to the algorithm developed by Subramanian et al (Subramanian et al. 2005) by using the R package piano (version 1.6.2) (Väremo et al. 2013). This analysis re-

sulted in metabolic pathways enriched (upregulated) and enriched (downregulated) in cancer vs normal samples, for each cancer type. In order to obtain a group of metabolic pathways that are commonly altered in different cancer types, I combined together all metabolic pathways found enriched in all cancer types and selected the pathways that resulted enriched (up- or down-regulated) in at least 25% of cancer types.

I then validated this list of commonly altered metabolic pathways by performing the same analysis on an independent dataset comprising 67 human breast cancer samples and 65 normal tissue controls, obtained from Terunuma et al (Terunuma et al. 2014). Differential gene expression analysis of breast cancer vs normal samples was performed by applying Shapiro Wilks test for normality followed by two-sided Students t-test and promiscuity-corrected t-values were used to perform metabolic GSEA as described above. The same approach was adopted for validation of metabolic adaptation in metastatic 786-O cell lines, compared to parental (Vanharanta et al. 2013; GEO accession code: GSE32299). Metastatic and parental groups were composed of 4 and 3 samples, respectively. These and all subsequent analyses were performed in R software, version 3.1.3 (2015.03.09) Smooth Sidewalk.

2.3 Correlation analyses

All correlations were calculated using Spearman's method. Final correlation p-values were adjusted for multiple testing using Benjamini-Hochberg correction method. Gene expression data and growth rate values of NCI-60 cancer cell lines were downloaded via CellMiner (http://discover.nci.nih.gov/cellminer/). Correlation between expression of purine biosynthesis and growth rate of NCI-60 cancer cell lines was calculated by comparing mean expression of genes involved in purine biosynthesis pathway and growth rate in each cancer cell line. Correlation between Phosphoribosylaminoimidazole carboxylase phosphoribosylaminoimidazole succinocarboxamide synthetase (*PAICS*) and growth rate was calculated by comparing expression of *PAICS* and growth rate values in each cancer cell line. Gene expression data and metabolite abundance of breast cancer and normal samples were obtained from (Terunuma et al. 2014). Correlation between expression of metabolic pathways and metabolite abundance was calculated by comparing mean expression of genes and abundance of metabolites involved in each pathway. Correlation between oxidative phosphorylation (OXPHOS) and epithelial-to-mesenchymal transition (EMT) levels was determined, for each cancer type, between median expression levels of OXPHOS and EMT genes for High and Low survival patients (see below), respectively. EMT gene signature was obtained from the Hallmark Epithelial Mesenchymal Transition gene set (M5930), publicly available at http://www.broadinstitute.org/gsea/msigdb.

2.4 Survival analysis

To investigate the link between alteration of metabolic pathways and survival of cancer patients, I took advantage of the survival data included in the TCGA database, from which I calculated the overall survival (OS) by using the R package "survival" (https://cran.r-project.org/web/packages/survival/index.html).

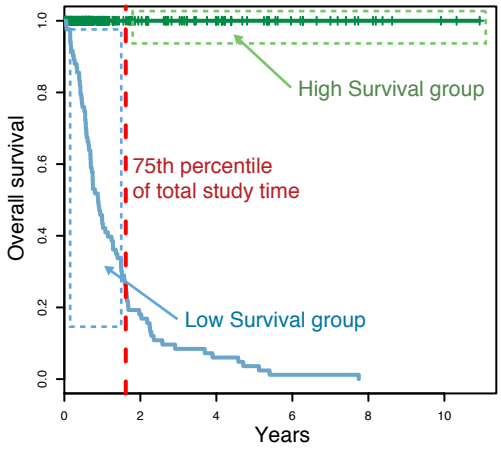

Figure 2.2: Example of classification of cancer patients into high and low survival groups. Overall survival (OS) times of bladder urothelial carcinoma (BLCA) patients. Green points correspond to patients that have been censored alive, while red points are patients who died during the study. The dashed red line indicates the 75^{th} percentile of all patients OS times. The green dashed square represents patients included in the high survival group, while blue dashed square denotes patients included in the low survival group.

Based on the calculated OS data for each patient, in each cancer type, I divided patients into "high survival" and "low survival" groups. To avoid potential biases, such as low censoring time or study drop-outs, in order for a patient to be included into the high survival group, he/she had to be censored "alive" for a certain amount of time (see below). This method avoids inclusion into the high survival group of patients that have been censored for only few months or patients that have dropped out of the study and the study lost their track. Moreover, this method allows to include patients that have survived, after diagnosis of cancer, for a certain amount of time (i.e. high survival patients).

I then included patients into the low survival group if they died during the study. In order to avoid overlaps between high and low survival groups (e.g. a patient might have died after being part of the study for a long time, see (**Figure 2.2**)), I only included in the low survival group patients that have died within a certain amount of time (**Figure 2.2**). The time threshold between high and low survival groups was determined empirically, by comparing the group sizes of high and low survival groups and by choosing the threshold that was resulting into similar group sizes, across all cancer types. This *ad hoc* parameter was implemented in order to avoid either group sizes to be highly different, or some groups to be not represented due to low number of patients in a particular cancer type. Following this method I chose a time threshold corresponding to the 75^{th} percentile of all patients OS times. Due to different OS times in different cancer types, the time threshold is different for different cancer studies.

For example, in the bladder urothelial carcinoma (BLCA) dataset the 75^{th} percentile observation time corresponds to 1.62 years. I included in the high survival group only patients that have been censored alive for 1.62 years or more, while the low survival group was composed of patients that have died within the first 1.62 years of the follow-up study. This resulted in a high survival group formed of 61

patients and low survival group formed of 61 patients as well. I excluded from gene expression analysis of low vs high survival patients those cancer types that displayed n $<$ 5 in one of the two groups (CHOL, PCPG, PRAD, READ, THCA).

Differential gene expression analysis coupled with GSEA of low survival versus high survival patients was performed as described above. GSEA of hallmarks cellular functions was performed on cancer types that showed downregulation of OXPHOS in low vs high survival patients. Gene sets were obtained from the HALLMARKS collection of the MSigDB database, publicly available at http://www.broadinstitute.org/gsea/msigdb.

2.5 Tissue-independent metabolic clustering of cancer samples

In order to perform clustering of cancer samples based on expression of metabolic pathways independently of the tissue of origin, all cancer samples were assembled into a data matrix. RNAseq Raw Counts of metabolic genes of each sample were normalised with variance stabilizing transformation (VSN) (Huber et al. 2002), distributed into metabolic pathways according to the metabolic signature described above and mean expression of genes in each metabolic pathway was calculated. For example, the citric acid cycle (CAC) pathway is composed of 58 genes, therefore to calculate mean expression of the CAC pathway I averaged the normalised gene expression values of all 58 genes. Optimal number of clusters was determined via Gap statistic, a technique that compares the change in within-cluster dispersion with what would be expected under a reference null distribution (Tibshirani et al. 2001). Gap statistic was performed with the function "clusGap" from the R package "cluster" (https://cran.r-project.org/web/packages/cluster/index.html). Mean expression levels of metabolic pathways for all cancer samples were then subjected to partitioning around medoids (PAM) clustering, a clustering technique that defines, for a pre-defined number of clusters, a medoid as the object in the cluster with minimal dissimilarity to all other objects in the cluster (Barbakh et al. 2009). PAM clustering was performed with k number of clusters obtained via Gap statistics.

2.6 Analysis of tissue-specific metabolic rewiring

Samples from all normal tissues and all cancer tissues were grouped and VSN transformation (Huber et al. 2002) was applied independently on RNAseq raw counts of metabolic genes belonging to the normal tissues data set and on the cancers data set. For each metabolic gene we calculated the mean expression across patients, in each normal tissue or cancer:

$$P = \frac{p_1 + ... + p_n}{n} \tag{2.1}$$

where n is the number of samples in each normal or cancer data set and P defines the mean of all patients, for each metabolic gene. The ratio between expression of each metabolic gene in a tissue and the average expression across all tissues (normal or cancer) was calculated:

$$r_{i,t} = \frac{P_{i,t}}{Q_i} \tag{2.2}$$

where $P_{i,t}$ is the result of equation 2.1 i.e. the average expression of the i^{th} metabolic gene in the t^{th} tissue (normal or cancer); and Q_i is the average P_i expression across all tissues (normal or cancer). Hence, $r_{i,t}$ defines the fold change, for each gene, between normal (or cancer) tissue and the average of all normal (or cancer) tissues. To find out tissue-specific activation or suppression of metabolic pathways, pathway mean was calculated as follows:

$$S_p = \frac{r_{1i,t} + ... + r_{ji,t}}{j} \tag{2.3}$$

where j is the number of genes in each pathway p and S_p denotes the mean r fold change in the pathway p, thus obtaining a fold change of each metabolic pathway in each tissue, compared to average tissue. Given C_p and N_p as the S_p values for cancer tissues and normal tissues, respectively, the correlation between metabolic competence in normal and cancer tissues can be calculated from:

$$G_p = cor(N_p, C_p) \tag{2.4}$$

where G denotes the correlation between normal and cancer samples and p denotes each pathway.

Metabolic diversity between normal and cancer tissues was quantified by calculating the standard deviation of the N_p and C_p distributions, for each normal and cancer tissue, respectively.

In order to obtain tissue-specific functions, I calculated the average expression levels for each gene, among all normal tissues. I then performed differential gene expression and promiscuity-corrected GSEA comparing each normal tissue against the average expression of all normal tissues. Tissue-specific cancer metabolic adaptation was determined by comparing the metabolic pathways that were enriched in cancer vs normal and the metabolic functions specific of that particular tissue. Tissue-dependent and -independent metabolic adaptation of cancer were obtained by extracting metabolic pathways that, if up- or down-regulated in normal are up- and down-regulated in cancer, and viceversa. To investigate whether tissue-specific functions are associated with tissue-specific essentiality, I downloaded data from the Achilles 2.4 study, a shRNA screening performed on 216 cancer cell lines, derived from different tissues (Cowley et al. 2014). shRNAs targeting metabolic genes (based on previously described metabolic gene signature) were extracted from the list of all shRNAs. Association between gene essentiality and tissue of origin was obtained by using ANOVA and p-values were adjusted using Benjamini-Hochberg method and FDR = 5%. To determine tissue-independent pathway essentiality I obtained, for each cell line, a list of essential metabolic genes by extracting the top 5% essential genes, based on Analytic Technique for Assessment of RNAi by Similarity (ATARiS) gene-level score (Cowley et al. 2014; Shao et al. 2013). I then combined cell lines into tissues of origin, thus obtaining a list of essential genes for each tissue. To assess pathway essentiality across different tissues, I measured the occurrence of each essential gene across tissues and calculated the average occurrence per pathway, thus obtaining the mean number of tissues were metabolic genes, in each pathway, are essential.

2.7 Cell culture

2.7.1 Subpassaging

Cells were cultured in Dulbeccos modified Eagles medium (DMEM, Life Technology cat. no. 41966-029) containing 25 mM glucose and 4 mM glutamine, with added 10% v/v fetal bovine serum (FBS) and grown in a humidified incubator at 37°C and 5% CO_2. After subpassaging cells were allowed to grow for two to three days until 90-95% confluent before next subpassaging.

2.7.2 Cell growth assays

For cell proliferation assays $2*10^4$ cells were seeded in 24-well plates and allowed to attach for at least 16 hours. Medium was then changed to normal DMEM or DMEM with added nutrients or drugs. Cell growth in galactose was performed by culturing cells in glucose-free and pyruvate-free DMEM (Life Technology cat. no. 11966-025), with added 10% v/v FBS, 25 mM D-galactose (Sigma, G0750) and 1 mM sodium pyruvate (Sigma, P2256). To assess cell proliferation in the presence of aminooxiacetate (AOA) and aspartate normal DMEM was supplemented with varying concentrations of AOA (Sigma-Aldrich, C13408) and 4 mM L-aspartic acid (Sigma-Aldrich, A9256). Cell growth was assessed with an IncuCyteő FLR (Essen Bioscience) and assay was stopped when all cell conditions reached full confluency or confluency started to decrease consistently.

2.8 Oxygen consumption and extracellular acidification rate measurements

To assess oxygen consumption rate (OCR) and extracellular acidification rate extracellular acidification rate (ECAR) $6*10^4$ cells were seeded the night before experiment in XFe24 Cell Culture microplate in 100 μL normal DMEM. The next day cells were washed twice in phosphate buffer saline (PBS) and medium was replaced with 675 μL of bicarbonate-free DMEM (Sigma-Aldrich, D5030) supplemented with 25 mM glucose, 1 mM pyruvate, 4 mM glutamine, 40 μM phenol red and 1% v/v FBS. To eliminate residues of carbonic acid from medium, cells were incubated for at least 30 minutes at 37°C with atmospheric CO_2 in a non-humidified incubator. OCR and ECAR were assayed in a Seahorse XF-24 extracellular flux analyser by the addition via ports AC of 1 μM oligomycin (port A), 1 μM carbonyl cyanide-p-trifluoromethoxyphenylhydrazone (FCCP, port B), 1 μM rotenone and 1 μM antimycin A (port C). Two or three measurement cycles of 2-min mix, 2-min wait, and 4-min measure were carried out at basal condition and after each injection. At the end of the experiment, each well was washed twice with 1 mL of PBS and proteins were extracted with 100 μL of radioimmune precipitation assay (RIPA) lysis medium (150 mM NaCl, 50 mM Tris, 1 mM EGTA, 1 mM EDTA, 1% (v/v) Triton X-100, 0.5% (w/v) sodium deoxycholate, 0.1% (v/v) SDS, pH 7.4) at room temperature. Plates were incubated at -80°C for 30 min and allowed to thaw at room temperature. Protein concentration in each well was measured by a BCA assay according to the manufacturer's instructions (Thermo). OCR and ECAR values were normalised on total μg of proteins in each well.

2.8.1 Assessment of activity of individual respiratory complexes

Activity of individual respiratory complexes was assessed by following a modified version of the method proposed by Salabei and colleagues (Salabei et al. 2014). Cells were seeded in XFe24 Cell Culture microplate as mentioned above. On the day of experiment each well was washed twice with 500 μL of mannitol and sucrose (MAS) buffer (70 mM sucrose, 220 mM mannitol, 10 mM KH_2PO_4, 5 mM MgCl2, 2 mM HEPES, 1 mM EGTA, 4 mg/mL fatty acid-free bovine serum albumin, pH 7.2), replaced with 675 μL of MAS buffer with added 20 μg/mL digitonin (Sigma-Aldrich, cat. no. D141) and plate was immediately inserted into the Seahorse XF-24 analyser. Activity of complex I and II was assayed on the same plate by adding in port A-D 5 mM glutamate and 2.5 mM malate (port A), 1 μM rotenone (port B), 10 mM succinate (port C) and 1 μM antimicyn A (port D). Activity of complex III was assayed by addition via port A-B of 500 μM duroquinol (port A) and 1 μM Antimycin A (port B). Activity of complex IV was assessed by adding in port A-B 500 μM tetramethyl-p-phenylenediamine (TMPD) and 2 mM ascorbate (port A) and 20 mM sodium azide (port B). All drug solutions were prepared in MAS buffer. Two or three measurement cycles of 2-min mix, 2-min wait, and 3-min measure were carried out at basal condition and after each injection. Protein concentrations in each well were determined as detailed above. OCR measurements were normalised on total μg of proteins in each well.

2.8.2 Estimation of intracellular ATP turnover

Estimation of ATP production and consumption from oxidative phosphorylation and glycolysis was obtained as described by Mookerjee et al (Mookerjee et al. 2017). Briefly, $4*10^4$ cells were seeded in XFe24 Cell Culture microplate in 100 μL normal DMEM. The next day cells were washed twice with, and medium was replaced by, 675 μL Krebs-Ringer phosphate HEPES (KRPH) medium (2 mM HEPES, 136 mM NaCl, 2 mM NaH_2PO_4, 3.7 mM KCl, 1 mM $MgCl_2$, 1.5 mM $CaCl_2$, 0.1% (w/v) fatty-acid-free bovine serum albumin, pH 7.4 at 37°C) and incubated for 30 minutes at 37°C with atmospheric CO_2. OCR and ECAR were assayed in a Seahorse XF-24 extracellular flux analyser by the addition via ports AD of 10 mM glucose (port A), 1 μM oligomycin (port B), 1 μM carbonyl cyanide-p-trifluoromethoxyphenylhydrazone (FCCP, port C), 1 μM rotenone and 1 μM antimycin A (port D). To assess ATP consumption by cytoskeleton dynamics injections were: (A) 10 mM glucose, (B) 1 μM nocodazole (Sigma-Aldrich cat. no. M1404), (C) 1 μM oligomycin and (D) 1 μM rotenone and 1 μM antimycin A. Two or three measurement cycles of 1-min mix, 1-min wait, and 3-min measure were carried out at basal condition and after each injection. At the end of the experiment, protein concentration was quantified as described above. Calculations of J_{ATP} were performed as described in (Mookerjee et al. 2017).

2.9 Western blotting

For analysis of protein expression proteins were extracted in RIPA buffer (see above) at room temperature. 20-50 μg of protein was heated at 70°C for 10 min in the presence of sample buffer 1Œ (Bolt loading buffer 1Œ (Life Technologies cat.

no. B0007) supplemented with 4% β-mercaptoethanol (Sigma-Aldrich cat. no. M6250)). Samples were then loaded onto Bolt gel 412% Bis-Tris (Invitrogen cat. no. NW04122BOX) and run using MES 1Œ buffer (Life Technologies cat. no. B0002) at 200 V constant for 30-40 min. Dry transfer of the gels was carried out using IBLOT2 system (Life Technologies). Membranes were then incubated in blocking buffer (5% milk in TBS 1Œ + 0.01% Tween 20) for 30 minutes at room temperature. Primary antibodies in blocking buffer were incubated overnight at 4°C or 2 hours at room temperature. Secondary antibodies (conjugated with 680 or 800nm fluorophores from Li-Cor) were diluted 1:2000 in blocking buffer and incubated for 1h at room temperature. Images were acquired using a Li-Cor Odyssey CLx system linked with Image Studio 5.2 software (Li-Cor). Primary antibodies were: mouse anti-human GAPDH (Abcam cat. no. ab8245), mouse anti-human Mitochondria OXPHOS cocktail (Origene cat. no. MS601-360), rabbit anti-human LDH (Abcam cat. no. ab47010), rabbit anti-human MDH1 (Abcam cat. no. ab180152), rabbit anti-human Calnexin (Abcam cat. no. ab22595), rabbit anti-NDI-1 (Cambridge Research Biochemicals), mouse anti-human TOMM20 (Abcam cat. no. ab56783).

2.10 Immunoprecipitation assay

For immunoprecipitation assay cells were seeded in 15 cm dishes and allowed to grow until 95% confluent. Cells were then washed twice with PBS on ice, 500 μL of lysis buffer (140 mM NaCl, 5mM EDTA, 1% Triton X-100, 20 mM Tris pH 7.4) was added and cells were scraped and collected. Extracted samples were incubated overnight at -20°C, centrifuged at 16000 $\times$ g for 2 minutes at 4°C and supernatant was collected. For each immunoprecipitation reaction, 35 μg of mouse anti-human GAPDH (Abcam cat. no. ab8245) or mouse anti-human MDH1 (Abcam cat. no. ab76616) were coupled to 1.5 mg Dynabeads M-270 Epoxy beads (Life Technologies, cat. no. 14311D) following manufacturers instructions. Antibody-coupled beads were incubated with 3 mg of protein lysate per condition (total volume 1 mL) on a spinning wheel for 30 minutes at 4°C. After incubation, samples were placed on a magnet rack and beads were washed three times with lysis buffer. Elution was performed by two cycles of beads resuspension in 20 μL of sample buffer 1Œ (see above) followed by incubation at 70°C for 10 minutes. Immunoprecipitation and co-immunoprecipitation were assayed via western blotting.

2.11 Immunofluorescence assay

$2*10^4$ cells were seeded in 8-well μ-Slide chambers (Ibidi Labware cat. no. 80821). The next day cells were washed twice with PBS, fixed with 4% formaldehyde for 10 min at room temperature and washed twice with tris-buffered saline (TBS, 50 mM Tris, 150 mM NaCl, pH 7.6). Cells were then permeabilised with 2% BSA, 0.1% Triton-X-100 in TBST (TBS + 0.1% Tween 20) for 10 min at room temperature, washed three times with TBS and blocked with 1% BSA, 10% goat serum (Abcam) in TBST for 30 min at room temperature. Cells were washed three times with TBS and incubated overnight at 4°C with a solution containing mouse anti-human GAPDH (Abcam cat. no. ab8245) and rabbit anti-human MDH1 (Abcam cat. no. ab180152) at a 1:100 dilution. After incubation with primary antibodies, cells were

washed three times with TBS (5 min each wash) and stained with goat anti-mouse IgG coupled with Alexa Fluor 488 (Thermo-Fisher Scientific cat. no. A11001) and goat anti-rabbit IgG coupled with Alexa Fluor 568 (Thermo-Fisher Scientific cat. no. A11011) for 2 hours at room temperature in the dark. Cells were washed three times with TBS, DNA was stained with a solution of 1 μg/mL of diamidino 2-phenylindole (DAPI) or with a solution of DAPI supplemented with 1 μM Alexa FluorTM Phalloidin 488 (Thermo Fisher cat. no. A12379) for ten minutes at room temperature and cells were washed three times with TBS before image acquisition. Images were acquired on Leica confocal microscope TCS SP5 with 63Œ objective. Each channel was acquired separately to avoid bleed through and laser intensity, magnification, and microscope settings were maintained equal for all conditions. Co-localisation of GAPDH and MDH1 or Actin and MDH1 was quantified by assessing the overlap coefficient between channels with the use of Volocity software v6.3 (PerkinElmer).

2.12 Proteomics

Cells were seeded in 15 cm dishes and allowed to grow until 95% confluent. Cells were then washed twice with PBS on ice and 500 μL of extraction buffer (20 mM HEPES, 8 M urea, protease inhibitors cocktail 1X (Sigma-Aldrich cat. no. P8340) and phosphatase inhibitors cocktail (Sigma-Aldrich cat. no. P2850 and P5726), pH 8) were added. Protein concentration was quantified as described above and 400 μg of proteins were submitted to further processing. Samples from three independent experiments were collected. Protein samples were then processed and analysis via mass spectrometry by the proteomics facility at the Laboratory of Molecular Biology (LMB), Cambridge, UK.

2.13 Quantification of m.8993 heteroplasmy

Heteroplasmy at position m.8993 was measured using a previously described PCR RFLP assay, exploiting the creation of a unique SmaI/XmaI site in the mutated molecule (Gammage, Gaude, et al. 2016). Inclusion of [^{32}P]-dCTP in a final cycle of PCR prevents false detection of wild-type mitochondrial DNA (mtDNA) due to heteroduplex formation. These measurements were performed by Dr Payam Gammage at the University of Cambridge, MRC Mitochondrial Biology Unit, Cambridge, UK.

2.14 Fluorescence associated cell sorting (FACS)

To assess mitochondrial mass 2.5*10^5 cells were seeded in 6-well plates and allowed to reach 90-95% confluency. On the day of experiment cells were incubated with normal DMEM containing 50 nM MitoTracker Green FM (Thermo Fisher Scientific, cat. no. M7514) for 30 minutes. Cells were detached with 0.25% trypsin and washed three times with PBS. Washed cells were then analysed by FACS using a LSRII (BD) flow cytometer by monitoring the fluorescence emission at 530 nm 15 nm upon excitation with a 488 nm laser. FACS data were analysed with FlowJo software (Treestar).

2.15 NADH measurements

To measure whole cell oxidised nicotinamide adenine dinucleotide (NAD^+)/reduced nicotinamide adenine dinucleotide (NADH) I applied an adapted version of the method proposed by Frezza et al (Frezza, Zheng, Tennant, et al. 2011). $6*10^4$ cells were seeded in a 96-well plate the day before experiment and an enzymatic cycling reaction was performed. On the day of experiment cells were washed twice with PBS and 100 μL of EB-DTAB buffer (1% w/v dodecyltrimethylammonium bromide (DTAB), 20 mM sodium bicarbonate, 100 mM sodium carbonate, 10 mM nicotinamide, 0.05% v/v Triton X100, pH 10.3) was added into each well, cell lysis was facilitated by pipetting and 50 μL of lysed cells were transferred into a new empty well. 25 μL of 0.4 N HCl were added to the last well (acid-treated sample) and plate was incubated at 60°C for 15 min. Plate was then equilibrated at room temperature for 10 min and 25 μL of 0.5 M Trizma base were added to the acid-treated wells. 50 μL of HCl/Trizma solution (0.4 N HCl : 0.5 M Trizma base 1:1 v/v) were added to the untreated wells (base-treated samples). 5 μL of each acid-treated and base-treated samples were transferred to a new 96-well plate and 195 μL of cycling solution (CS) were added. CS was composed of 84% v/v of reaction cocktail (120 mM bicine, 3.7% EtOH, 5 mM EDTA, pH 7.8), 3% v/v of 5 mg/mL alcohol dehydrogenase (ADH, Sigma-Aldrich cat. no. A3263) in doubly distilled H_2O (ddH_2O), 8.5% v/v 20 mM Phenazine Thiosulfate (PES, Sigma-Aldrich cat. no. P4544), 4.5% v/v 10 mM 3-[4,5-Dimethylthiazole-2-yl]-2,5-diphenyltetrazolium Bromide (MTT, Sigma-Aldrich cat. no. M2128). Plate was incubated at room temperature for 30 min and MTT absorbance was read at 570 nm with a Tecan 200 Pro microplate reader. Blank samples composed of EB-DTAB buffer only were prepared and subtracted to all other samples. Standard curves with NAD^+ and NADH in the range of 0.05-5 μM were prepared for quantification. To assess mitochondrial NADH the day before experiment $5*10^5$ cells were seeded on a 15 mm coverslip and incubated overnight in standard medium. The next day medium was washed and replaced with 500 μL of phenol red-free DMEM (Sigma-Aldrich cat. no. D5030) supplemented with 25 mM glucose, 1 mM pyruvate, 2 mM glutamax (Thermo Fisher Scientific cat. no. 35050061), 10 mM HEPES, pH 7.4. Each coverslip was then placed in a metal ring and fitted on a heated stage at 37°C. NAD(P)H fluorescence intensity time series were performed on an inverted LSM 510 laser scanning confocal microscope (Carl Zeiss) with 351 nm illumination from an argon ion laser (Coherent Enterprise UV). NAD(P)H fluorescence was detected using a 351 nm long-pass dichroic and 460 $\pm$ 25 nm band-pass emission filter with a Œ 40, 1.3 NA quartz oil immersion objective. Images (12-bit 512 Œ 512) were obtained with a pixel dwell time of 1.6 μs. To reduce noise, the image recorded at each time point was an average of two consecutive scans. Time series measurements were obtained by acquiring one image every minute following this pattern: 1) basal conditions (5 minutes); 2) dropwise addition of 100 μL of 6 mM cyanide was added (1 mM final concentration, 4 min); 3) replacement of medium with 800 μL of fresh medium (5 min); 4) dropwise addition of 200 μL of 5 μM FCCP (1 μM final concentration, 4 min). Three coverslips per condition were assayed in each experiment and three independent experiments were carried out. Images were analysed with Image J 1.49. Same value (1280) of thresholding was used to detect objects in each image for each condition, watershed processing was applied and intensity was analysed by detecting

particles larger than 20 pixels.

2.16 Metabolomics analysis

For steady-state metabolomics or metabolite tracing experiments $1.2*10^5$ cells were seeded in 12-well plates. After 24 hours cells were washed twice with PBS and medium was changed with normal DMEM or medium containing metabolite tracers. For glucose tracing experiments 25 mM U-^{13}C-glucose (Cambridge Isotope Laboratories Inc., cat. no. CLM-1396-MPT-PK) or 4-^{2}H-glucose (Cambridge Isotope Laboratories Inc., cat. no. DLM-9294-PK) was added to glucose-free and pyruvate-free DMEM (Life Technology cat. no. 11966-025), together with 10% v/v FBS and 1 mM sodium pyruvate. For glutamine tracing experiments 4 mM U-^{13}C-glutamine (Cambridge Isotope Laboratories Inc., cat. no. CLM-1822-SP-PK) or 1-^{13}C-glutamine (Cambridge Isotope Laboratories Inc., cat. no. CLM-3612-PK) was added to glutamine-free DMEM (Life Technology cat. no. 21969-0.35), together with 10% v/v FBS. For aspartate labelling experiments 4 mM U-^{13}C-aspartate (Cambridge Isotope Laboratories Inc., cat. no. CLM-1801-H) was added to normal DMEM with 10% v/v FBS. After incubation with normal medium or medium containing metabolite tracers, one well from each condition was used to estimate cell number. To extract extracellular metabolites, 50 μL of medium were collected from each well, centrifuged at 10000 $\times$ g for 1 min and metabolites were extracted by adding 750 μL of metabolite extraction buffer (MEB, 50% v/v methanol, 30% v/v acetonitrile, 20% v/v ddH_2O). To extract intracellular metabolites, cell plates were placed on ice, washed twice with ice-cold PBS and 1 mL of MEB / 10^6 cells was added to each well and cells were scraped. One cycle of freeze-thawing at -80°C was performed to further lyse the cells. Both extracellular and intracellular fractions were then incubated in a thermomixer (Eppendorf) at max speed for 15 min at 4°C. Proteins were then pelleted by centrifuging samples at 16000 $\times$ g for 10 minutes at 4°C and supernatants were transferred into glass vials and stored at -80°C until further analysis. Liquid chromatographymass spectrometry (LCMS) analysis was performed by Dr Sofia da Costa on a QExactive Orbitrap mass spectrometer coupled to a Dionex UltiMate 3000 Rapid Separation LC system (Thermo). The LC system was fitted with a SeQuant ZIC-pHILIC (150 mm Œ 2.1 mm, 5 μm) with the corresponding guard column (20 mm Œ 2.1 mm, 5 μm) both from Merck. The mobile phase was composed of 20 mM ammonium carbonate and 0.1% ammonium hydroxide in water (solvent A), and acetonitrile (solvent B). The flow rate was set at 200 μL/min with a previously described gradient (Mackay et al. 2015). The mass spectrometer was operated in full MS and polarity switching mode scanning a range of 50-750 m/z. Samples were randomised, in order to avoid machine drift, and were blinded to the operator. The acquired spectra were analysed using XCalibur Qual Browser and XCalibur Quan Browser software (Thermo Scientific) by referencing to an internal library of compounds. Calibration curves were generated using synthetic standards of the indicated metabolites.

2.17 Metabolic modelling

Modelling of metabolic rewiring following mitochondrial dysfunction was performed with flux balance analysis (FBA) (Orth et al. 2010), under the assumption of mass conservation. To investigate metabolic rewiring, I constrained a recently published metabolic reconstruction of central carbon metabolism (Zieliski et al. 2016) with experimental data obtained from consumption and release (CORE) of extracellular metabolites and oxygen consumption driven by individual complexes. CORE data were obtained by seeding cells in two 12-well plates (total 6 wells per cell line), as described above, and allowing cells to attach until next day. Once cells attached, medium was changed to normal DMEM (see above) and one well was used for quantification of protein abundance (time point 0). Cells were allowed to grow for 24 hours, after which extracellular medium was harvested and submitted to LC-MS metabolomic analysis (see above). One well was used for quantification of protein abundance (time point 1). Change in protein abundance from time point 0 to time point 1 was used as a predictor of biomass generation during the experiment. Levels of extracellular metabolites were quantified via LC-MS by comparing with external standards that were run in parallel, together with media samples. Consumption and release of metabolites were obtained by subtracting the quantified metabolite levels of reference media samples (DMEM medium incubated for 24 hours without cells) from media samples of each cell line. Finally, CORE data were obtained by calculating the ratio between total moles of metabolite produced or consumed from the extracellular medium and the biomass generated during the 24 hours of experiment (moles/min/μg protein).

I maximised adenosine triphosphate (ATP) yield as objective function and calculated the flux difference between N7 and N80 models by subtracting the predicted flux of each reaction for N7 from N80 model. Top 10% altered reactions were considered. To assess contribution of each reaction to ATP production, I individually blocked (upper bound = 0, lower bound = 0) each reaction in N80 and N7 models and calculated the difference in ATP yield against the complete model. Contribution of reductive carboxylation to metabolic rewiring was predicted by blocking isocitrate dehydrogenase 1 (IDH1) reaction in N80 model and calculating the flux difference of each reaction against the complete N80 model. Top 10% altered reactions were considered. Simulations were performed with Matlab R2016A (Mathworks) with the COBRA toolbox 2.0 and by using GLPK 4.48 as solver.

2.18 Lentiviral vectors generation and transduction

The viral supernatant for cell transduction was obtained from the filtered growth media of the packaging cells HEK293T transfected with with 3 μg psPAX, 1 μg pVSVG, 4 μg of shRNA constructs and 24 μl Lipofectamine 2000 (Life Technology). 1×10^6 cells were then plated on a 6 cm dish and infected with the viral supernatant in the presence of 4 μg/ml polybrene. After 2 days, the medium was replaced with selection medium containing 2 μg/ml puromycin. The expression of the shRNA constructs was induced by incubating cells with 2 μg/ml doxycycline. The shRNA sequence were purchased from Thermo Scientific and are as follows: shNTC #RHS4743; shIDH1 #1: TTTCGTATGGTGCCATTTG; shIDH1 #2: TTGACGCCAACATTATGCT; shIDH2 #1: TCTTGGTGCTCATGTACAG;

shIDH2 #2: TTCTTGTCGAAGTCGGTCT; shMDH1 #1: CAATTTGAGCTTTAGCTCG; shMDH1 #2: TATTCTTGATTACAACAGG. For NDI-1 expression, $3*10^6$ HEK293T cells were plated in 10 cm dishes, allowed to attach overnight, and transfected with 5 μg psPAX, 5 μg pMD2G and 2 μg of pWPI control or NDI-1 plasmids (Cannino et al. 2012). Viral supernatant was used as described above for infecting N80 cells.

2.19 Cell migration

$6*10^6$ cells were seeded in a 96-well plate and cultured overnight in standard conditions. A 700-800 μm wound was obtained in each well with a 96 pins IncuCyteő WoundMaker (Essen Bioscience). After applying the wound, cells were washed with PBS twice and medium was replaced with 100 μL DMEM. Images were acquired with an IncuCyte FLR (Essen Bioscience) every 2 hours for at least 10 consecutive hours. Wound widths at time point 0 hours and 6 hours were extracted and used to calculate migration speed. 8-16 wells per condition were used as technical replicates in each experiment, and at least 4 independent experiments were acquired.

2.20 qPCR

mRNA was extracted using RNeasy Kit (Qiagen) following manufacturers instructions. 1 μg of mRNA was retrotranscribed into cDNA using High Capacity RNA-to-cDNA Kit (Applied Biosystems, Life Technologies, Paisley, UK). For the qPCR reactions 0.5 μM primers were used. 1 μl of Fast Sybr green gene expression master mix; 1 μl of each primers and 4 μl of 1:10 dilution of cDNA in a final volume of 20 μl were used. Real-time PCR was performed in the Step One Real-Time PCR System (Life Technologies Corporation Carlsbad, California) using the fast Sybr green program and expression levels of the indicated genes were calculated using the $\Delta\Delta^{Ct}$ method by the appropriate function of the software using actin as calibrator. Primer sequences are as follows: IDH1: Fwd: GTGTGCAAAATCTTCAATTGACTT; RV: GGTGACATACCTGGTACATAACTTTG; IDH2: Fwd: GGAGCCCGAGGTCAAAATAC; RV: TGGCAGTTCATCAAGGAGAA; Actin: QuantiTect primer QT00095431 (Qiagen), sequence not disclosed.

2.21 Statistical analysis

Statistical analysis was performed with Graphpad Prism 5.0a. At least 3 independent experiments were used for each test. Statistical analysis of metabolomics data was performed with the R package muma v1.4 (Gaude, Chignola, et al. 2013) on R software 3.3.2.

CHAPTER 3

Results.
The metabolic landscape of cancer transformation and progression

CANCER has been defined as a genetic disease whereby the evolution from benign to malignant lesions occurs via a series of mutations over time (Vogelstein, Papadopoulos, et al. 2013). The process of transformation is accompanied by profound alterations of cellular metabolism that fulfill the energy requirements of cancer cell growth and proliferation (Hanahan and Weinberg 2011). A recent systematic analysis of expression of metabolic genes across several cancer types showed that, together with increased glycolysis, other metabolic pathways, including nucleotides and protein synthesis, are activated in cancer (Hu, Locasale, et al. 2013). Although these metabolic features of cancer are now exploited for diagnostic and therapeutic purposes, their broader clinical implications are still under intense investigation. In this chapter I will investigate the landscape of metabolic alterations experienced by different cancer types. I will focus on both metabolic alterations peculiar of each cancer type (tissue-specific) and alterations that are commonly undertaken by different cancer types (convergent). Finally, in order to assess the clinical implications of altered metabolism in cancer, I will assess the link between metabolic alterations and survival of cancer patients. This analysis led me to the discovery of novel and clinically relevant aspects of the metabolic transformation of cancer, with important implications for patient stratification, prognosis, and therapy. Complete datasets and raw results of this chapter can be found in Gaude and Frezza 2016.

3.1 The metabolic landscape of cancer

3.1.1 Data set and analysis pipeline

In order to investigate the metabolic landscape of cancer, I analysed the expression of metabolic genes across 20 different types of solid cancers from the cancer genome atlas (TCGA), encompassing a total of 8161 cancer and normal samples **(Table 3.1)**.

Table 3.1: List of tumour and normal samples that underwent bioinformatic analysis. Abbreviations and group sizes are shown.

Cancer type	Abbreviation	Tumour samples (n)	Normal tissues (n)
Bladder Urothelial Carcinoma	BLCA	408	19
Breast Invasive Carcinoma	BRCA	1093	112
Cervical Squamous Cell Carcinoma and Endocervical Adenocarcinoma	CESC	304	3
Cholangiocarcinoma	CHOL	36	9
Colon Adenocarcinoma	COAD	285	41
Esophageal Carcinoma	ESCA	184	13
Glioblastoma Multiforme	GBM	186	5
Head and Neck Squamous Cell Carcinoma	HNSC	519	43
Kidney Renal Clear Cell Carcinoma	KIRC	533	72
Kidney Renal Papillary Cell Carcinoma	KIRP	290	32
Liver Hepatocellular Carcinoma	LIHC	371	50
Lung Adenocarcinoma	LUAD	511	58
Lung Squamous Cell Carcinoma	LUSC	502	51
Pancreatic Adenocarcinoma	PAAD	178	5
Pheochromocytoma and Paraganglioma	PCPG	179	3
Prostate Adenocarcinoma	PRAD	497	52
Rectum Adenocarcinoma	READ	94	10
Stomach Adenocarcinoma	STAD	611	70
Thyroid Carcinoma	THCA	505	59
Uterine Corpus Endometrial Carcinoma	UCEC	174	24
Subtotal		7430	731
Total			8161

Figure 3.1: Proportion of promiscuous genes among metabolic pathways. Genes belonging to each metabolic pathway have been divided based on their promiscuity, i.e. the number of pathways they are associated with. Pathways that are mainly composed of specific genes display few dots, while pathways composed of mainly promiscuous genes are divided into several dots. Blue shading indicates the proportion of specific and promiscuous genes in each pathway.

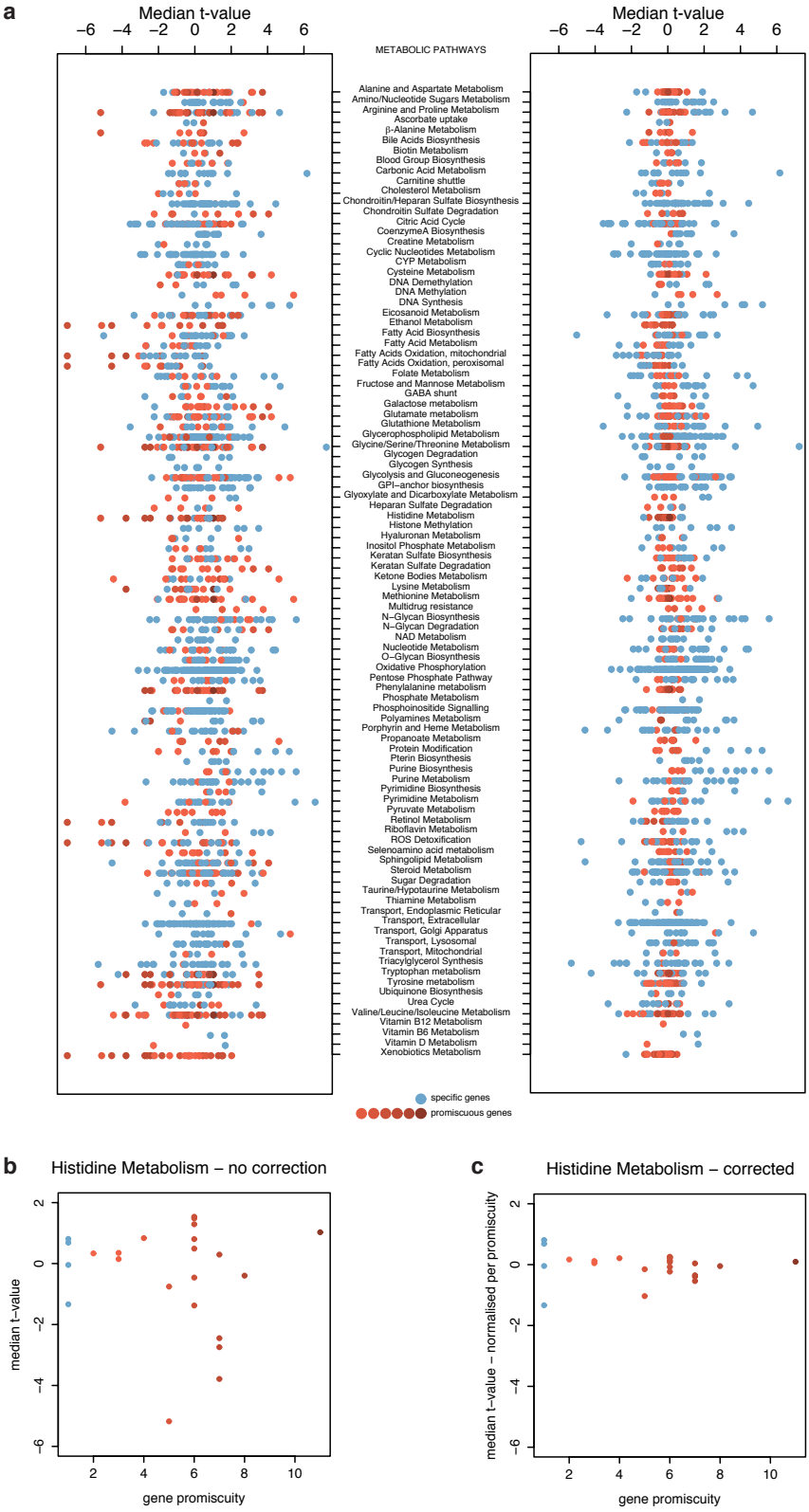

Figure 3.2: Effect of promiscuity correction on gene significance. a) Non corrected (left) and promiscuity-corrected (right) median t-values of cancer vs normal for metabolic genes across all cancer types. **(b-c)** Median t-value of cancer vs normal for Histidine Metabolism before **(b)** and after **(c)** promiscuity correction. Specific genes (blue dots) and promiscuous genes (red shading) are highlighted in order to compare the effect of promiscuity correction on differential gene expression.

mRNA sequencing (RNAseq) data from each cancer data set were analysed using a negative binomial generalized linear model (Love et al. 2014), comparing the expression of metabolic genes in cancer tissues against tissues of origin. I then applied gene set enrichment analysis (GSEA)(Subramanian et al. 2005) against a manually-curated metabolic gene signature. To identify metabolic alterations common to different cancers, I selected metabolic pathways that were enriched (up- or down-regulated) in 5/20 (25%) cancers, compared to normal tissues. The threshold of 25% of cancers was based on a conservative variation of the 20/20 method proposed by Vogelstein (Vogelstein, Papadopoulos, et al. 2013).

3.1.2 Promiscuity of the metabolic network

While composing metabolic gene signatures I noticed that several genes (∼20%) were associated with multiple metabolic pathways (**Figure 3.1**), in line with an interconnected topography of the metabolic network. The association of a gene across multiple metabolic pathways, or *promiscuity*, could be a confounding factor when linking the differential expression of a gene to a specific function. Of note, distribution of genes across gene signatures has been recently reported to be an accountable factor in gene set enrichment analyses and correction for overlapping genes could improve the performance of GSEA (Tarca et al. 2012). I observed that, in some cases, enrichment of metabolic pathways was driven by promiscuous genes only, even without significant contribution from pathway-specific genes. For instance, the pathway *Histidine Metabolism* was significantly enriched in several cancers, but such enrichment was driven entirely by promiscuous, rather than specific, genes (**Figure 3.2b**). To account for this factor, I applied an *ad hoc* correction for gene promiscuity in metabolic pathways by penalising the score of genes proportionally to their promiscuity across the metabolic network (see Materials and Methods for a full explanation). Briefly, for each gene, t-values obtained from differential gene expression analysis were divided by the number of pathways that gene is associated with. This correction successfully decreased the significance of promiscuous genes, while having no effect on specific genes (**Figure 3.2a**). Accordingly, Histidine Metabolism pathway, as well as other pathways whose enrichment was predominantly driven by promiscuous genes, did not score an enrichment upon application of the correction (**Figure 3.2c**).

3.1.3 Nucleotide synthesis and mitochondrial metabolism are convergent features of cancer transformation

Differential gene expression between cancer and normal tissues, after correction for promiscuity, was subjected to GSEA and significantly enriched metabolic pathways for each cancer type were obtained (**Figure 3.3**).

Besides glycolysis, a well-established metabolic feature of cancer (Pavlova and Thompson 2016), purine biosynthesis and DNA synthesis were the most frequently up-regulated pathways across different cancers (14/20, 70% and 10/20, 50%, respectively). Phosphoribosylaminoimidazole carboxylase phosphoribosylaminoimidazole succinocarboxamide synthetase (*PAICS*) was the most frequently up-regulated gene (71%) within the purine biosynthesis pathway (**Figure 3.4**).

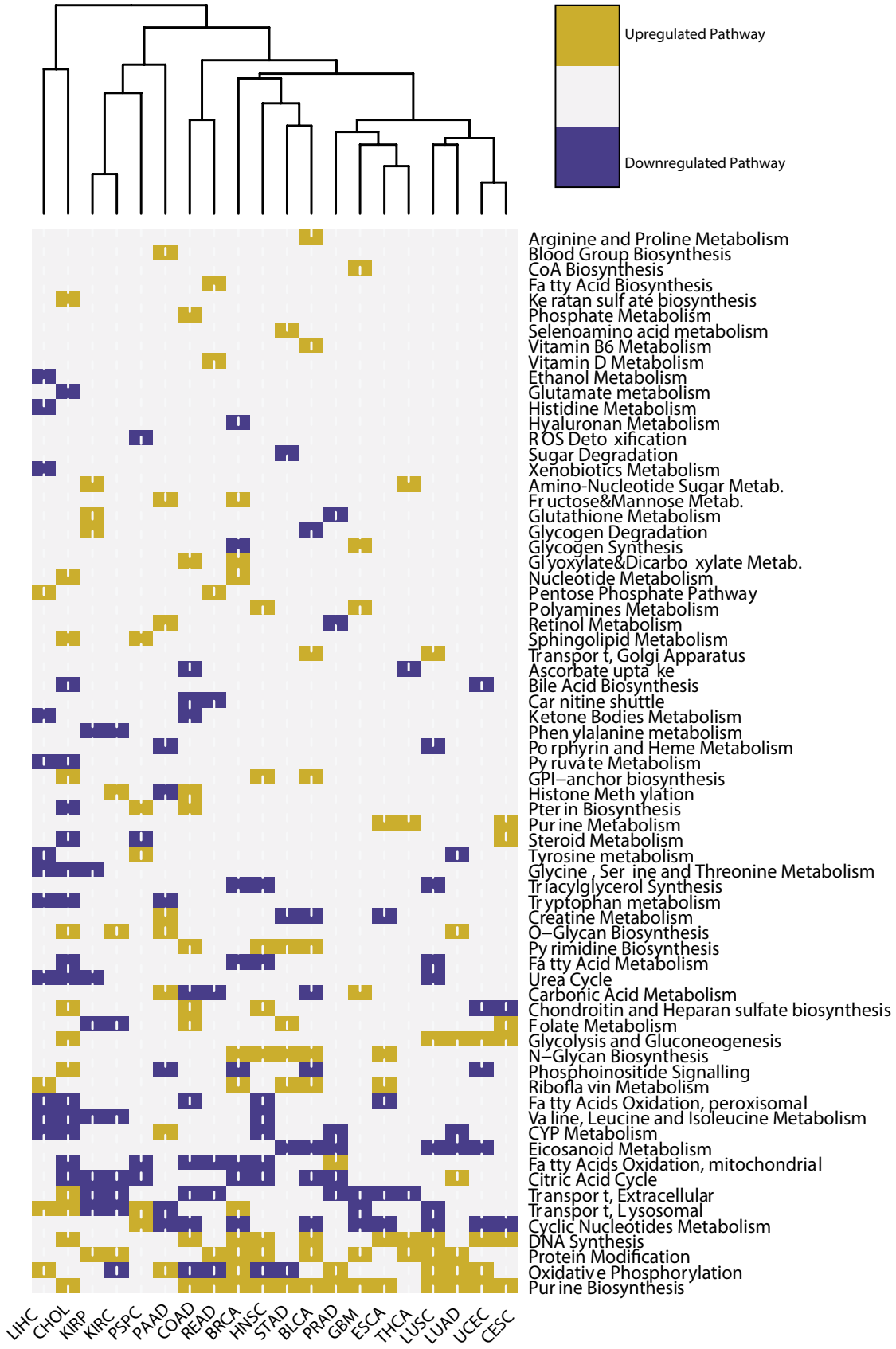

Figure 3.3: Altered metabolic pathways in cancers compared to normal tissues. Heatmap representation and hierarchical clustering of enriched up-regulated (gold) and enriched down-regulated (blue) metabolic pathways in cancers compared to normal tissues. For abbreviations of cancers and normal tissues see Table 3.1.

To validate the relevance of these pathways for proliferation of cancer cells, I assessed the correlation of purine biosynthesis pathway and *PAICS* expression with the growth rate of the NCI-60 panel of cancer cell lines (**Figure 3.5a-b**). Both purine biosynthesis and *PAICS* expression showed significant positive correlation with proliferation rate of cancer cell lines, confirming the relevance of this pathway in an independent dataset.

Another shared metabolic feature of cancers that emerged from this analysis is the dysregulation of genes encoding for mitochondrial metabolism (**Figure 3.4**). Overall, 65% of cancers exhibited down-regulation of at least one mitochondrial pathway, while the remaining 35% showed its over-expression. In particular, down-regulation of citric acid cycle (CAC) and mitochondrial fatty acids oxidation (mFAO) genes was observed in 40% and 30% of cancer types, respectively. oxidative phosphorylation (OXPHOS) was found up-regulated in 35% and down-regulated in 25% of cancers (**Figure 3.4**). Of note, this result is in accordance with recent evidence showing heterogenous regulation of OXPHOS across different cancer types (Hu, Locasale, et al. 2013).

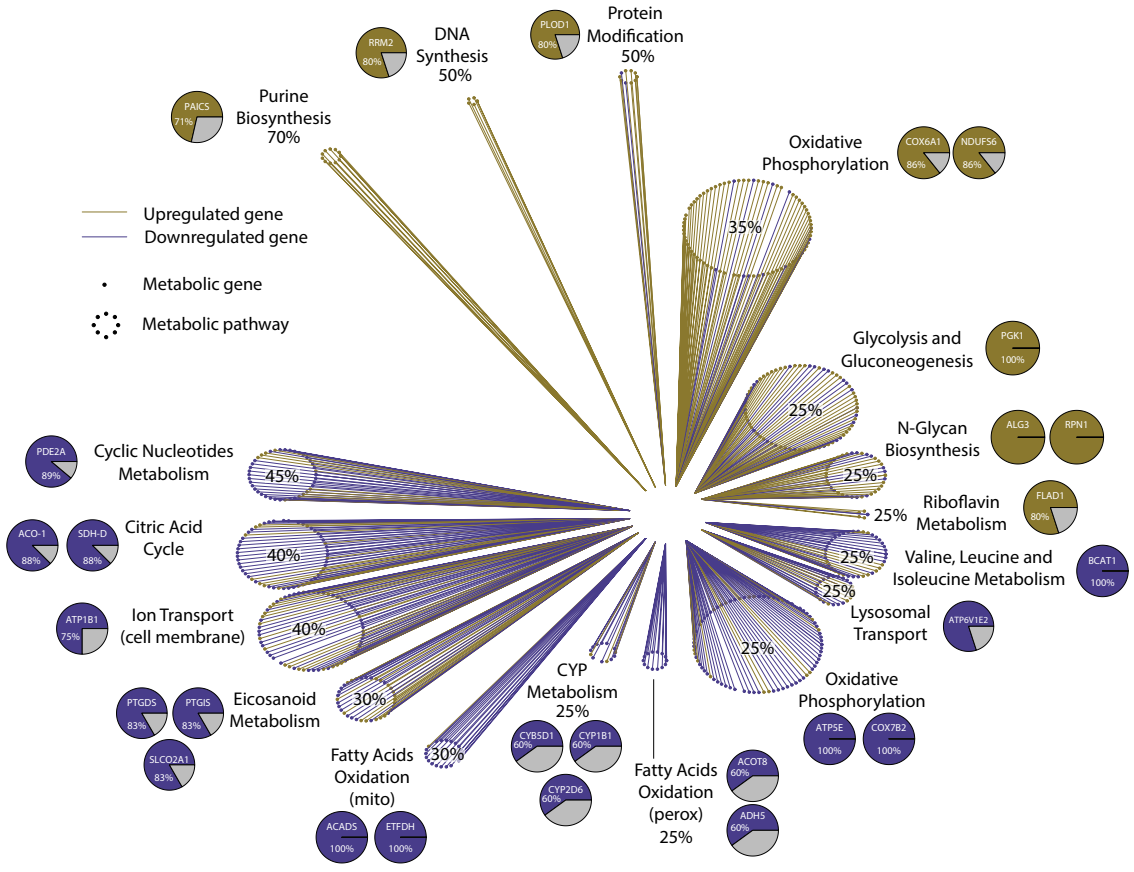

Figure 3.4: Convergent metabolic alterations in cancer tissues compared to normal. Gene expression effect plot of metabolic pathways enriched in more than 25% of cancers. Circles indicate metabolic pathways and dots in each circle represent individual metabolic genes. Gold and blue lines indicate up-regulated and down-regulated genes in cancers compared to normal tissues, respectively. Pie charts represent the most frequently up- or down-regulated genes in the corresponding pathway; percentage values indicate frequency of up- or down-regulation.

To validate these findings I took advantage of a recently published study where gene expression and metabolite abundance were measured in a cohort of breast cancer patients (Terunuma et al. 2014). First, I wanted to assess whether expression of metabolic genes correlated to expected changes in metabolite concentration. Expression levels of glycolytic genes positively correlated with accumulation of lactate, and expression of Purine biosynthesis and DNA synthesis correlated with abundance of nucleotides (**Figure 3.5c-e**). Moreover, gene expression of mFAO negatively correlated with palmitate levels (**Figure 3.5f**). I then applied metabolic GSEA on these cancer samples. Among metabolic pathways enriched between breast cancer and normal samples, purine biosynthesis and DNA synthesis were up-regulated, whilst CAC, mFAO and cyclic nucleotides metabolism were down-regulated (**Figure 3.5g**), thus confirming my findings with an independent and cross-platform data set.

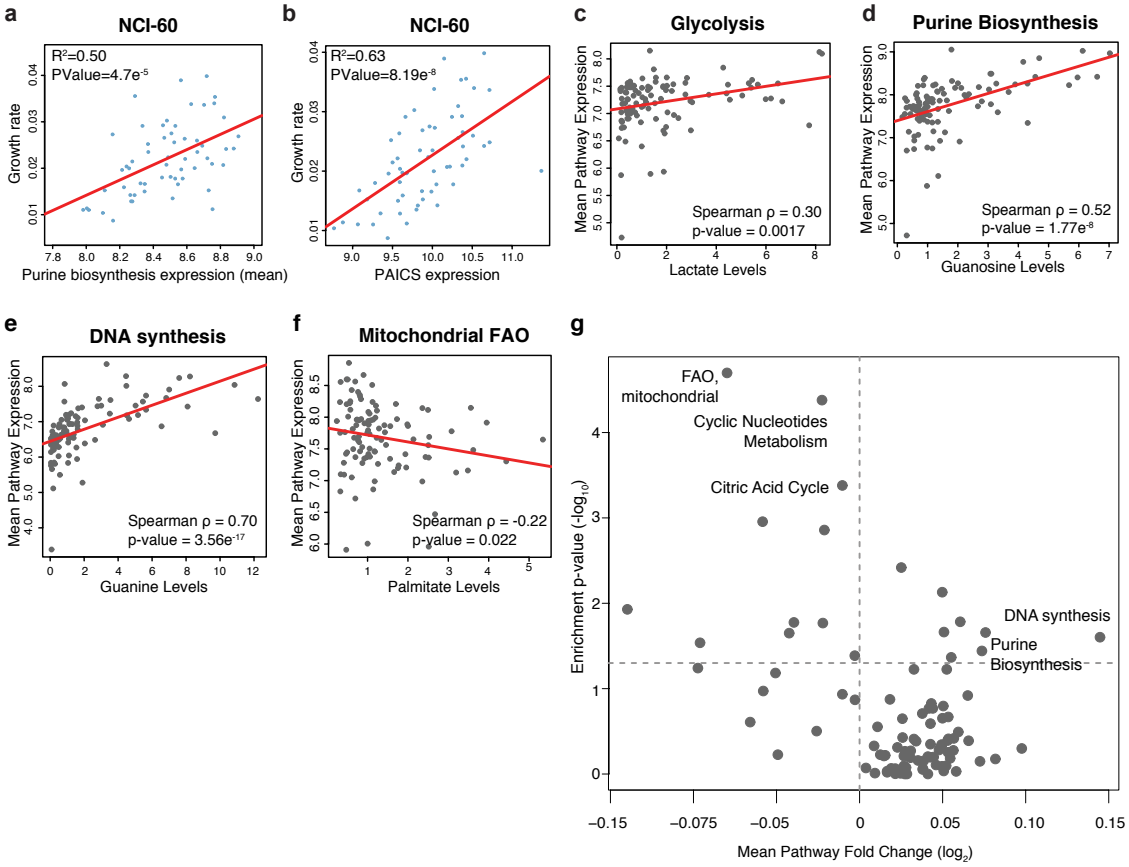

Figure 3.5: Validation of convergent metabolic landscape of cancer with an independent data set. **a)** Scatter plot representation of Purine Biosynthesis genes (x axis) and growth rate of the NCI-60 panel of cancer cell lines (y axis). **b)** Scatter plot representation of expression of *PAICS* (x axis) and growth rate of the NCI-60 panel of cancer cell lines (y axis). **c-f)** Scatter plot indicating correlation between mean expression of indicated metabolic pathways and levels of **(c)** Lactate, **(d)** Guanosine, **(e)** Guanine, **(f)** Palmitate. Red lines indicate the linear trend between variables. Correlation coefficient and p-values are indicated. **g)** Volcano plot representation of mean fold change expression of genes in each pathway (x axis) vs enrichment p-values (y axis) in breast cancer vs normal samples.

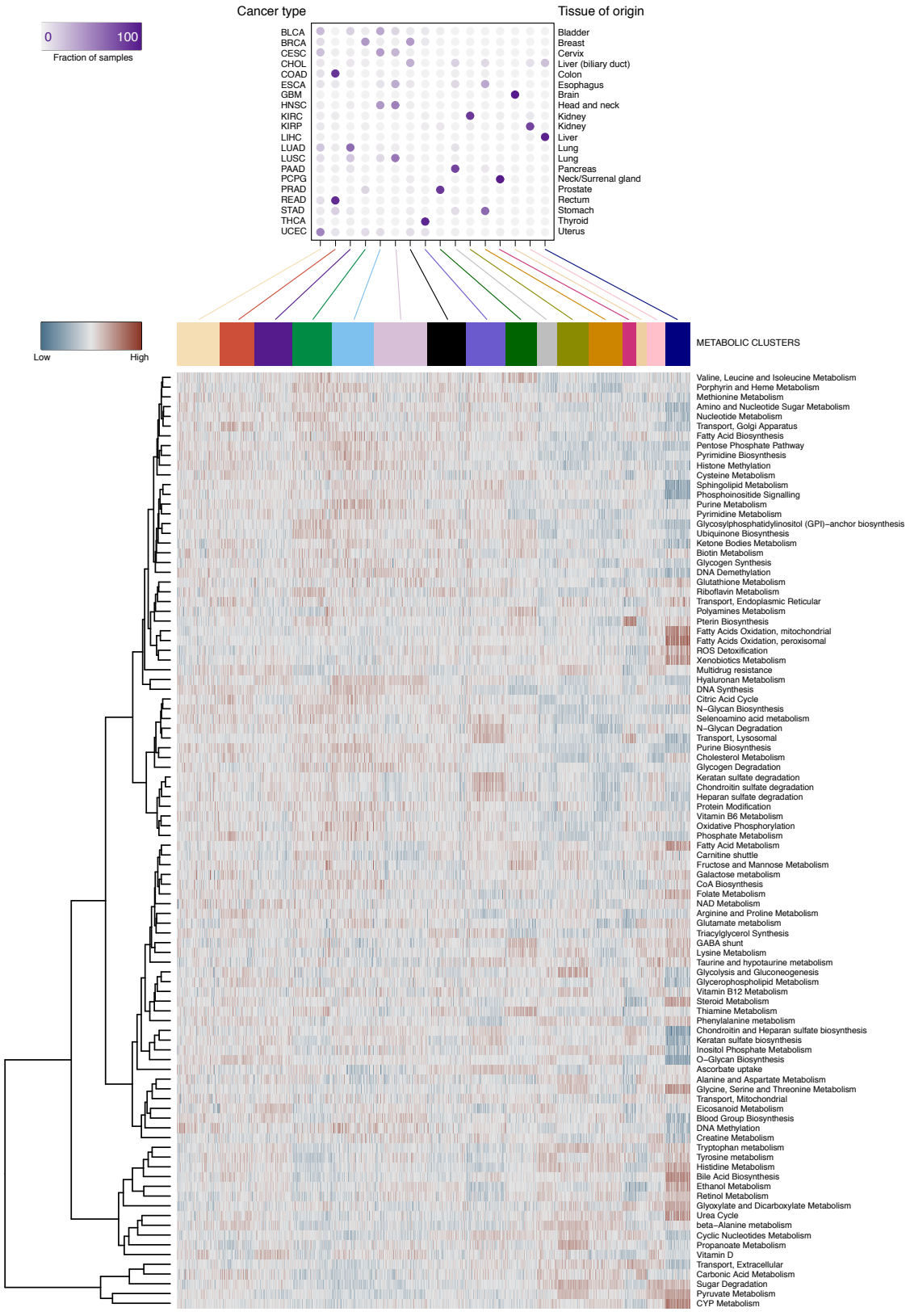

Figure 3.6: Unsupervised clustering of cancer samples based on expression of metabolic pathways. Heatmap representation of metabolic pathways in cancer samples only, divided into 16 clusters (top colored banner). Samples from each cancer type were overlapped on the 16 metabolic clusters and proportion of samples found in each cluster is reported in the top dot plot (purple shading indicates proportion of samples).

3.1.4 Metabolic traits reminiscent of tissue of origin

Hierarchical clustering of enriched metabolic pathways (**Figure 3.3**) indicates that cancers arising from the same tissue might exhibit similar metabolic features. This observation suggested that cancer cells retain metabolic features of their tissues of origin. To further investigate the extent of such metabolic "imprinting", I applied unsupervised hierarchical clustering to all cancer samples. Optimal number of clusters was obtained via bootstrapping (see Methods). Interestingly, I observed a high degree of overlap between the obtained clusters and tissues of origin of each cancer (**Figure 3.6**), thus indicating that tissue-specific metabolic features are intrinsically maintained in cancer cells.

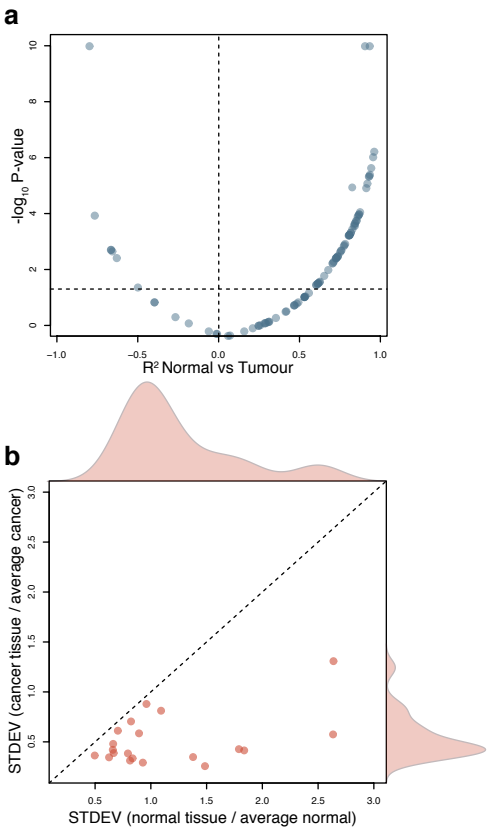

Figure 3.7: Association between tissue of origin and metabolic transformation of cancer. a) Scatter plot representation of correlation coefficient (Spearman, x axis) and correlation p-value (-$\log_{10}$, y axis) of metabolic pathways in normal tissue compared to cancer. Horizontal dashed line indicates FDR of 5% (-$\log_{10}$). **b)** Scatter plot representation of the variance of metabolic pathways among normal (x-axis) and cancer (y-axis) tissues.

To corroborate this observation, I performed correlation analysis between the metabolic signatures of distinct cancers and corresponding normal tissue (**Figure 3.7a**). Most correlations were positive and significant (57/96, Spearman ρ, Benjamini-Hochberg adjusted p-value ≤ 0.05), confirming that the metabolic landscape of cancer is reminiscent of its tissue of origin. Interestingly, I also observed few significant negative correlations (4/96), including highly expressed pathways in normal tissues that were down-regulated in cancer. Moreover, the overall loss of tissue-specific metabolic functions and the convergence to a common metabolic landscape across cancers was confirmed by the finding that the variance of metabolic pathways among cancers was lower than the variance among normal tissues (**Figure 3.7b**).

To further investigate tissue-specific metabolic rewiring of cancer I first identified metabolic pathways that are enriched in each normal tissue, compared to average, thus obtaining normal tissue-specific metabolic features (see Materials and Methods for more detail). To determine the extent of tissue-specific metabolic rewiring in cancers I assessed whether metabolic pathways that characterise a normal tissue are altered in the corresponding cancer tissue. Whilst most tissue-specific metabolic functions were not altered in cancer (**Figure 3.8**), 38% of the metabolic pathways that were highly expressed in normal tissue were down-regulated in cancer. Also, 22% of pathways that were down-regulated in normal tissues were up-regulated in cancer (**Figure 3.8**). For instance, while normal breast tissue has

a low expression of *Fructose and Mannose metabolism*, breast cancer samples show an up-regulation of this pathway. Viceversa, *Glycogen synthesis* is up-regulated in normal breast, while it is down-regulated in breast cancer (**Figure 3.8**).

Finally, I wanted to investigate whether the observed metabolic rewiring of cancer generates tissue-specific metabolic liabilities, i.e. whether cancer cells arising from the same tissue are dependent on similar metabolic pathways for their growth or survival. To this aim I took advantage of a recently published RNA interference screening (Achilles 2.4) of a large panel of genomically characterised cancer cell

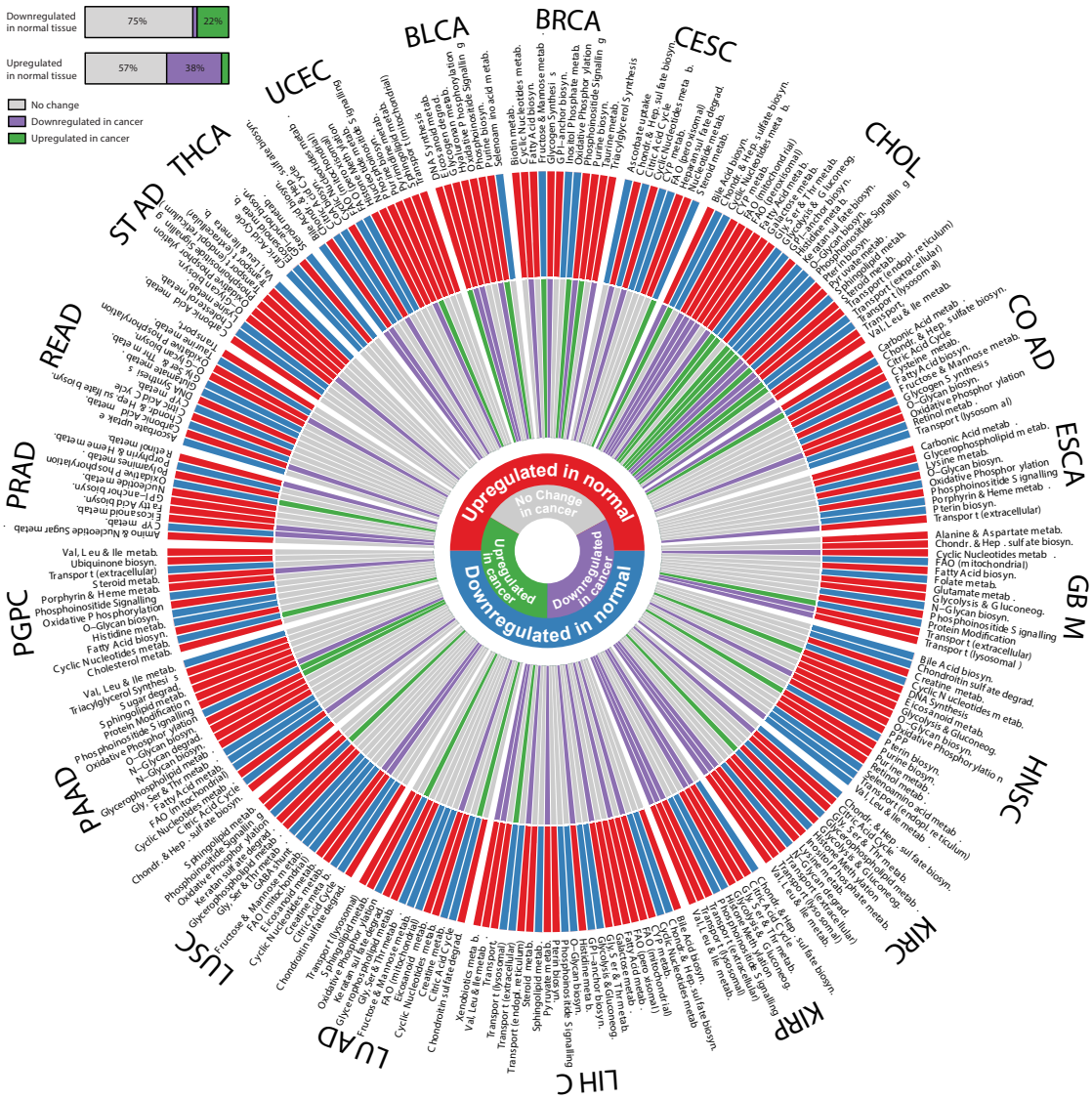

Figure 3.8: Tissue-specific metabolic traits in all cancer types. Tissue-specific metabolic signatures in normal and cancer tissues are represented in a *polar histogram*. The external circle displays metabolic pathways found enriched up-regulated (red) or down-regulated (blue) in normal tissues, compared to average. The internal circle shows the enrichment of individual metabolic pathways in cancer compared to normal. Grey bars indicate no change in cancer compared to normal. The horizontal histogram indicates the proportion of metabolic pathways altered in cancer compared to pathways down-regulated or up-regulated in normal tissues.

lines (Cowley et al. 2014). In line with a tissue-specific metabolic reprogramming of cancer, tissue of origin predicted gene essentiality of 59% of metabolic genes (349/595, ANOVA adjusted p-value ≤ 0.05), suggesting that proliferation of cancer cells is dependent on tissue-defined metabolic determinants.

3.2 OXPHOS is linked to patient survival and metastasis

3.2.1 Classification of cancer patients based on overall survival

I then wanted to investigate whether the observed metabolic alterations correlated with the clinical outcome of cancer patients. To this aim, I took advantage of survival data collected by TCGA. In order to investigate metabolic alterations linked to patient survival, patients from each cancer type were divided into a High Survival and Low Survival group. For each cancer type, I included in the High Survival group patients that have been censored alive for longer than the 75th percentile of the total duration of the follow-up study. On the other hand, the Low Survival group included patients that have died within the 75th percentile of the total follow-up study duration (**Figure 2.2**). This method of classification avoids overlap between High and Low survival groups and potential biases that could arise from short follow-up recordings and drop-outs. Of note, this conservative classification affected group size of High and Low survival patients for each cancer type, resulting in some groups being poorly represented. Therefore, I excluded from gene expression analysis those cancer types where the High or Low survival group were smaller than 5 patients. Cancer types excluded were CHOL, PCPG, PRAD, READ, THCA.

3.2.2 OXPHOS is down-regulated in cancer patients with poor survival

Then, I performed differential gene expression analysis in Low and High survival patients and applied promiscuity-corrected metabolic GSEA. I found that several metabolic pathways were significantly altered in the Low Survival compared to the High Survival group (**Figure 3.9a**). Overall, poor survival was associated with inhibition of at least one mitochondrial pathway in 10/15 cancers (67%). OXPHOS was the most affected pathway in Low vs High survival patients and was found down-regulated in the low survival group of 9 out of 15 (60%) cancer types (**Figure 3.9b**). Of note, the most frequently down-regulated genes in this group were subunits of Complex I and IV of the respiratory chain.

To investigate the possible relation between mitochondrial metabolism and poor clinical outcome, I performed GSEA on Low and High Survival patients, taking advantage of a large collection of cancer-associated gene signatures from the Broad Institute. Among cancers that exhibited down-regulation of OXPHOS, the most up-regulated cellular function was epithelial-to-mesenchymal transition (EMT) (**Figure 3.9c**), a gene signature associated with cancer aggressiveness and poor prognosis (Tsai and Yang 2013). Notably, OXPHOS showed significant (FDR = 0.05) negative correlation with EMT in 19/20 cancer types (**Figure 3.9d**).

3.2.3 OXPHOS is associated with cancer metastasis

Given the role of EMT in cancer metastasis (Tsai and Yang 2013), I hypothesized an association between down-regulation of OXPHOS, induction of EMT, and the

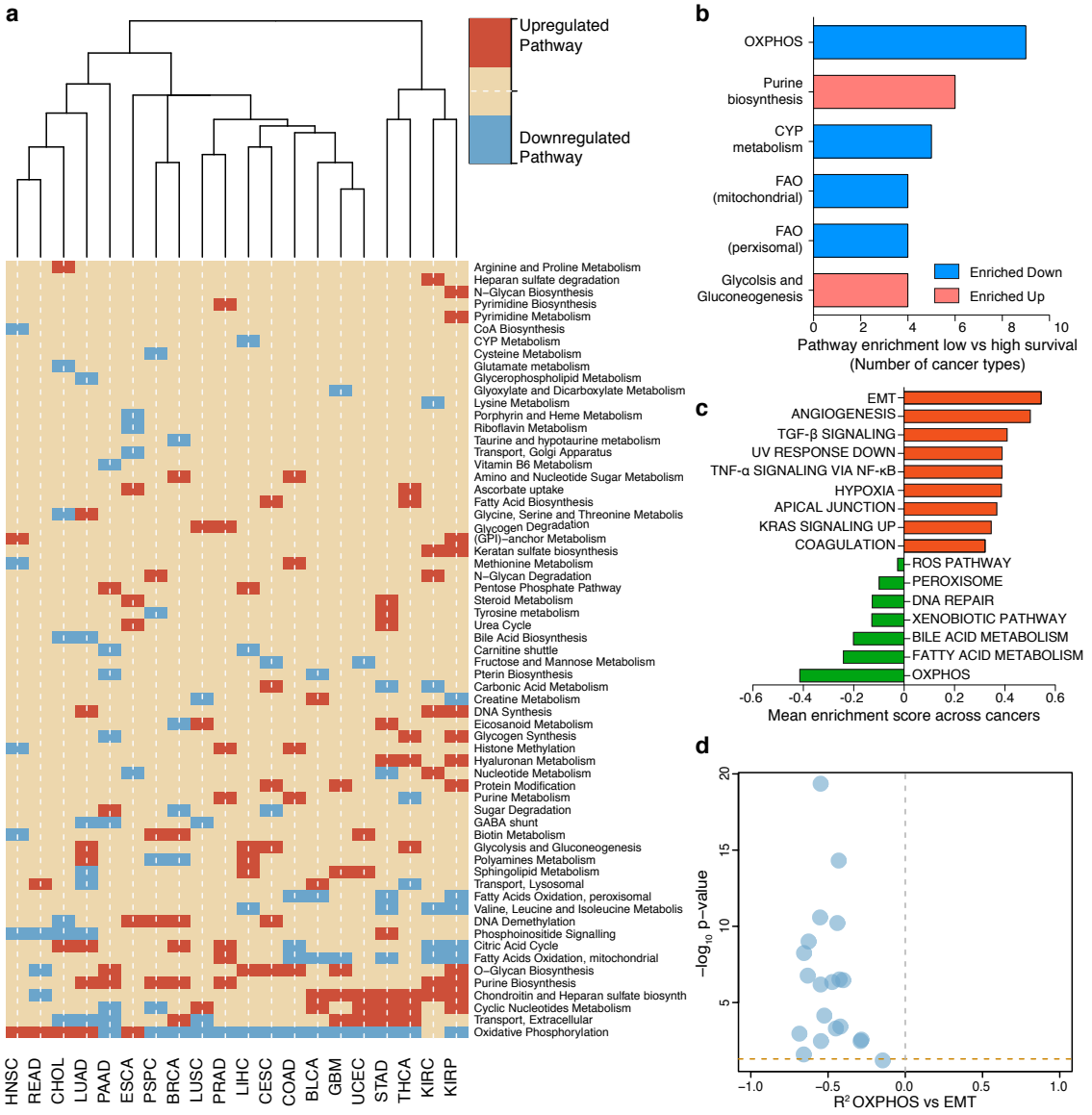

Figure 3.9: Down-regulation of OXPHOS genes is associated with poor clinical outcome and EMT gene signature. **a)** Heatmap representation of enriched up-regulated and down-regulated metabolic pathways in High vs Low survival patients. Metabolic pathways enriched in at least 25% of cancers are highlighted as blue or red square, based on down- or up-regulation, respectively. **b)** Frequency of metabolic pathways found enriched up-regulated (pink) or down-regulated (blue) between Low and High survival patients in at least 25% of cancer types. **c)** Top 10 enriched up-regulated and down-regulated cancer hallmarks between Low and High Survival patients across cancer types that showed OXPHOS down-regulation (9 cancers). Mean enrichment scores of Low vs High Survival patients across the 9 cancer types considered are shown. **d)** Volcano plot showing correlation coefficient (Spearman, x axis) and correlation p-values (Spearman, -$\log_{10}$, y axis) of mean expression of OXPHOS genes compared to mean expression of genes involved in EMT. Horizontal dashed line indicates FDR = 5%.

metastatic potential of cancer, which is directly linked to patient prognosis. To validate this hypothesis, I took advantage of the Skin Cutaneous Melanoma data set provided by TCGA, composed of 367 metastatic and 103 primary cancer samples. I performed differential metabolic gene expression and GSEA on metastatic vs primary cancer samples. Of note, EMT was strongly up-regulated in metastatic vs primary cancer samples (**Figure 3.10a**). Furthermore, OXPHOS was the most significantly down-regulated metabolic pathway in metastatic vs primary cancers (**Figure 3.10b**). In line with the findings on Low vs High survival patients, Cyclic Nucleotides metabolism and Purine biosynthesis were both up-regulated in metastatic vs primary cancers (**Figure 3.10b**).

To further validate the link between reduced expression of mitochondrial genes and metastasis, I compared the metabolic gene expression profile of metastatic

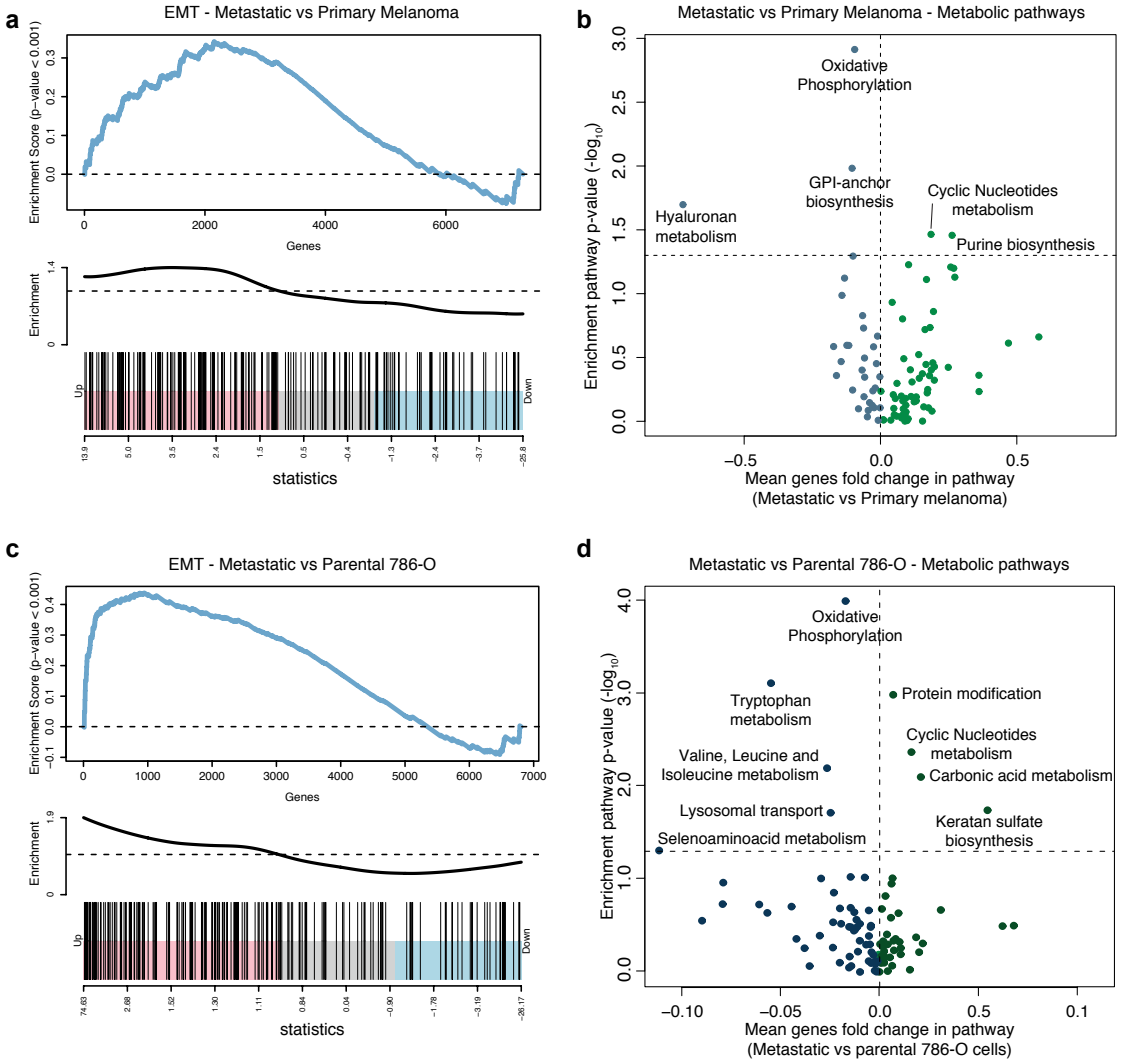

Figure 3.10: Suppression of OXPHOS is a key metabolic feature of Skin Cutaneous Melanoma. a,c) Enrichment plot of Epithelial-to-Mesenchymal Transition (EMT) in metastatic vs primary melanoma cancer samples (a) and in metastatic vs parental 786-O cell lines (c). **b,d)** Volcano plot representations of mean fold change (log_2) of genes in each pathway (x axis) vs enrichment p-values (y axis) of metastatic vs primary cancer samples (b) and of metastatic vs parental 786-O cell lines (d).

and parental 786-O kidney cancer cell lines generated by Vanharanta et al (Vanharanta et al. 2013). Briefly, this panel of cell lines were generated by intravenous injection of parental 786-O cells into nude mice and performed subsequent isolation of cells that spontaneously formed metastases in the lungs. The comparison of metastatic and parental 786-O cells allows for the investigation of gene signatures associated with metastasis. In line with my findings in cancer patients, EMT was strongly up-regulated in metastatic vs parental cells (**Figure 3.10c**) and OXPHOS was the most down-regulated metabolic pathway in metastatic cells compared to parental (**Figure 3.10d**). Moreover, cyclic nucleotides metabolism, one of the pathways found up-regulated in metastatic vs primary melanoma, was also found up-regulated in 786-O metastatic vs parental cell lines (**Figure 3.10d**).

3.3 Discussion

Dysregulation of cellular metabolism is an established feature of cancer. Yet, the contribution of this metabolic reprogramming to cancer biology and to the clinical outcome of patients is still under investigation. Taking advantage of a large collection of cancer samples from the cancer genome atlas (TCGA) consortium, I systematically investigated the mRNA expression of metabolic genes in 20 different cancer types and assessed the link between altered gene expression and survival of cancer patients. This analysis revealed that different cancer types exhibit similar metabolic features, which are reminiscent of their tissue of origin, and that specific metabolic features correlate with metastatic potential and patient prognosis.

Previous studies have highlighted important features of altered metabolism between tumor and normal tissues in a pan-cancer perspective. For instance, Hu and colleagues performed an extensive analysis of metabolic gene expression changes in cancer compared to normal tissues, observing common patterns of metabolic adaptation among different cancer types (Hu, Locasale, et al. 2013; Reznik and Sander 2015; Gross et al. 2015). In accordance with this study, I found that distinct cancers display up-regulated expression of glycolysis and nucleotide metabolism, and down-regulation of mitochondrial fatty acids oxidation (mFAO), whereas oxidative phosphorylation (OXPHOS) presented heterogeneous regulation. Subtle differences between the study by Hu et al (Hu, Locasale, et al. 2013) and my findings, including expression changes of citric acid cycle (CAC) genes, can be explained by differences in the curation of metabolic pathways, which I obtained by integrating multiple databases. Interestingly, the observation that expression of mFAO is diminished across several cancer types is in line with the results from a recent pan-cancer analysis where signals from mRNA, miRNA and DNA methylation levels were integrated to find common expression changes in cancer (Gross et al. 2015). Together with these findings, my results showed diminished expression of CAC enzymes in cancer, and succinate dehydrogenase (SDH)D ranked among the most frequently down-regulated mitochondrial genes, in line with its role as mitochondrial tumor suppressor (Selak et al. 2005). This finding is in line with a previous study indicating the loss of co-expression of genes of the mitochondrial respiratory chain in kidney cancer (Reznik and Sander 2015), and with the decrease of mitochondrial DNA (mtDNA) in tumor samples from TCGA database (Reznik, Miller, et al. 2016). Together with the observation that direct inhibition of mitochondrial metabolism is responsible for p53 genetic inactivation and increased tumorigenic potential (Bartesaghi et al. 2015), my results support the notion that down-regulation of several mitochondrial pathways is a common feature of the metabolic rewiring occurring in different cancer types.

Although these data seem to support a role for mitochondrial dysfunction in cancer initiation and progression, mitochondria are far from being an accessory organelle in cancer cells. Cells completely devoid of mtDNA (ρ^0) have lower ability to form tumors in mice (Morais et al. 1994) and ρ^0 cells need to acquire mtDNA from host cells to recover mitochondrial function and achieve growth in vivo (Tan, Baty, et al. 2015). Indeed, mitochondria are important for the generation of several precursor molecules, such as aspartate, citrate and succinyl-CoA for supporting nucleotide, lipid and heme biosynthesis, respectively. Moreover, mitochondrial metabolism is flexible and can engage in both oxidative and reductive metabolism to support the generation of cytosolic citrate even in the presence of mitochondrial dysfunction

triggered by genetic or environmental cues. For instance, reductive citrate has been shown to support lipid synthesis under hypoxia (Metallo et al. 2012), in the presence of CAC truncation (Mullen et al. 2012), or in the presence of respiratory chain inhibitors (Fendt et al. 2013). Together with this evidence, my results suggest that partial, rather than complete, loss of mitochondrial function supports the growth of cancer cells. Suboptimal mitochondrial function would induce a metabolic switch towards aerobic glycolysis, which is known to support anabolic programs in fast growing cells (Vander Heiden et al. 2009), while maintaining the ability to carry out important mitochondrial functions required for metabolism and signaling. Importantly, recent work demonstrated that partial mitochondrial dysfunction induces migration, invasion and metastasis, while complete loss of mitochondrial function leads to inhibition of the metastatic phenotype (Porporato et al. 2014).

My study established for the first time a link between metabolic alteration and survival of cancer patients. By comparing low and high survival patients from 15 different cancer types I observed that down-regulation of OXPHOS gene expression is almost invariably associated with poor clinical outcome. This result suggests that, despite activation of OXPHOS could have different effects during cancer initiation depending on the tissue of origin, suppression of OXPHOS genes is a common feature of cancer progression and could have important implications for patient survival. Low OXPHOS was strongly associated with induction of epithelial-to-mesenchymal transition (EMT), a process linked to cancer invasion and metastasis, one of the most common causes of cancer deaths. Consistently, OXPHOS was amongst most down-regulated pathways in distant melanoma metastases, compared to primary cancer. These results support at much broader scale the finding that partial mitochondrial dysfunction increases metastatic potential of cancer cells (Porporato et al. 2014). At the same time, these results partially disagree with recent work from the Kalluri's laboratory, where LeBleu and colleagues investigated the metabolic phenotype of circulating tumour cells and metastasis from various breast cancer models (LeBleu et al. 2014). In accordance with my findings, they found that metastatic cells exhibited low expression of OXPHOS genes, compared to the primary tissue and circulating cancer cells. However, they found that invasive ductal breast cancers are characterized by high expression of the master regulator of mitochondrial biogenesis nuclear coactivator PPARγ coactivator-1α (PGC1α), which also correlated with metastasis. Of note, I could not find significant changes in the expression of PGC1α between metastatic and primary melanoma tumors (BH p-value=0.37) suggesting that the findings of LeBleu might not represent a common feature of cancer but, likely, apply to a specific subset of breast cancers. In line with the interpretation of possible tissue-specific roles of PGC1α, a recent study found that PGC1α down-regulation is linked with prostate cancer progression and metastasis, and its genetic reactivation suppresses the formation of prostate cancer metastases (Torrano et al. 2016).

Beyond conclusions that can be drawn from the results presented in this chapter, it is important to highlight that the analytical approach applied herein is not devoid of limitations. First, establishing a link between mRNA levels of metabolic enzymes and cellular function can be a daunting task, not only because of the lack of correlation between transcript abundance and protein concentration (Zhang, Wang, et al. 2014), but also because of lack of large-scale information about downstream regulation of protein activity (e.g. acetylation, phosphorylation, etc).

Moreover, regulation of metabolic pathways can be very intricate and often occurs at nodal points in the pathway, rather than at the level of every gene; therefore, mean expression of metabolic pathways is only a partial estimate of their activity. Second, the association between down-regulation of OXPHOS and metastatic behavior via induction of an EMT signature is based on correlation. This hypothesis is in line with previous studies (Porporato et al. 2014), and I further confirmed such link in two independent data sets of metastatic melanoma and metastatic cell lines. Nevertheless, more experimental work is required to corroborate the molecular underpinnings linking mitochondrial function to metastasis.

Finally, my results have multiple implications. First, they suggest that, during the process of cancer transformation, cancer cells explore different molecular paths that entirely depend on the tissue of origin. Second, they indicate that, despite the overwhelming genetic complexity that underlines transformation, cancer cells contrive common metabolic strategies to support their proliferation. Importantly, these convergent *pathways* of transformation are achieved despite the vast genetic heterogeneity of cancer cells and appear to be independent of genetic mutations at the level of specific oncogenes or tumour suppressor genes. Therefore, I hypothesise that the metabolic reprogramming of cancer is degenerated, i.e. different oncogenes and tumor suppressor genes lead to similar metabolic signatures to support proliferation. It is therefore tempting to speculate that evolution of cancer might be driven by phenotypic traits, and that oncogenes and tumor suppressors might be selected for their efficiency in regulating these metabolic changes. In line with this hypothesis, a recent study found that metabolic and cancer-causing genes undergo co-altered somatic copy number variation (Sharma et al. 2016), indicating that alteration of cancer-associated genes is often linked with metabolic rewiring. These findings may catalyse a better understanding of the role of dysregulated metabolism in cancer and provide novel means to stratify patients based on their metabolic features.

CHAPTER 4

Results. Metabolic determinants of mitochondrial dysfunction

One of the main findings presented in the previous chapter is that inhibition of mitochondrial function is a common feature of metabolic rewiring in different cancer settings and is associated with patient survival. Given the importance of mitochondrial metabolism in cancer, I wanted to investigate further the effect of altered mitochondrial function on cellular metabolism. To this aim I decided to exploit an *in vitro* system of mitochondrial dysfunction.

A consistent obstacle to clarifying the link between mitochondrial function and cell metabolism has been the difficulty of disentangling the direct consequences of dysregulated mitochondrial metabolism from secondary and indirect effects. Cytoplasmic hybrids (cybrids) have been used to investigate the effects of mitochondrial function on cell physiology (King and Attardi 1989). Cytoplasts with wild type or mutated mitochondrial DNA (mtDNA) are fused with the nucleus from a donor cell to evaluate the effect of a specific mtDNA mutation. However, cybrid generation is notoriously prone to artefacts. For instance, ethidium bromide used to eliminate mtDNA of the host cells also induces mutations in the nuclear genome. Moreover, the selection of individual clones often leads to unrepresentative clone-specific phenotypes, with the marked interclonal heterogeneity being attributable to simple founder effects (King and Attardi 1989; Martnez-Reyes et al. 2016). To overcome these issues, the selective digestion of mutated mtDNA with mitochondrially-targeted zinc-finger nucleases (mtZFNs) has been recently used to generate isogenic cell lines (from parental 143B human osteosarcoma cell line) with different levels of heteroplasmy of the mtDNA mutation m8993T>G (Gammage, Rorbach, et al. 2014). This mutation affects ATP6, a key subunit of ATP synthase, leading to neuropathy ataxia and retinitis pigmentosa (NARP) syndrome and fatal childhood maternally inherited Leigh's syndrome (MILS). Importantly, these cells exhibit distinct and stable metabolic phenotype (Gammage, Gaude, et al. 2016). The precise and selective regulation of mitochondrial function offered by the NARP model might yield novel insight into the effects of mitochondrial (dys)function on cell metabolism, as well as other cellular functions.

In this chapter I will present the results obtained by employing this new model of *progressive* mitochondrial dysfunction to investigate how mitochondrial function impacts upon cell metabolism. I will show that reduced turnover of mi-

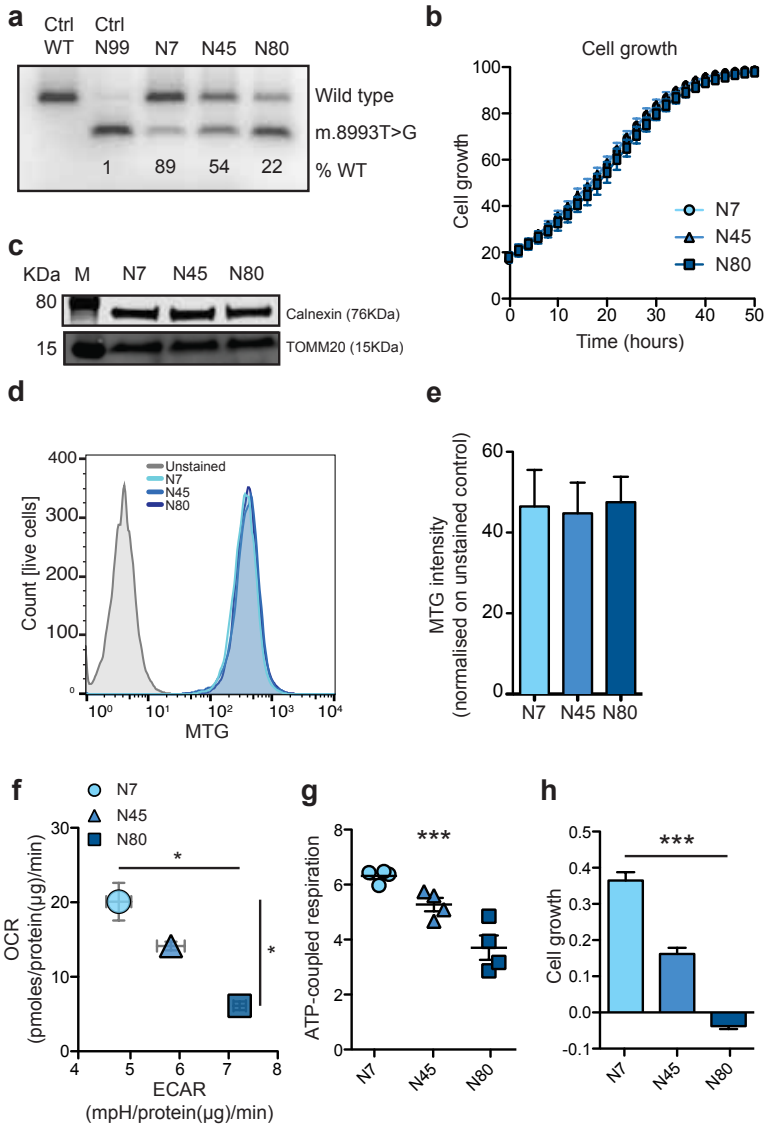

Figure 4.1: Increasing levels of m8993T>G mutation are associated with changes in mitochondrial function. **a)** Restriction fragment length polymorphism (RFLP) analysis of last cycle hot PCR products (mtDNA nt positions 8339-9334) amplified from total DNA samples of 143B cells harbouring indicated levels of m.8993T>G, obtained by sequential treatment with mtZFNs. Wild-type cells and 99% m.8993T>G cybrids were used as controls. **(b)** Cell growth of N7, N45 and N80 cells in standard conditions measured using Incucyte. **c)** Western blot analysis of the mitochondrial membrane marker TOMM20. Calnexin was used as loading control. **d)** Representative fluorescence distributions of cells with or without Mitotracker Green (MTG) staining from FACS analysis and **(e)** mean MTG intensity after subtraction of intensity from unstained control. Data are mean $\pm$ s.e.m. from three independent cultures. **f)** Basal extracellular acidification rate (ECAR) and oxygen consumption rate (OCR) in N7, N45 and N80 cells. **g)** ATP-coupled respiration in N7, N45 and N80 cells as calculated by subtracting oxygen consumption rate (OCR) values after treatment with 1 μM oligomycin from basal OCR (after correction for non-mitochondrial respiration). **h)** Proliferation of N7, N45 and N80 cells in the presence of D-galactose as unique sugar supply. Cell growth was determined by calculating the slope of respective proliferation curves. All data are mean $\pm$ s.e.m. from 3 independent cultures. *, *** indicate one-way ANOVA p-value $\leq$ 0.05 and 0.001, respectively.

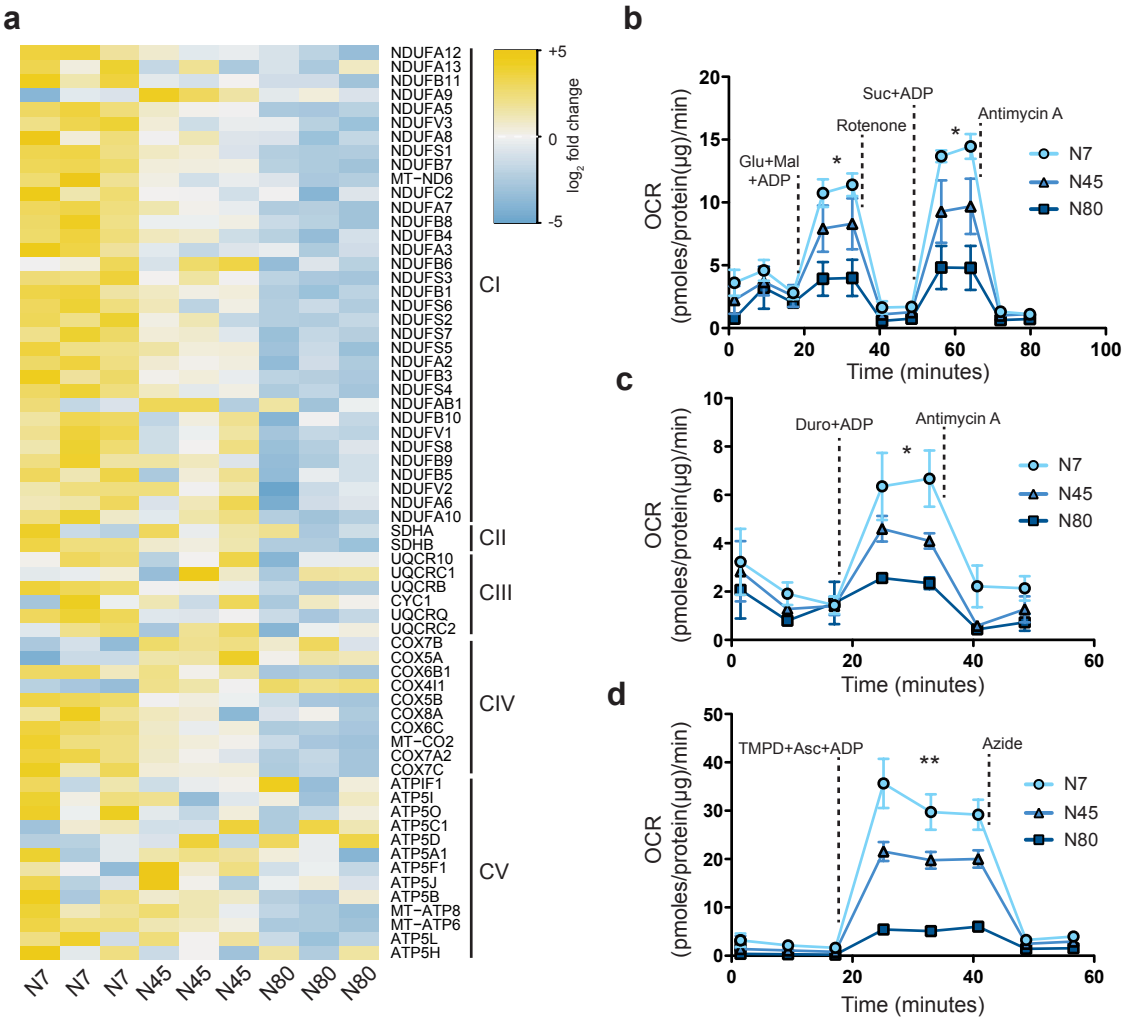

Figure 4.2: m8993T>G mutation induces global defects of the mitochondrial respiratory chain. a) Heatmap representation of protein expression of mitochondrial respiratory complexes in N7, N45 and N80 cells as analysed by proteomics analysis (see Materials and Methods). Data represent values from three independent experiments and $\log_2$ fold change values against mean of all cell lines are colour-coded as indicated. **(b-d)** Respiration of digitonin-permeabilised N7, N45 and N80 cells in the presence of **(b)** glutamate-malate (complex I) and succinate (complex II), **(c)** duroquinol (Complex III) and **(d)** TMPD-Ascorbate (Complex IV). Data are mean $\pm$ s.e.m. from 3 independent cultures. *, ** indicate one-way ANOVA p-value $\leq$ 0.05 and 0.01, respectively.

tochondrial reduced nicotinamide adenine dinucleotide (NADH) due to mitochondrial dysfunction induces redox state imbalance and triggers cytosolic reductive glutamine metabolism. By supporting the generation of cytosolic malate, reductive carboxylation allows metabolic channelling of NADH between malate dehydrogenase 1 (MDH1) and glyceraldehyde 3-phosphate dehydrogenase (GAPDH), which become physically associated in cells with dysfunctional mitochondria. Finally, I found that mitochondrial dysfunction is associated with increased migratory capacity and that increased MDH1 activity directly supports this increased motility. These results propose a link between reductive carboxylation and the glycolytic switch, a hallmark of mitochondrial dysfunction and cancer metabolism. These findings lend insight towards understanding the metabolic rewiring that accompa-

nies mitochondrial dysfunction and that contributes to increased cell proliferation and motility during carcinogenesis.

4.1 m8993T>G heteroplasmy affects mitochondrial function and cellular metabolism

To investigate the effects of primary mitochondrial dysfunction on cellular metabolism I used a panel of isogenic cell lines with stable low (N7), medium (N45), or high (N80) levels of m8993T>G heteroplasmy (Gammage, Gaude, et al. 2016) (**Figure 4.1a**). These cells exhibited comparable growth rate in basal conditions (**Figure 4.1b**). I then characterised the mitochondrial phenotype of the neuropathy ataxia and retinitis pigmentosa (NARP) model. Mitochondrial mass of these cells was comparable, as shown by protein expression of the mitochondrial membrane transporter TOMM20 (**Figure 4.1c**) and by staining with the mitochondria-specific, membrane potential-independent, dye Mitotracker Green (**Figure 4.1d-e**). Despite this, I observed a decrease in basal and ATP-coupled oxygen consumption rate (OCR) and increase of extracellular acidification rate (ECAR) (**Figure 4.1f-g**) in N80 compared to N45 and N7 cells, consistent with a gradual decline of mitochondrial function. In line with the presence of mitochondrial dysfunction, I demonstrated that N80 cells fail to grow in galactose (**Figure 4.1h**), a substrate whose slower catabolism depends on intact mitochondrial function (Marroquin et al. 2007).

Correspondingly, whilst the m8993T>G mutation affects complex V, the entire respiratory chain (RC) was influenced by this mutation. Indeed, a proteomic analysis revealed that, together with low levels of ATP6 and other subunits of ATP synthase, the abundance of most of RC components (**Figure 4.2a**) was decreased in N80 compared to N45 and N7 cells, with subunits of Complex I showing lowest levels of expression compared to other respiratory complexes. To confirm these findings at the functional level I measured the activity of individual respiratory complexes in

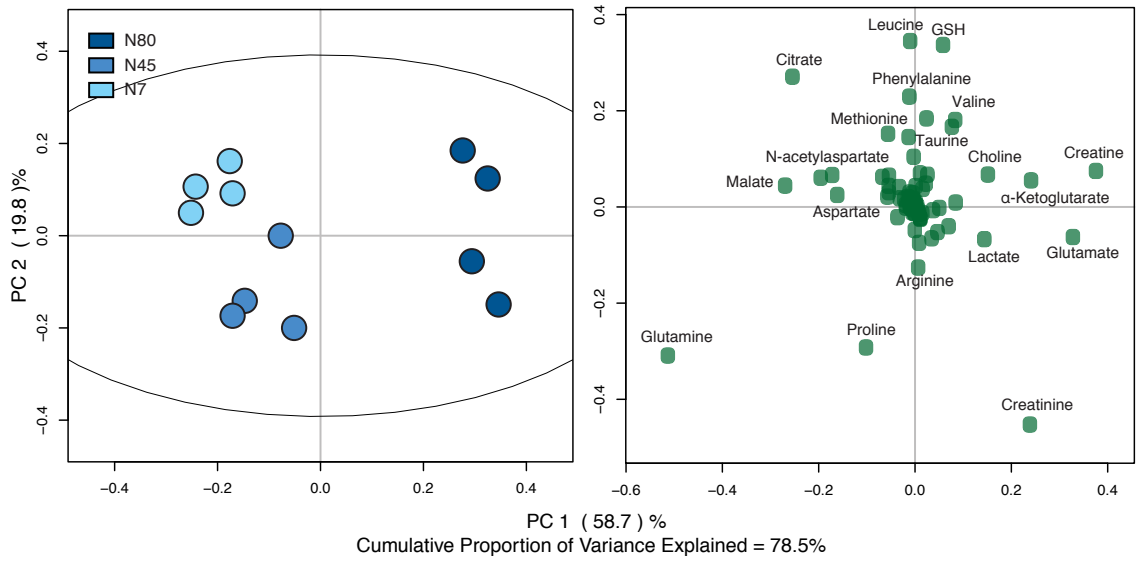

Figure 4.3: m8993T>G mutation affects cellular metabolism. PCA score plot (left) and loading plot (right) of metabolite levels as measured by LC-MS in N7, N45 and N80 cells.

permeabilised cells. By combining complex-specific substrates and inhibitors, this technique allows to assess the consumption of oxygen driven by individual complexes during ADP-dependent respiration (Salabei et al. 2014). In line with decreased protein expression of respiratory complexes, as well as with decreased OCR (**Figure 4.1f-g**), the activity of all individual RC complexes was decreased in correlation with the level of heteroplasmy (**Figure 4.2b-d**). Although the activity of all complexes was significantly altered in NARP cell lines, complex IV showed the most significant alteration. This result could be due to the architecture of the respiratory chain, with complex IV being the site of oxygen consumption and potentially acting as a bottleneck for the respiratory chain. Together, these data indicate that increasing levels of m8993T>G heteroplasmy correspond to defects across all complexes of the respiratory chain and lead to increasing levels of mitochondrial dysfunction.

Finally, I wanted to investigate whether m8993T>G heteroplasmy can affect cellular metabolism. To this aim I performed LC-MS-based metabolomics of intracellular metabolites in N7, N45 and N80 cells, followed by statistical analysis with PCA. The PCA score plot (**Figure 4.3left**) represents biological replicates of each cell line and groups sample points together based on multivariate similarities (i.e. points close to each other are more similar compared to points far apart). Interestingly, the PCA score plot showed a clear separation between cell lines, with N80 cells forming a clear cluster along the principal component 1, while N45 and N7 being clustered apart by principal component 2 (**Figure 4.3left**). This result indicates that metabolite levels of N80 cells are most different, compared to N7 and N45 cells. The PCA loading plot (**Figure 4.3right**) shows the importance of each metabolite in determining the separation observed in the score plot. Metabolites far from the centre of the plot, i.e. having high loading values for principal components 1 and 2, are the most different among cell lines. Interestingly, intermediates of the citric acid cycle (CAC), such as citrate and malate, as well as metabolites associated with mitochondrial function, such as aspartate (Birsoy et al. 2015; Sullivan, Gui, et al. 2015) co-clustered with N7 and N45 cells, while the glycolytic metabolite lactate co-clustered with N80 cells (**Figure 4.3**). Glutamine and glutamate show opposite trends, suggesting that conversion of glutamine into glutamate might be altered in the NARP model. This evidence suggests that mitochondrial dysfunction associated with m8993T>G can affect several metabolic pathways.

4.2 Constraint-directed metabolic modelling predicts association between cytosolic reductive carboxylation and glycolysis

To systematically investigate the metabolic changes associated with mitochondrial dysfunction in the m8993T>G mutation model, I took advantage of a recently published *in silico* metabolic model of mitochondrial and central carbon metabolism (Zieliski et al. 2016). Metabolic models provide detailed reconstructions of interconnected metabolic reactions and allow prediction of intracellular fluxes, under the assumption of steady state (Orth et al. 2010). Importantly, experimental measurements of e.g. extracellular nutrients availability or enzyme activity, can be implemented to refine the model and tailor its predictions on the experimental system under investigation.

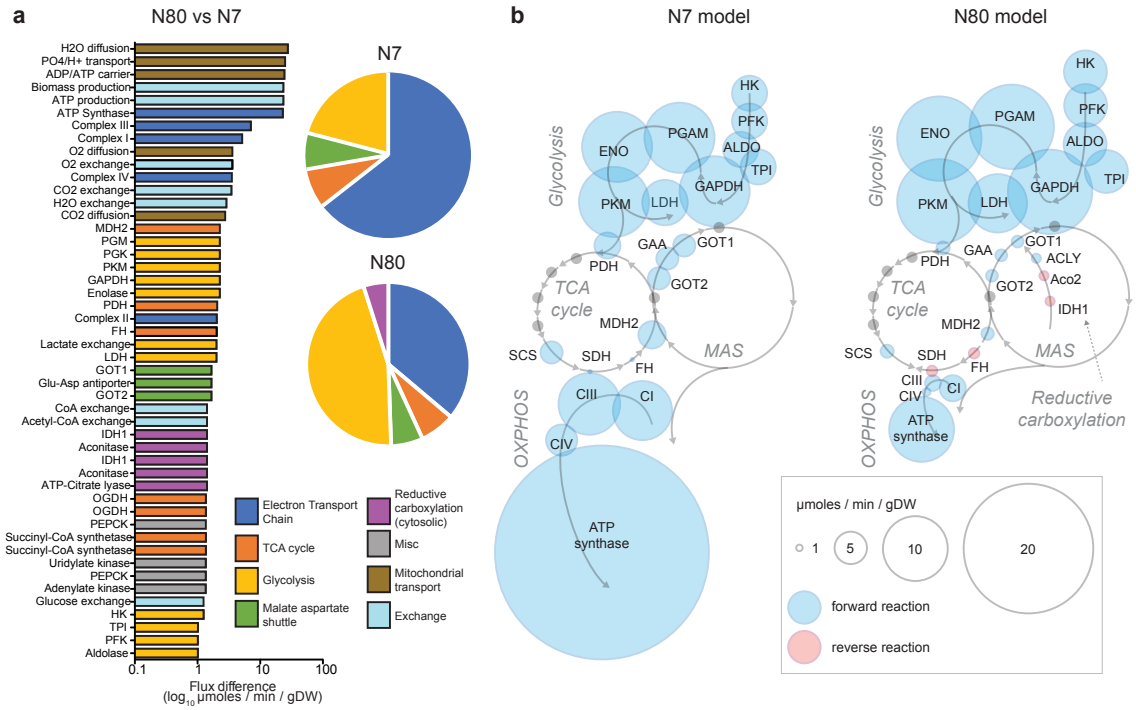

Figure 4.4: Metabolic model predicts activation of cytosolic reductive carboxylation in cells with mitochondrial dysfunction. **a)** Top 10% affected reactions between N80 and N7 as predicted by metabolic modelling. Flux difference of each reaction between N80 and N7 was obtained by subtracting the predicted flux for N7 to the predicted flux for N80. Log_{10} of the flux difference is shown. Duplicated reactions indicate intermediates of reactions. **b)** Bubble representation of reactions involved in glycolysis, OXPHOS, MAS and cytosolic reductive carboxylation. Bubble size is indicative of reaction flux (μmoles / min / gDW). Blue and red bubbles indicate forward and reverse reactions. Grey arrows show the predicted direction of reactions, while grey dots represents reactions present in the depicted pathways, but with no predicted flux change.

I refined this model by including consumption and release rates of metabolites as measured by LC-MS metabolomics and by constraining RC activity with RC complex-dependent measurements of OCR (**Figure 4.2b-d**). I then computed the intracellular metabolic fluxes and compared the predicted enzymatic activities in N7 and N80 models. Besides the expected changes in RC activity, oxygen exchange, and ATP production, the model predicted an increase in several glycolytic reactions and decreased activity of multiple enzymes of the CAC and MAS in N80 model, compared to N7 (**Figure 4.4**). Interestingly, the model predicted the activation of cytosolic reductive carboxylation of glutamine in N80 cells, while this pathway was inactive in N7 cells (**Figure 4.4**).

To test the predictions of the model, I cultured cells in the presence of uniformly labelled (U)-^{13}C-glucose (**Figure 4.5a**) and (U)-^{13}C-glutamine (**Figure 4.6a**) and assessed by LC-MS the labelling profile of downstream metabolites. I observed increased levels of the glycolytic metabolites ^{13}C-phosphoenolpyruvate (PEP) and ^{13}C-lactate (**Figure 4.5b**) and decreased levels of ^{13}C-labelled CAC intermediates, such as 2-oxoglutarate, fumarate, and malate, in N80 cells (**Figure 4.5c**) upon incubation with (U)-^{13}C-glucose. Consistent with an increased dependency on glycolysis, N80 cells were more sensitive to inhibition of GAPDH by heptelidic acid,

compared to N7 (**Figure 4.5d**), as measured by inhibitory concentration 50 (IC50).

The incubation of cells with (U)-^{13}C-glutamine revealed changes in glutamine oxidation in N80, compared to N45 and N7 cells (**Figure 4.6a-b**). In particular, I observed a decrease in m+4 isotopologues in citrate and aconitate, consistent with reduced oxidation of glutamine via the TCA cycle (**Figure 4.6b**). I also observed a substantial increase in aconitate and citrate m+5, and in malate and fumarate m+3 in N80 cells compared to N7 and N45 (**Figure 4.6c**), indicative of reductive carboxylation of glutamine proportional to level of heteroplasmy. To assess whether induction of reductive carboxylation in N80 cells occurs in the cytosolic or mitochondrial compartment, I silenced either IDH1 or IDH2 in N80 cells (**Figure 4.6d**), the key enzymes of cytosolic and mitochondrial reductive carboxylation, respectively. I then followed incorporation of (U)-^{13}C-glutamine carbons into downstream metabolites using LC-MS. Accumulation of aconitate and citrate m+5 were significantly reduced when IDH1 was suppressed, while downregulation of IDH2 had only minor effects (**Figure 4.6e**). Together, these data confirm the predictions of the metabolic model and indicate that mitochondrial dysfunction induces a glycolytic switch and triggers reductive carboxylation of glutamine in the cytosolic compartment.

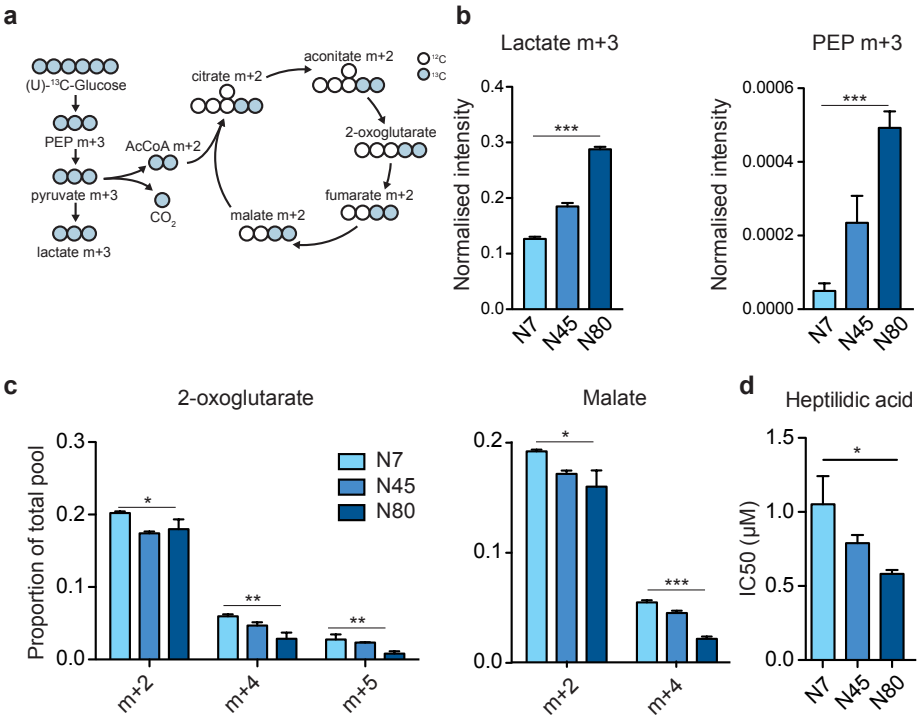

Figure 4.5: Mitochondrial dysfunction is associated with increased glycolysis and decreased glucose oxidation. a) Schematic representation of metabolite labelling pattern from (U)-^{13}C-glucose. **b)** Normalised intensities (total metabolite count) of lactate m+3 (left) and PEP m+3 (right) after incubation with (U)-^{13}C-glucose. **c)** Labelling patterns of the indicated CAC intermediates after incubation with (U)-^{13}C-glucose. **d)** IC50 values of the GAPDH inhibitor heptelidic acid on the proliferation of N7, N45 and N80 cells. All data are mean ± s.e.m. from at least three independent cultures. *, ** and *** indicate one-way ANOVA p-value $\leq$ 0.05, 0.001 and 0.001, respectively.

4.3 Reductive carboxylation is regulated by NAD$^+$ /NADH ratio

I then wanted to investigate the possible determinants of cytosolic reductive carboxylation triggered by mitochondrial dysfunction. Reductive carboxylation has been associated with altered levels of NAD$^+$/NADH ratio (Fendt et al. 2013), though it is not clear whether these changes are sufficient to drive reductive carboxylation. To

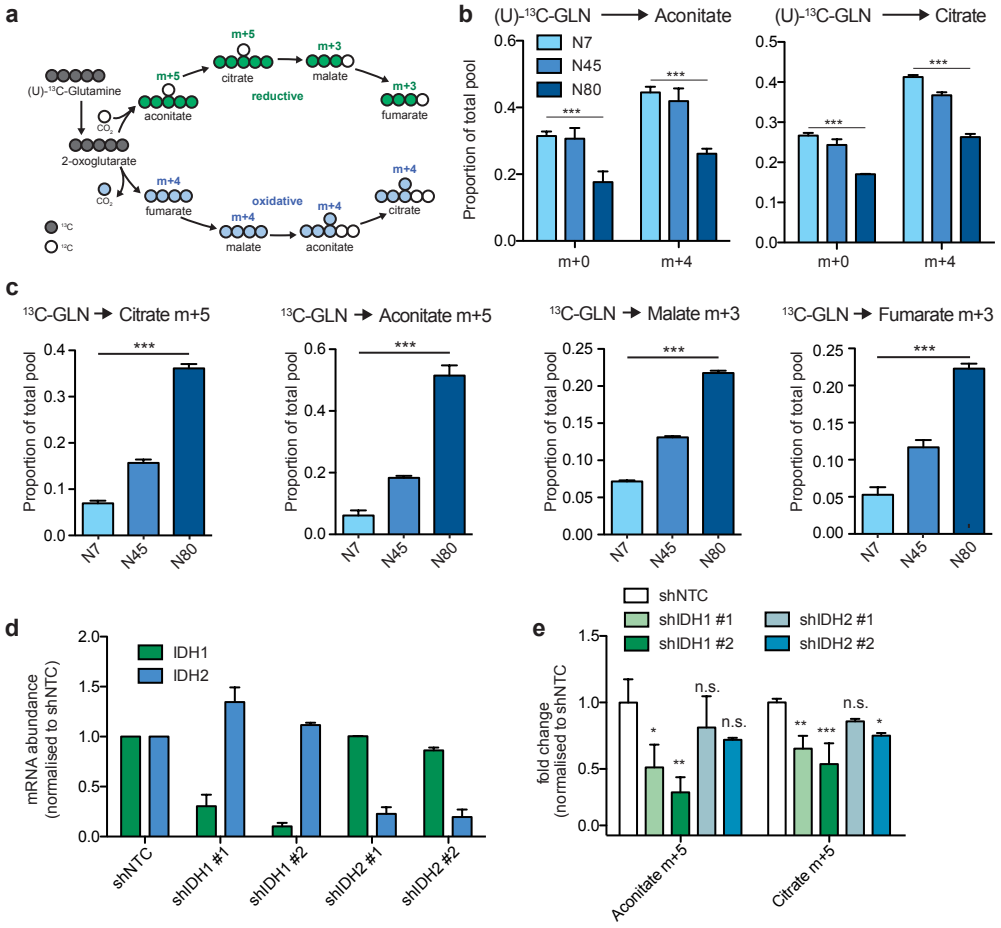

Figure 4.6: Mitochondrial dysfunction is associated with increased cytosolic reductive carboxylation of glutamine. **a)** Schematic representation of metabolite labelling pattern from (U)-^{13}C-glutamine. **b)** Labelling patterns of aconitate and citrate m+0 and m+4 intermediate originating from oxidation of (U)-^{13}C-glutamine in the mitochondria. **c)** Proportion of total pool of metabolites originating from reductive carboxylation of (U)-^{13}C-glutamine; aconitate m+5, citrate m+5, malate m+3 and fumarate m+3 are shown. **d)** mRNA expression of IDH1 and IDH2 genes upon selective knock down of IDH1 and IDH2 with two independent shRNA constructs. Actin mRNA expression was used as endogenous control and data were normalised on shNTC control. Data are mean $\pm$ s.d. from one representative experiment. **e)** Relative metabolite levels (normalised on shNTC control) from reductive carboxylation of U-^{13}C-Glutamine in N80 cells infected with shRNA constructs targeting IDH1 or IDH2. Data are mean $\pm$ s.e.m. from three independent cultures. **(b-c)** *** indicate one-way ANOVA p-value $\leq$ 0.001. **(e)** *, **, *** indicate Dunnetts p-value $\leq$ 0.05, 0.01 and 0.001, respectively. n.s. = not significant.

investigate whether mitochondrial function affects NAD^+/NADH ratio in N7, N45 and N80 cell lines, I measured NAD^+/NADH levels using an enzymatic assay, which measures total cellular NAD^+/NADH levels. Total NAD^+/NADH was decreased in N80, compared to N7 and N45 cells (**Figure 4.7a**), suggesting that mitochondrial dysfunction is associated with NADH redox imbalance.

To assess the levels of mitochondrial NAD^+/NADH more directly, I measured NAD(P)H autofluorescence using confocal microscopy. This imaging technique allows to assess NADH levels in live cells, therefore avoiding cell lysis and gaining information of compartmentalised NADH pools. Moreover, the combination of live cell imaging together with treatment with specific mitochondrial inhibitors, allows to investigate the specific consumption of NADH by the RC. Briefly, NAD(P)H autofluorescence levels are acquired in basal conditions, after which cells are treated with the complex IV-specific inhibitor cyanide (CN). This blocks flux through the RC and induces accumulation of NADH due to reduced consumption by complex I. Accumulation of NADH upon CN depends on the extent to which complex I is coupled to the respiratory chain and on the ability of the CAC to provide new

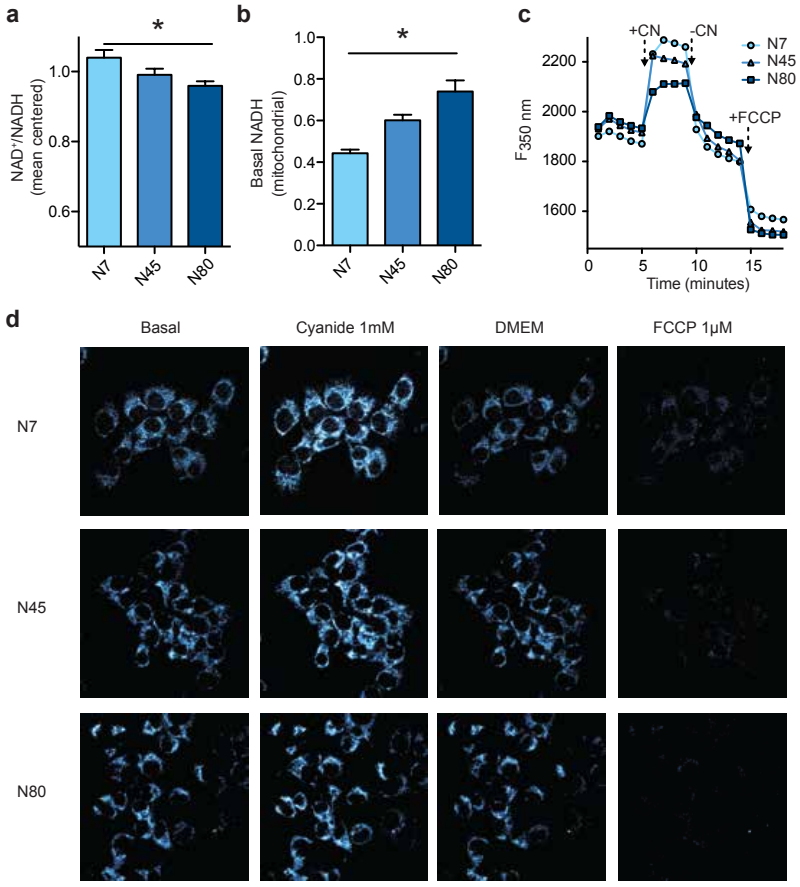

Figure 4.7: NAD^+/NADH imbalance in cells with mitochondrial dysfunction. a) Total levels of NAD^+/NADH in N7, N45 and N80 cells, as measured by enzymatic assay. **b)** Levels of mitochondrial NADH as measured by NAD(P)H autofluorescence. **c)** Fluorescence intensity after excitation at 350 nm extracted from image time series analysis of N7, N45 and N80 cells in basal conditions or after addition of indicated drugs. Data are mean $\pm$ s.e.m. from three independent cultures. * indicates one-way ANOVA p-value ≤ 0.05. **d)** Representative images of N7, N45 and N80 cells excited at 350 nm.

NADH molecules. Slower flux through the RC and/or through the CAC will result in lower NADH accumulation. Media is then changed to allow for CN wash out and requilibration (**Figure 4.7c**), after which cells are treated with carbonyl cyanide-p-trifluoromethoxyphenylhydrazone (FCCP). FCCP uncouples electron transport and oxygen consumption from ATP production and induces maximal respiration, thus leading to depletion of mitochondrial NADH pools. Cells with dysfunctional CAC will experience profound NADH depletion due to inability of the CAC to supply NADH. This experiment showed that basal levels of mitochondrial NADH are increased in N80 cells, compared to N7 and N45 (**Figure 4.7b-d**), suggesting that reduced consumption of NADH by the RC can lead to accumulation of NADH in the mitochondrial compartment. These results indicate that impairment of respiratory activity in N80 cells alters NADH oxidation in the mitochondria, leading to a decreased total cellular NAD^+/NADH ratio.

To further assess the link between NAD^+/NADH balance and reductive carboxylation in these cell lines, I rescued mitochondrial NADH oxidoreductase activity by expressing yeast-derived NADH dehydrogenase internal (NDI-1) in N80 cells (**Figure 4.8a-b**), where respiratory complex I activity is compromised. NDI-1 constitutes an alternative NADH oxidoreductase that transfers electrons from NADH to ubiquinone, delivering electrons to downstream complexes and therefore can be used

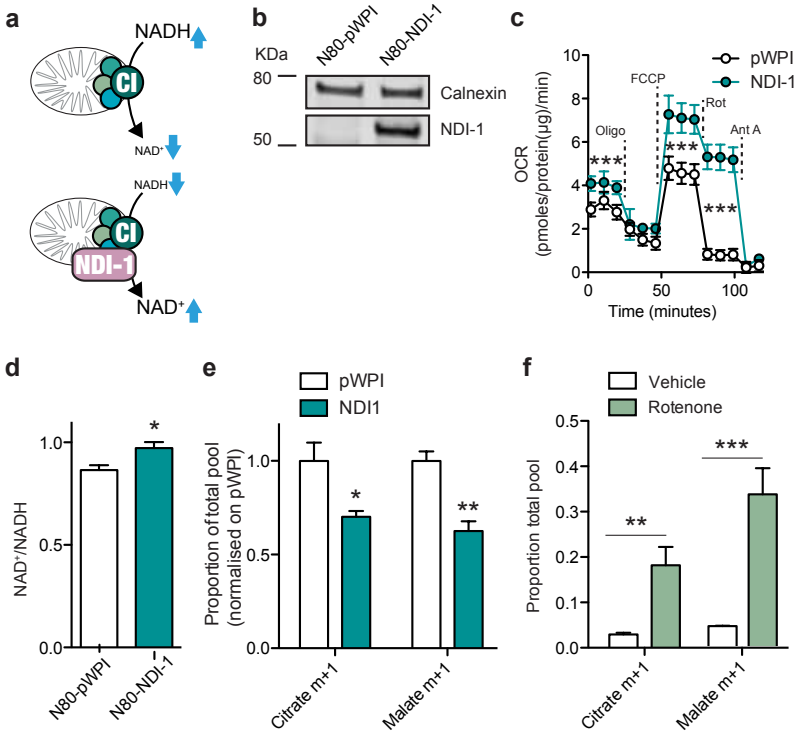

Figure 4.8: Reductive carboxylation is dependent on mitochondrial NADH oxidation. **a)** NDI-1 expression affects mitochondrial NADH oxidation. **b)** Protein expression of NDI-1 upon transduction of N80 cells with lentiviral vectors. **c)** OCR of pWPI and NDI-1 N80 cells in basal conditions or after indicated injections. **d)** Total levels of NAD^+/NADH. **e-f)** Proportion of total pool of citrate and malate m+1 upon incubation with 1-^{13}C-glutamine of **(e)** pWPI and NDI-1 N80 cells and **(f)** N7 cells treated with vehicle control or rotenone. Data are mean ± s.e.m. from 3 independent cultures. *, ** and *** indicate two-sided t-test p-value $\leq$ 0.05, 0.01 and 0.001, respectively.

to bypass electron transport in complex I (Seo et al. 1998; Bai et al. 2001). Since N80 cells display complex I deficiency and activation of reductive carboxylation, rescue of NADH oxidoreductase activity via NDI-1 expression in these cells allow to assess the link between mitochondrial NADH levels and reductive carboxylation.

In line with increased electron transport through the respiratory chain, expression of NDI-1 improved basal and maximal respiration of N80 cells, compared to N80 cells expressing an empty vector (**Figure 4.8c**). To assess whether the increase in respiration was due to NDI-1 expression, I treated NDI-1-expressing cells with the complex I-specific inhibitor rotenone, which does not inhibit NDI-1. Rotenone severely impaired respiration of control N80 cells, while had only minor effects on NDI-1-expressing cells (**Figure 4.8c**). Moreover, inhibition with the complex III-specific inhibitor antimycin A abolished respiration of both cell lines, indicating that the increase of respiration was, indeed, specifically caused by NDI-1 expression (**Figure 4.8c**). Importantly, not only NDI-1 resulted in increased respiration of N80 cells, but also was able to rescue the NAD^+/NADH ratio (**Figure 4.8d**), thus indicating that NDI-1 can successfully rescue mitochondrial NADH oxidoreductase activity.

Finally, in order to assess whether NDI-1 affected glutamine reductive metabolism, I performed 1-^{13}C-glutamine labelling, which selectively tracks reductive carboxylation (Metallo et al. 2012). Briefly, metabolism of 1-^{13}C-glutamine through oxidative reactions of the CAC will lead to loss of the labelled carbon via oxidation and decarboxylation of α-ketoglutarate (αKG) to succinyl-CoA by alpha-ketoglutarate dehydrogenase (AKGDH). Instead, reductive carboxylation of αKG to isocitrate by IDH1 or IDH2 will produce labelled isocitrate and the labelled carbon will be retained into downstream metabolites (Metallo et al. 2012).

Supplementation with 1-^{13}C-glutamine resulted in lower levels citrate m+1 and malate m+1 in NDI-1-expressing N80 cells, compared to control, indicating that NDI-1 expression can diminish the activation of reductive carboxylation (**Figure 4.8e**). In further support of a causative link between mitochondrial dysfunction, changes in NAD^+/NADH ratio, and cytosolic reductive carboxylation, the complex I-specific inhibitor rotenone led to increased reductive carboxylation (**Figure 4.8f**). Together, these data indicate that impairment of cellular NAD^+/NADH ratio by mitochondrial NADH turnover can affect the levels of cytosolic glutamine reductive carboxylation.

4.4 Reductive carboxylation is coupled with glycolysis via malate dehydrogenase 1 (MDH1)

I then assessed the functional relevance of cytosolic reductive carboxylation in the metabolic reprogramming of N7, N45 and N80 cells. To this end, I first simulated the complete knock out of IDH1 *in silico*, followed by computation of the changes in ATP production associated to knock out of individual enzymes. Briefly, ATP production upon knock out of individual enzymes is calculated and compared to ATP production under normal conditions (wild type). The difference of ATP yield is used as a readout of the contribution of a given enzyme to ATP production.

The *in silico* depletion of IDH1 suggested a significant impact on reactions belonging to glycolysis and MAS (**Figure 4.9a**). Indeed, among the top reactions

affected by blocking reductive carboxylation were major glycolytic enzymes, such as GAPDH and pyruvate kinase (PK), as well as glutamate-oxaloacetate transaminase 1 (GOT1) and MDH1, two components of MAS (**Figure 4.9a**). Interestingly, I found that the *in silico* deletion of IDH1 led to a 10% reduction of ATP yield in N80 (**Figure 4.9b**) but had no effects on ATP production in N7. Moreover, among components of MAS, I observed a striking increase in the contribution of MDH1 to ATP production in N80 compared with N7 model (**Figure 4.9b**). These results suggest that cytosolic reductive carboxylation and MDH1 are linked to glycolysis and subsequent ATP generation. In support of this hypothesis, lactate production decreased when IDH1, but not IDH2, was silenced in N80 cells (**Figure 4.9c**). These results are in line with the recent observation that MDH1 can support glycolysis via recycling of cytosolic NADH in proliferating cells (Hanse et al. 2017).

I then wanted to investigate whether the synthesis of cytosolic malate via MDH1 could support glycolysis in cells with mitochondrial dysfunction. To this aim, I first assessed the functional consequences of the suppression of MDH1 in N80 cells (**Figure 4.10a**). Production of malate m+1 and fumarate m+1 from 1-^{13}C-glutamine was markedly reduced in MDH1-depleted N80 cells, compared to non-

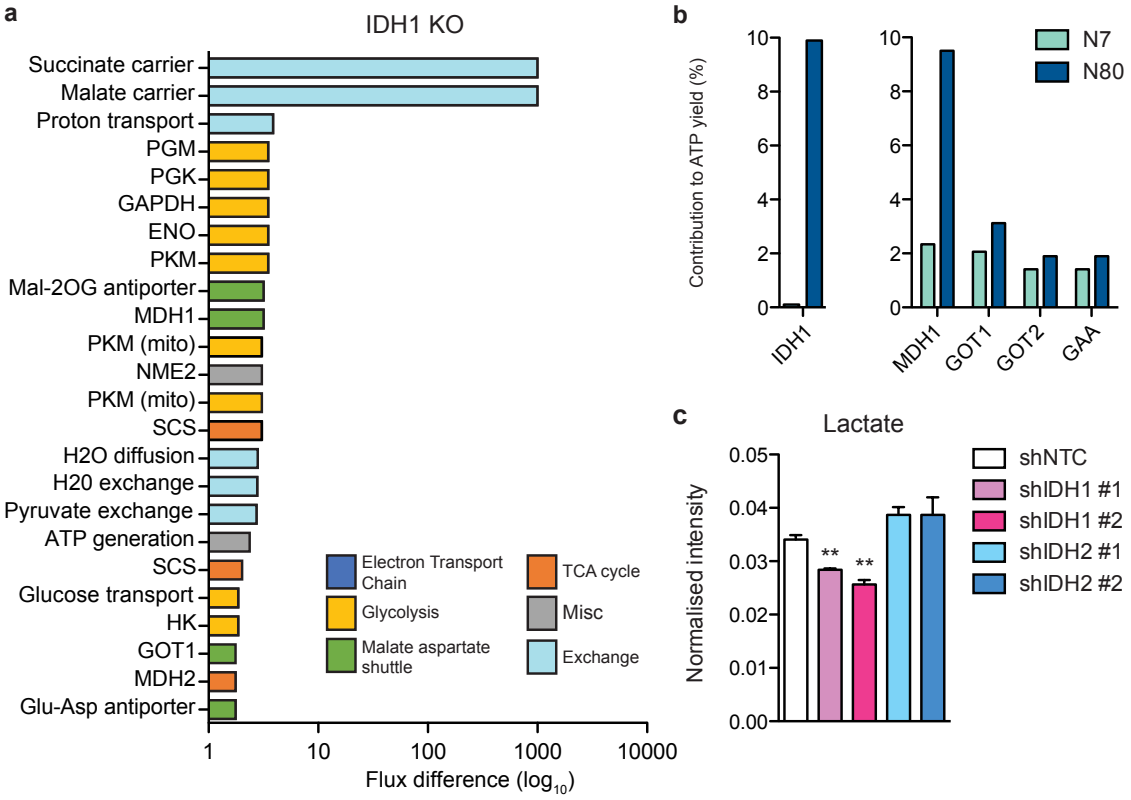

Figure 4.9: Metabolic modelling predicts association between reductive carboxylation, MDH1 and glycolysis. a) Top 10% affected reactions in N80 model upon deletion of IDH1 reaction as predicted by metabolic modelling. Each reaction is colour-coded based on distribution into metabolic pathways. **b)** Percentage of contribution to ATP production for the indicated enzymes, as predicted by metabolic modelling in N80 and N7 models. **c)** Intracellular lactate levels in N80 cells infected with shRNA constructs targeting IDH1 or IDH2. Data are normalised on non-targeting shRNA control (shNTC). Data are mean ± s.e.m. from three independent cultures. ** indicates two-sided t-test p-value ≤ 0.01.

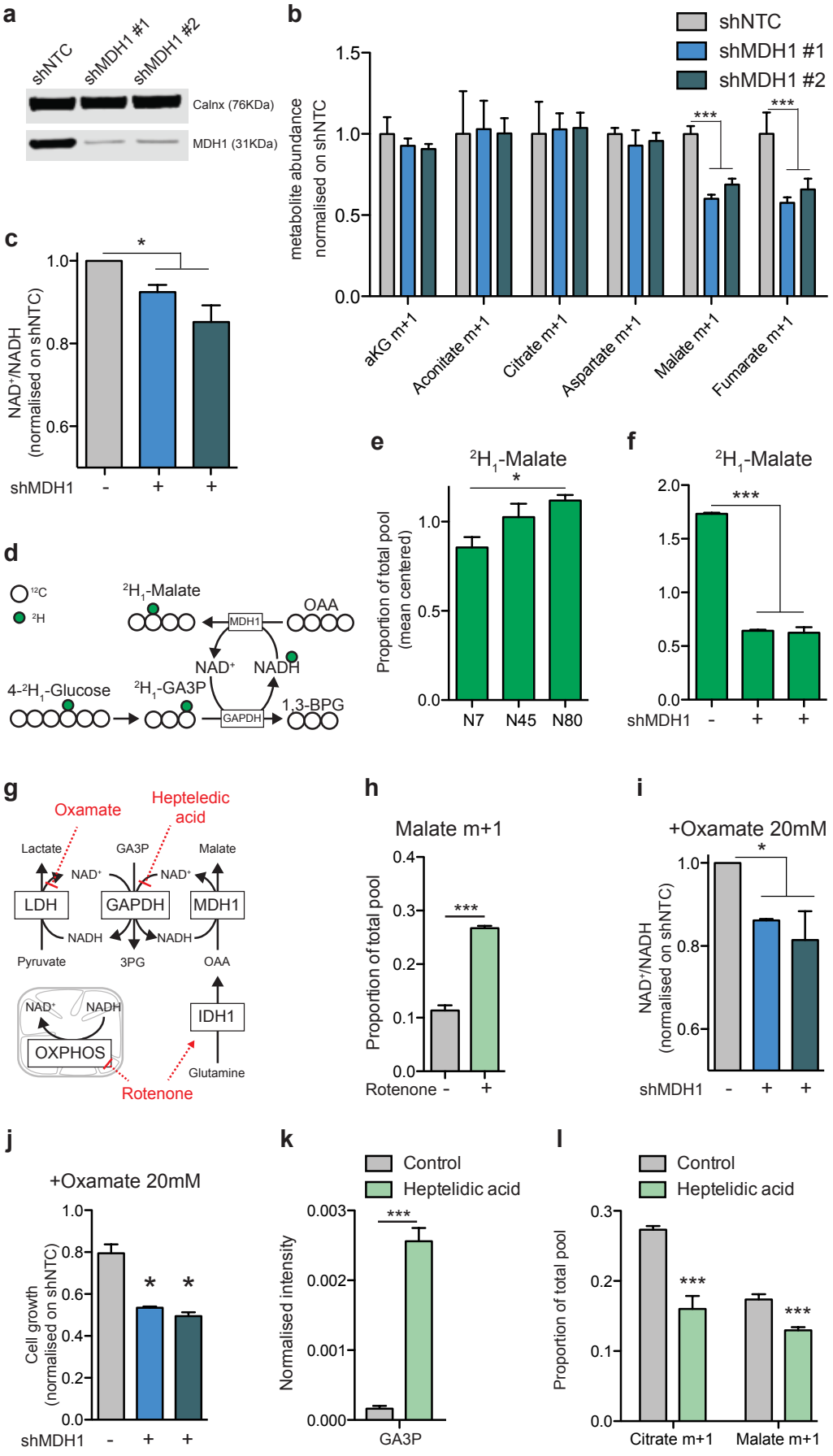

Figure 4.10: *Caption next page*

targeting control (**Figure 4.10b**). These results indicate that silencing of MDH1 has functional consequences in N80 cells, as well as confirm the prediction that reductive carboxylation can generate cytosolic malate via MDH1. Importantly, silencing of MDH1 led to a decrease of NAD^+/NADH ratio (**Figure 4.10c**), suggesting that MDH1 activity plays a role in NADH redox balance.

To directly assess the coupling between glycolytic NADH and MDH1 I performed a hydrogen tracing experiment with 4-^{2}H-glucose, which allows measurement of the transfer of hydrogen atoms from GAPDH-derived NADH to cytosolic metabolites (**Figure 4.10d**) (Lewis et al., 2014). I found that malate m+1 was markedly increased in N80 cells, compared to N45 and N7 (**Figure 4.10e**), confirming the functional coupling between GAPDH and MDH1 (**Figure 4.10f**), as well as the directionality of MDH1. To assess whether coupling of MDH1 and GAPDH is a consequence of mitochondrial dysfunction, I treated N7 cells with rotenone and measured the levels of malate m+1 upon incubation with 4-^{2}H-glucose. I found that treatment with rotenone led to increased levels of malate m+1 in N7 cells, demonstrating that the coupling of MDH1 and GAPDH can be induced by pharmacological suppression of mitochondrial function. To further the role of MDH1 in regulating NADH redox and supporting proliferation of cells with mitochondrial dysfunction, I inhibited LDH, one of the major regulators of NADH balance in the cytosol, with oxamate in shMDH1 N80 cells (**Figure 4.10i**). As shown by measurements of NADH redox state (**Figure 4.10i**) and cell proliferation (**Figure 4.10j**), silencing of MDH1 sensitised cells to LDH inhibition (**Figure 4.10i-j**), suggesting that MDH1 might play an important role in supporting NAD^+/NADH ratio and growth of cells with mitochondrial dysfunction.

The data shown above indicate that a cross-talk between reductive carboxy-

Figure 4.10: (Previous page) Mitochondrial dysfunction is associated with increased metabolic channelling between GAPDH and MDH1. a) Representative western blot analysis of MDH1 expression upon infection of N80 cells with non-targeting control (shNTC) or shRNA constructs targeting MDH1 (shMDH1 #1 and #2). **b)** Levels of metabolites from 1-^{13}C-glutamine in shMDH1 N80 cells. Data are normalised on non-targeting shRNA control (shNTC). **c)** Total levels of NAD+/NADH in shNTC and shMDH N80 cells in basal conditions. **d)** Schematic representation of labelling pattern originating from 4-^{2}H-glucose. Deuterium atoms are represented as green filled circles. **e-f)** Proportion of total pool of malate m+1 originating from 4-^{2}H-glucose in N7, N45 and N80 cells **(e)** and shMDH1 N80 cells **(f)**. **g)** Schematic representation of inhibition of LDH, GAPDH and OXPHOS by oxamate, heptelidic acid and rotenone, respectively. **h)** Proportion of total pool for malate m+1 in N7 cells treated with vehicle control or 0.5 ţM rotenone and incubated with 1-13C-glutamine. **i)** Total levels of NAD^+/NADH in shNTC and shMDH1 N80 cells after treatment with the LDH inhibitor Oxamate (20 mM). Data is normalised on vehicle control (no oxamate) and on shNTC control. **j)** Cell growth of shMDH cells upon treatment with 20 mM of LDH inhibitor Oxamate. Data are normalised on shNTC control. **k)** Normalised intensity of GA3P upon treatment of N7, N45 and N80 cells with vehicle control or 0.5 μM heptelidic acid. **l)** Proportion of total pool for citrate and malate m+1 originating from 1-^{13}C-glutamine in N80 cells upon treatment with 0.5 μM of the GAPDH inhibitor heptelidic acid. **(b-c, f, h-l)** * and *** indicate two-sided t-test p-value $\leq$ 0.05 and 0.001, respectively. **(e)** * indicates one-way ANOVA p-value $\leq$ 0.05.

lation, MDH1 activity, and glycolysis occurs in cells with mitochondrial dysfunction. To further corroborate this cross-talk, I inhibited GAPDH activity with the specific inhibitor heptelidic acid (**Figure 4.10g**) and assessed the activation of reductive carboxylation. Of note, treatment with heptelidic acid led to significant accumulation of GA3P (**Figure 4.10k**). Moreover, I observed diminished levels of citrate m+1 and malate m+1 (**Figure 4.10l**) upon incubation of N80 cells with 1-^{13}C-glutamine. Together with data shown above, this evidence confirms that a cross-talk between reductive carboxylation and glycolysis occurs at the level of MDH1 and GAPDH and suggest that the metabolic channelling between these two enzymes is important for the mutual regulation of these two metabolic pathways.

The hydrogen tracing experiments with 4-^{2}H-glucose (**Figure 4.10d-f**) indicate that metabolite channelling between GAPDH and MDH1 exists. Of note, substrate channeling is known to be facilitated by interaction of individual enzymes into multi-enzymatic complexes (You et al. 2012). I wanted to investigate whether NADH channelling between GAPDH and MDH1 could be supported by physical interaction of these two enzymes. To this aim, I performed co-immunoprecipitation assay and I found that GAPDH interacts with MDH1 (**Figure 4.11a**). Strikingly, I observed that N80 cells display a higher interaction between GAPDH and MDH1, compared to N45 and N7 (**Figure 4.11a**). Importantly, increased interaction between GAPDH and MDH1 in N80 cells was not due to higher protein expression of MDH1 in N80 cells (**Figure 4.11b**). In addition, I observed that a complex of GAPDH and LDH is formed in N7, N45 and N80 cells (**Figure 4.11c**) thus confirming previous evidence of interaction between these two enzymes (Svedrui and Spivey 2006). Finally, immunofluorescence assay showed increased co-localisation between GAPDH and MDH1 in N80 cells, compared to N45 and N7, thus confirming an increased interaction between the two enzymes in the presence of mitochondrial dysfunction (**Figure 4.11d**).

Together, these data support the hypothesis that GAPDH and MDH1 form a multi-enzymatic complex that may facilitate NADH recycling from reductive carboxylation to glycolysis in cells with mitochondrial dysfunction.

4.5 Aspartate supports flux via MDH1 and generates malate

My results indicate that mitochondrial dysfunction reduces the ability of mitochondria to consume NADH and that cytosolic reductive carboxylation provides carbons to recycle NADH via MDH1. In this scenario, the cytosolic component of the MAS, including GOT1, would function as an additional source of oxaloacetate for MDH1 (**Figure 4.12a**). To investigate the directionality of the MAS, cells were cultured in the presence of (U)-^{13}C-aspartate. Strikingly, I found that aspartate is converted to m+4 malate and fumarate, displaying the highest proportion of labelling in N80, compared to N45 and N7 cells (**Figure 4.12b**). Yet, I could not detect labelled succinate and the labelling of citrate from aspartate did not correlate with mitochondrial function (**Figure 4.12c**), indicating that utilisation of aspartate is predominantly cytosolic. In support of this hypothesis, defects of cellular respiration in N80 cells were not rescued by exogenous aspartate (**Figure 4.12d**), indicating that aspartate does not contribute to CAC in the mitochondria. Treatment with rotenone led

to increase m+4 labelling of malate and fumarate (**Figure 4.12b**) from (U)-^{13}C-

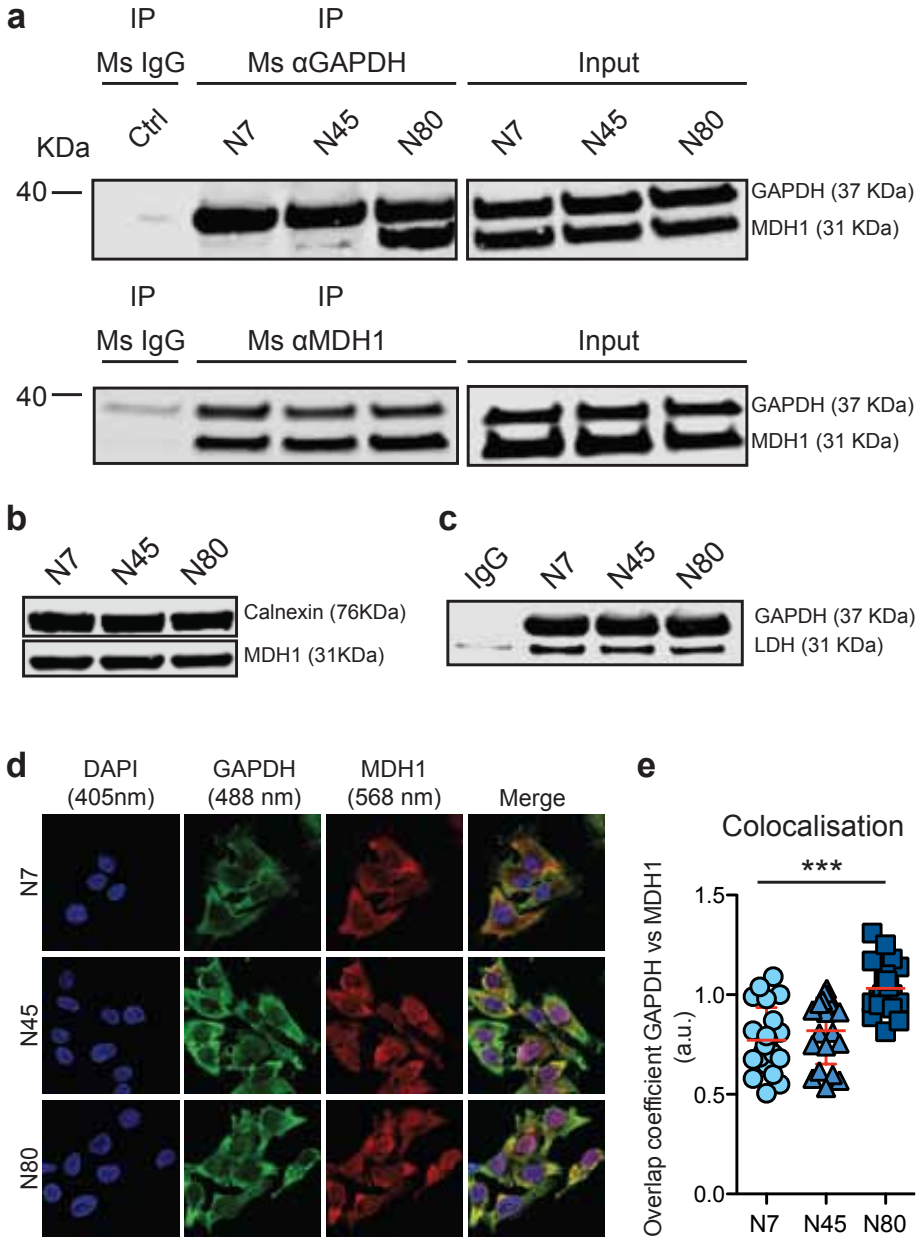

Figure 4.11: A complex between GAPDH and MDH1 is formed in cells with mitochondrial dysfunction. a) GAPDH (top) and MDH1 (bottom) were used as baits in an immunoprecipitation assay on lysates obtained from N7, N45 and N80 cells. The interaction between GAPDH and MDH1 is shown by co-IP. Immunoglobulin G (IgG) is used in negative isotype controls. Representative images from two independent experiments. **b)** Western blot analysis of MDH1 expression in N7, N45 and N80 cells. Calnexin was used as loading control. **c)** Immunoprecipitation analysis of GAPDH in N7, N45 and N80 cells. Interaction between GAPDH and LDH is shown by co-IP. Mouse IgG were used as isotype control for the IP reaction. **d)** Representative immunofluorescence images of N7, N45 and N80 cells stained with DAPI (blue), GAPDH (green) and MDH1 (red). **e)** Co-localisation of fluorescence signals from GAPDH and MDH1 is shown. Data are mean $\pm$ s.d. from 20-30 cells per conditions. * indicates one-way ANOVA p-value ≤ 0.05.

aspartate, thus suggesting that contribution of aspartate to these metabolite pools is linked with mitochondrial function. The synthesis of cytosolic malate from aspartate requires transamination to oxaloacetate (OAA), followed by reduction of OAA to malate via MDH1. I reasoned that N80 cells might be dependent on aspartate transamination. Consistent with this hypothesis, aspartate supplementation could rescue proliferation of N80 cells grown in galactose, while only minor effects were observed in N7 and N45 cells (**Figure 4.12e**). Moreover, treatment with aminooxiacetate (AOA), an inhibitor of transaminases, prevented the beneficial effects of aspartate for N80 cells grown in galactose (**Figure 4.12f**).

These results indicate that transamination of aspartate supports flux through MDH1 and synthesis of cytosolic malate to support proliferation of cells with mitochondrial dysfunction.

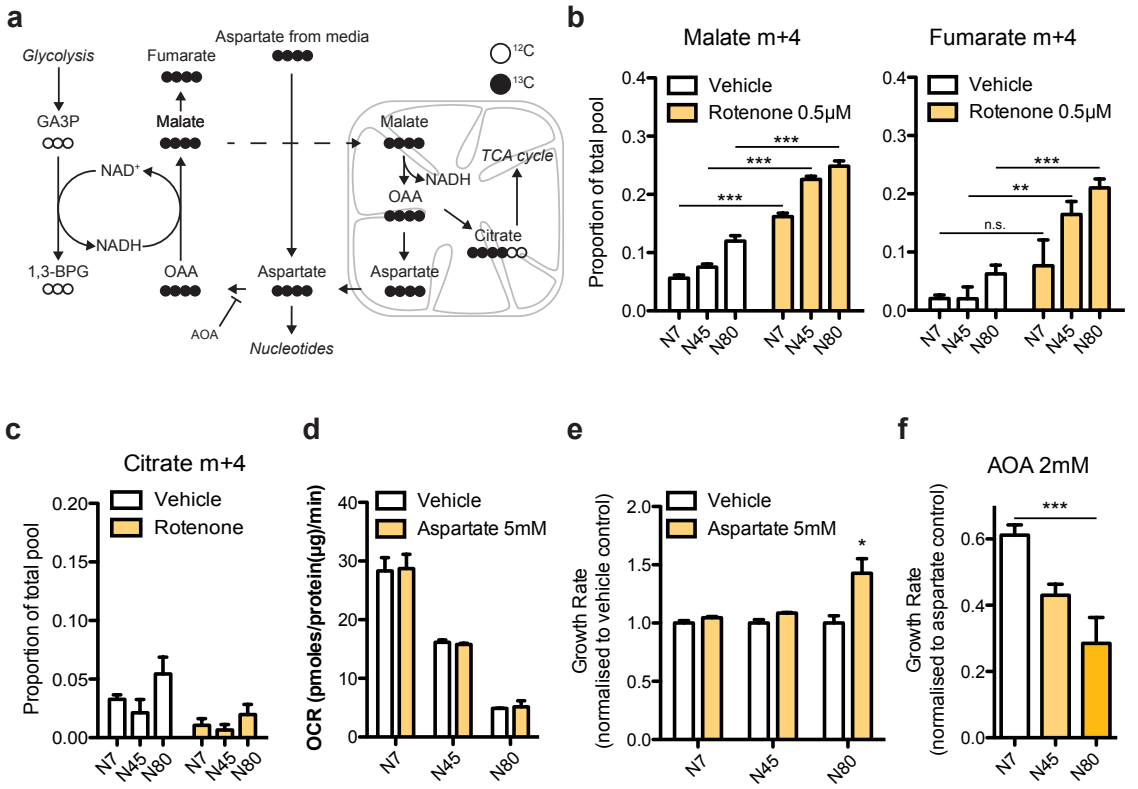

Figure 4.12: Aspartate transamination supports flux through MDH1 and generation of malate. a) Schematic representation of malate-aspartate shuttle (MAS) and labelling patterns originating from U-^{13}C-aspartate. **b-c)** Proportion of total pool of malate and fumarate m+4 **(b)** and citrate m+4 **(c)** in N7, N45 and N80 cells grown in the presence of U-^{13}C-aspartate upon treatment with vehicle control or 0.5 μM rotenone. **d)** Oxygen consumption rate (OCR) of N7, N45 and N80 cells in basal conditions or upon supplementation with 5 mM aspartate. **e-f)** Cell growth of N7, N45 and N80 cells grown in 25 mM galactose and supplemented with 5 mM aspartate **(e)** upon treatment with 2 mM of aminooxyacetate **(f)**. Data are mean $\pm$ s.e.m. from at least three independent cultures. **(b-e)** *, ** and *** indicate two-sided t-test p-value $\leq$ 0.05, 0.01 and 0.001, respectively. **(f)** *** indicates one-way ANOVA p-value $\leq$ 0.001.

4.6 MDH1 regulates cell migration

Finally, I investigated the functional outcome of the metabolic rewiring prompted by dysfunctional mitochondria. Recently, it was shown that production of ATP by glycolysis, rather than by mitochondrial OXPHOS, supports cell migration (Yizhak

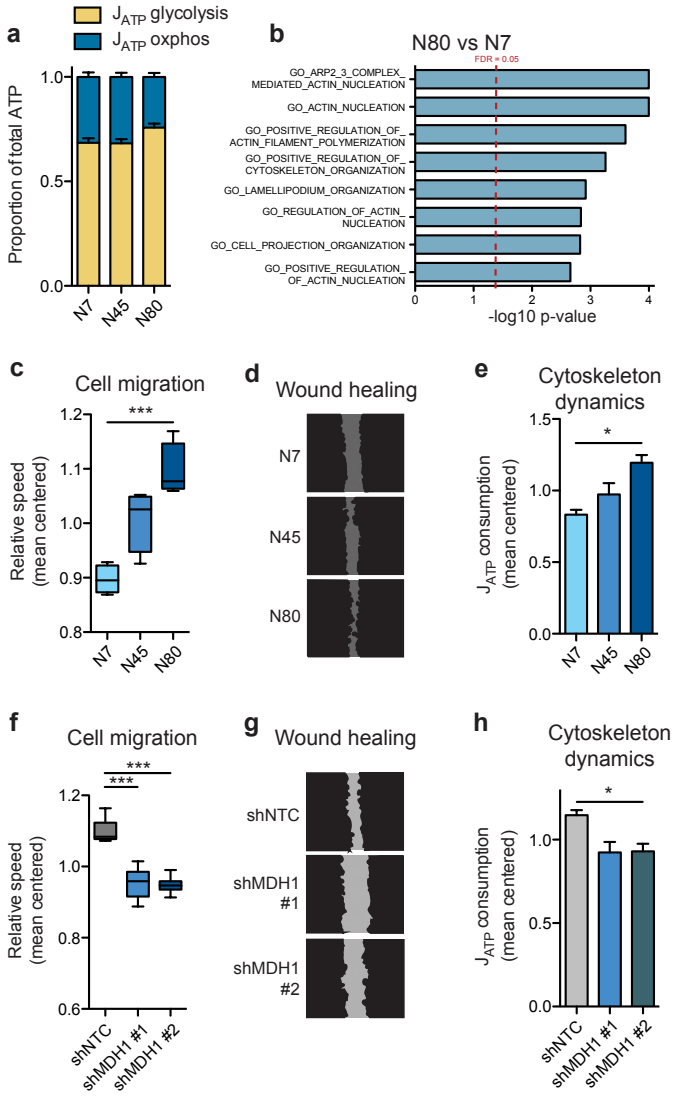

Figure 4.13: Mitochondrial dysfunction is linked with cell migration. **a)** Proportion of total ATP originating from glycolysis and oxidative phosphorylation in N7, N45 and N80 cells, as calculated from OCR and ECAR measurements. **b)** Enrichment p-values (-$\log_{10}$) of gene ontology (GO) biological processes involved in cell migration and cytoskeleton remodelling. Red dashed line indicates false discovery rate (FDR) = 0.05. **c, f)** Migration speed of N7, N45 and N80 cells **(c)** or shMDH1 cells **(f)** as measured by wound healing assay. **d, g)** Representative images of wound-healing assay 6 hours after application of wound in N7, N45 and N80 **(d)** and shMDH1 **(g)** cells. **e, h)** Values of J_{ATP} consumption due to cytoskeleton remodelling based on calculations from OCR and ECAR data upon treatment with 1 ţM nocodazole in N7, N45 and N80 cells **(e)** or shMDH1 cells **(h)**. All Data are mean $\pm$ s.e.m. from three to four independent cultures. * and *** indicate p-value $\leq$ 0.05 and 0.001, respectively, from ANOVA **(c, e)** or Dunnetts test **(f, h)**.

et al. 2014). I measured the contribution of glycolysis and OXPHOS to ATP production in N7, N45 and N80 cells via quantification of intracellular metabolic flux (Mookerjee et al. 2017) and found that N80 cells displayed an increased reliance on the glycolytic pathway for the ATP production (**Figure 4.13a**). Therefore, I hypothesised that switching to glycolytic ATP production might be associated with increased cell motility in this cell model. A proteomics analysis of N7 and N80 cells followed by Gene Ontology (GO) enrichment analysis revealed that processes involved in cell migration and cytoskeleton remodelling were significantly altered between N7 and N80 cells (**Figure 4.13b**). I therefore assessed cell migration in N7, N45 and N80 cells by performing wound-healing assay *in vitro*. I found that migratory capacity increased proportionally with the levels of mitochondrial dysfunction, with N80 cells displaying highest migration speed (**Figure 4.13c-d**). In line with this result, higher amounts of ATP were used for cytoskeletal remodelling in N80, compared to N7 and N45 (**Figure 4.13e**).

Finally, I assessed the role of MDH1 in supporting this process. I found that the migratory abilities of N80 were markedly reduced upon silencing of MDH1, compared to non-targeting control (**Figure 4.13f-g**), and shMDH1 cells showed reduced utilisation of ATP for cytoskeleton dynamics (**Figure 4.13h**). In addition, I observed that co-localisation of MDH1 with actin followed the trend of mitochondrial dysfunction in N7, N45 and N80 cells (**Figure 4.13i-j**).

Together, these results indicate that mitochondrial dysfunction is associated with increased migration and that, by sustaining glycolytic ATP generation, MDH1 plays an important role in supporting cell migration.

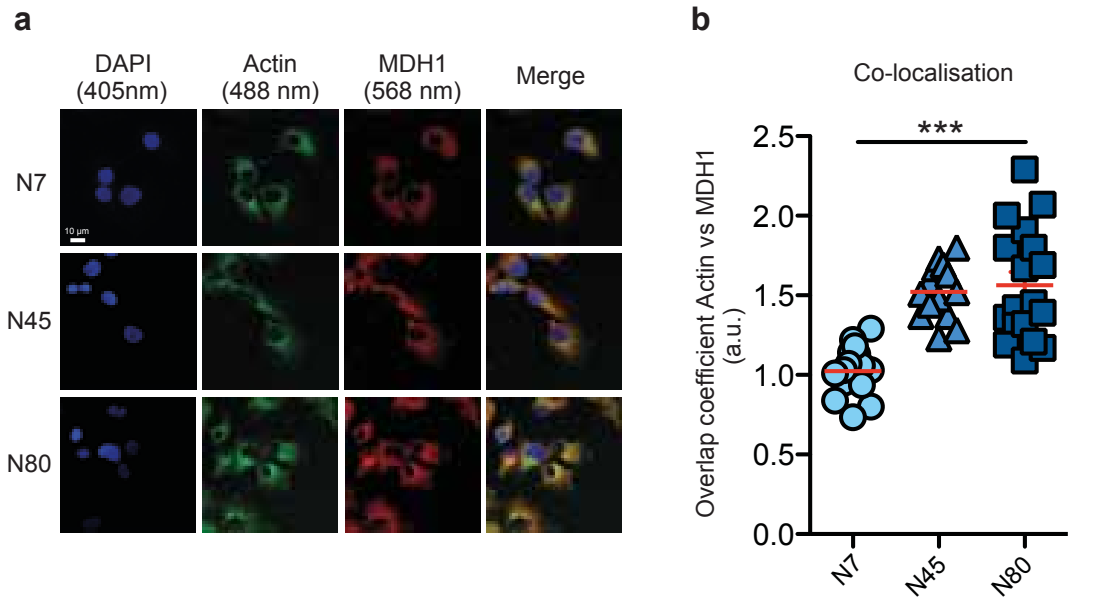

Figure 4.14: Co-localisation of MDH1 with actin cytoskeleton. a) Immunofluorescence images of N7, N45 and N80 cells stained with DAPI (DNA, blue), phalloidin (actin, green) or antibody against MDH1 (red). White arrows indicate areas of co-localisation between MDH1 and actin in N80 cells. **b)** Quantification of co-localisation between MDH1 and Phalloidin (actin). Data were obtained from 20-30 cells per condition. *** indicates ANOVA p-value ≤ 0.001.

4.7 Discussion

In this chapter I exploited a panel of isogenic cell lines that harbour a varying degree of heteroplasmy for a mitochondrial DNA (mtDNA) mutation that affects ATP synthase. I applied this unique cell model to investigate the link between mitochondrial dysfunction and glycolysis. This model is greatly improved in respect to possible gross chromosomal alterations occurring during the long-term selection of cybrid clones (King and Attardi 1989; Martnez-Reyes et al. 2016). Using *in silico* metabolic modeling, I predicted and experimentally validated that increasing levels of heteroplasmy result in an overall impairment of the respiratory chain and in a decreased utilisation of mitochondrial reduced nicotinamide adenine dinucleotide (NADH). This respiratory chain defect indirectly affects several pathways involved in the generation of mitochondrial reducing equivalents, such as the citric acid cycle (CAC) and malate-aspartate shuttle (MAS). Indeed, reduced oxidation of NADH by the mitochondrial respiratory chain (RC) would result in a depletion of oxidised nicotinamide adenine dinucleotide (NAD^+) from the mitochondrial matrix and this could affect the activity the CAC and MAS enzyme malate dehydrogenase 2 (MDH2). Importantly, reduced activity of MDH2 would limit the availability of oxaloacetate, a rate-limiting metabolite that supports generation of citrate, and would likely result in slow CAC flux. In addition, reduced flux through MDH2 would result in a block of the MAS, therefore limiting the entry of NADH into mitochondria and forcing cytosolic enzymes, such as lactate dehydrogenase (LDH), to maintain NAD redox balance. This is a very well known scenario under hypoxia, where disruption of MAS, NAD redox imbalance and activation of LDH have been extensively reported (Lu, Zhou, et al. 2008; Chouchani et al. 2014).

Among most striking metabolic adaptation that I observed upon mitochondrial dysfunction is the activation of cytosolic reductive carboxylation of glutamine. Increased reductive carboxylation was also accompanied by decreased oxidation of glutamine in the mitochondria. Although the determinants of this effect have not been investigated it is possible that this phenomenon is due, at least in part, to diminished availability of NAD^+ for mitochondria-specific glutamate dehydrogenase. The inhibition of glutamate oxidation in the mitochondria would then favour the transamination of glutamate by glutamate-oxaloacetate transaminase 1 (GOT1) in the cytosol and lead to reductive carboxylation.

Reductive carboxylation supports proliferation of cancer cells with mitochondrial dysfunction (Mullen et al. 2012) and cells grown under hypoxia use reductive carboxylation for *de novo* lipid synthesis (Metallo et al. 2012). Yet, its biochemical determinants remain unclear. In this work, I found that reductive carboxylation is driven by changes in $NADH/NAD^+$ levels and that it supports metabolic flux through the NADH-consuming malate dehydrogenase 1 (MDH1). Together these data indicate, for the first time, that reductive carboxylation, beyond being used for biosynthetic pathways, is directly involved in the regeneration of cytosolic NAD^+ to maintain redox balance and glycolytic flux. In this scenario, cytosolic reductive carboxylation operates as substitute for MAS, tightly coupling the oxidation of glutamine with glycolysis, likely enabling glycolytic flux for ATP synthesis and biomass generation. My findings indicate that MDH1 is an important enzyme when high glycolytic capacity is needed to support anabolic demands or to compensate for NAD redox imbalance upon mitochondrial dysfunction. These results are in line

with a recent study that demonstrated that MDH1 can recycle glycolytic NADH and support proliferation of cancer cells and activated lymphocytes (Hanse et al. 2017), two settings characterised by diminished mitochondrial function and high reliance on glycolysis (Vander Heiden et al. 2009; Pearce, Poffenberger, et al. 2013).

I also showed evidence that MDH1 physically interacts with the key glycolytic enzyme glyceraldehyde 3-phosphate dehydrogenase (GAPDH) enhancing the recycling of glycolytic NADH. Interaction of glycolytic enzymes into a single multienzymatic complex has been previously observed (Menard et al. 2014). Importantly, multienzymatic complexes can offer several advantages, including higher solvation and substrate channelling. Formation of a multienzymatic complex between GAPDH and LDH has already been reported (Svedrui and Spivey 2006) and NADH channelling between these two enzymes is known to be rate-limiting for glycolytic flux. My data suggest that a multienzymatic complex between GAPDH, LDH, and MDH1 can be formed and this can be regulated by changes in the metabolic state of the cell induced by mitochondrial dysfunction. Indeed, the extent of interaction and of NADH channelling between MDH1 and GAPDH depends on mitochondrial function and is not due to transcriptional or translational regulation, as protein levels of MDH1 are comparable between N7, N45 and N80 cells. This observation suggests that the interaction between MDH1 and GAPDH might be dictated by mitochondria-driven changes in cytosolic chemical environment, such as the availability of NAD^+. More work is required to establish the biophysical basis of the formation of this multienzymatic complex.

Recently published work has highlighted the link between mitochondrial dysfunction and acquisition of cell migratory abilities, whereby pharmacological inhibition of the respiratory chain (Porporato et al. 2014), genetic impairment of the TCA cycle (Loriot et al. 2012; Sciacovelli, Gonçalves, et al. 2016), or loss of transcriptional regulation for mitochondrial biogenesis (Torrano et al. 2016) can lead to acquisition of migratory properties and induce metastasis of cancer cells. In addition, these results support the findings reported in the previous chapter whereby downregulation of genes encoding for mitochondrial enzymes is associated with the induction of epithelial-to-mesenchymal transition (EMT), a genetic signature supporting migration and metastasis (Gaude and Frezza 2016). Yet, the sustaining mechanisms remain unclear. My results show that mitochondrial dysfunction is associated with increased production of ATP from glycolysis and increased migratory capacity. These results are in line with the observation that increased glycolytic vs oxidative generation of ATP increases cell migration (Yizhak et al. 2014). Of note, silencing of MDH1, which supports glycolysis upon mitochondrial impairment, can reduce cell migration. My findings are also in line with the recent evidence that glycolytic enzymes can sustain cell motility by localising with components of the cytoskeleton and providing local generation of ATP (De Bock et al. 2013).

Together, my results suggest that, in the presence of mitochondrial dysfunction, enhanced ATP yield from glycolysis, due to interaction and metabolic channelling between MDH1 and GAPDH, may increase local availability of ATP for cytoskeleton remodeling. Finally, these results demonstrate, for the first time, that MDH1 is an important mechanism to support cell migration.

In conclusion, my study is the first to provide a biochemical explanation for the emergence of cytosolic reductive carboxylation in the presence of mitochondrial dysfunction. This work might help to elucidate metabolic vulnerabilities of cells

that rely on aerobic glycolysis for their proliferation and migration, such as activated lymphocytes and metastatic cancer cells.

Perspectives

This study identifies for the first time the association of mitochondrial dysfunction with patient prognosis across several different types of cancer. Poor patient prognosis is associated with the induction of a migratory and invasive phenotype, a major determinant of cancer metastasis. The molecular underpinnings of this association entail the induction of a glycolytic state known to support anabolic growth (Vander Heiden et al. 2009). My findings expand the general understanding of glycolysis as a promoter of anabolism and link such metabolic state to increased migration. Importantly, the interaction of the enzymes MDH1 and GAPDH is reported for the first time, and is found to support cell migratory abilities.

These results raise critical questions regarding cancer development and progression. Selection of a metabolic state where mitochondrial function is depressed may occur at different stages of cancer transformation. Signalling from mutated oncogenes and tumour suppressors may partially inhibit mitochondrial function to increase the production of anabolic intermediates through glycolysis, while maintaining minimal flux through the CAC and OXPHOS. Notably, selection of heteroplasmic mtDNA mutations might result in bioenergetic defects and lead to a similar anabolic state. Furthermore, upon cell proliferation and tumour expansion, limited availability of nutrients and oxygen might induce hypoxic signalling and further reduce mitochondrial function of inner areas in a tumour mass. Cancer cells that successfully activate a glycolytic program might concomitantly be endorsed with increased migratory abilities, thus facilitating access to oxygen and nutrients and increasing cell survival. In this scenario, induction of cell migration by chance could become a necessity (Monod 1971) and invasion to different tissues might constitute a bottleneck for the survival of cancer cells that successfully abandoned the primary tumour mass.

The finding that a novel multienzymatic complex is formed between MDH1 and GAPDH might have important implications for cancer therapy. Inhibition of this interaction via silencing of MDH1 could reduce proliferation and migration of cells with mitochondrial dysfunction. Inhibition of protein-protein interaction that are specifically engaged in cancer cells is a therapeutic strategy that recently showed increased success in limiting proliferation of cancer cells (Shangary and Wang 2009; Taylor et al. 2009). Despite metabolic channeling between MDH1 and GAPDH has recently been shown to occur also in activated lymphocytes (Hanse et al. 2017), the interaction between these two enzymes might be selective for cancer cells. In light of this, development of a chemical inhibitor aimed at blocking the interaction between MDH1 and GAPDH might constitute a novel therapeutic strategy to inhibit migration of cancer cells.

It is important to mention that my study is not devoid of limitations and more experiments are required to improve our understanding of the mechansims as-

sociated with mitochondrial dysfunction. For instance, I observed that the level of interaction between GAPDH and MDH1 correlates with the degree of mitochondrial dysfunction. Though, the mechanisms linking altered mitochondrial function to interaction of the two enzymes have not been addressed by my study and more conclusive data on the association between mitochondrial dysfunction and GAPDH-MDH1 interaction is needed. A possible explanation of the cross-talk between mitochondria and interaction of metabolic enzymes could come from the ability of mitochondria to alter the levels of intracellular metabolites, potentially inducing a chemical environment that facilitates enzyme interaction. For instance, reduced availability of NAD^+ could induce conformational changes of NAD^+-dependent GAPDH, exposing protein residues for the interaction with other enzymes. Further investigation of such molecular underpinnings might help to clarify the link between mitochondrial dysfunction and selective interaction of metabolic enzymes. Furthermore, the finding that mitochondrial dysfunction induces cell migration has not been linked to increased metastatic ability of cancer cells. The role of mitochondrial function in supporting cancer cell metastasis could be validated in an *in vivo* experimental setting. For instance, intravenous injection of N7, N45 and N80 cells in nude mice might shed light on the ability of cells with mitochondrial dysfunction to colonise tissues and form metastases.

In conclusion, my study identifies an association between mitochondrial dysfunction and survival of cancer patients and helps describing the link between mitochondrial metabolism and cell migration. Despite further investigation is needed to understand the relevance of these findings for cancer metastasis, my study identifies a metabolic liability of cells with mitochondrial dysfunction that could be harnessed for cancer therapy.

Acknowledgements

I am extremely thankful, foremost, to Doctor Christian Frezza for giving me the great opportunity to further my career as a PhD student in his laboratory. As my scientific supervisor, he was able to diffuse his authority through a very unique mixture of expertise, humility and respect. The brightness of his mind and his constant curiosity have been, and will be, highly inspiring for me. Christian has also been an invaluable mentor and friend. Extremely understanding, he patiently guided me through the several obstacles I encountered during this journey, and helped me finding my way amongst scientific concerns and career decisions. His level of care and preoccupation went well beyond the academic duties of a PhD supervisor, supporting me during important life decisions and stimulating me with countless cultural and life-style inputs. In these years Christian has become a model of leadership that I wish to follow in my future career.

I am very thankful to Doctor Marco Sciacovelli for the extensive support during my PhD. Marco has been extremely helpful through all these years by carefully instructing me on numerous laboratory techniques, and by always sparing his time with generosity for the wide range of questions and doubts an inexperienced researcher can have. In addition, he has been a great lab companion, with his positive attitude and sense of humour helping to transform frustrating moments into fun memories. I have been very lucky to share this experience with a researcher of his caliber and with such a good friend, and I wish him a bright future in science.

My warmest thanks are for Doctor Katherine Bird for supporting me outside the lab in the journey through my PhD. She has been able to combine a genuine interest for my scientific findings together with an infinite patience for all the concerns, complaints, and changes of direction that I experienced in the past three years as a PhD student, and as a man. Her positive attitude and unconditioned caring made me enjoy even the most frustrating moments of my PhD, partly because I understood that life cannot be too bad if you have someone like Katy next to you.

I want to thank Doctor Sophia da Costa for the extreme patience with the countless samples that I collected and persistently submitted to her for mass spec metabolomics. Her precision and professional attitude have been instrumental for the accuracy and reproducibility of many of my findings.

I am very thankful to all the people that helped me collecting the data for this thesis. I am very thankful to Christina Schmidt for her help with immuno-precipitation assays. The period she spent under my supervision resulted in a key finding for my PhD thesis. Her passion and dedication to her summer project have been outstand-

ing and I am sure she will have a bright career in science or wherever else life will lead her.

I also thank Dr Payam Gammage and Dr Michal Minczuk for providing the NARP cell lines, as well as for their help with quantification of heteroplasmy and data interpretation. Dr Thomas Blacker and Dr Gyorgy Szabadkai taught me how to perform UV microscopy and obtain NADH autofluorescence measurements. I thank Dr John O'Neill for performing proteomics analysis of the NARP cell lines and Aurelien Dugourd and Julio Saez Rodriguez for analysing proteomics data.

Bibliography

Adam, Julie et al. (2011). "Renal cyst formation in Fh1-deficient mice is independent of the Hif/Phd pathway: roles for fumarate in KEAP1 succination and Nrf2 signaling". In: *Cancer Cell* 20.4, pp. 524–537.

Ahn, Christopher S and Christian M Metallo (2015). "Mitochondria as biosynthetic factories for cancer proliferation". In: *Cancer & Metabolism* 3.1, p. 1.

Almuhaideb, Ahmad, Nikolaos Papathanasiou, and Jamshed Bomanji (2011). "^{18}F-FDG PET/CT imaging in oncology". In: *Annals of Saudi Medicine* 31.1, p. 3.

Amary, M Fernanda et al. (2011). "IDH1 and IDH2 mutations are frequent events in central chondrosarcoma and central and periosteal chondromas but not in other mesenchymal tumours". In: *The Journal of Pathology* 224.3, pp. 334–343.

Anastasiou, Dimitrios (2017). "Tumour microenvironment factors shaping the cancer metabolism landscape". In: *British Journal of Cancer* 116.3, p. 277.

Avery, Oswald T, Colin M MacLeod, and Maclyn McCarty (1944). "Studies on the chemical nature of the substance inducing transformation of Pneumococcal types". In: *Journal of Experimental Medicine* 79.2, pp. 137–158.

Bai, Yidong et al. (2001). "Lack of Complex I Activity in Human Cells Carrying a Mutation in MtDNA-encoded ND4 Subunit Is Corrected by theSaccharomyces cerevisiae NADH-Quinone Oxidoreductase (NDI1) Gene". In: *Journal of Biological Chemistry* 276.42, pp. 38808–38813.

Barbakh, Wesam Ashour, Ying Wu, and Colin Fyfe (2009). "Review of clustering algorithms". In: *Non-Standard Parameter Adaptation for Exploratory Data Analysis*. Springer, pp. 7–28.

Bartesaghi, Stefano et al. (2015). "Inhibition of oxidative metabolism leads to p53 genetic inactivation and transformation in neural stem cells". In: *Proceedings of the National Academy of Sciences of the United States of America* 112.4, pp. 1059–1064.

Barthel, Andreas et al. (1999). "Regulation of GLUT1 gene transcription by the serine/threonine kinase Akt1". In: *Journal of Biological Chemistry* 274.29, pp. 20281–20286.

Baudot, Alice D et al. (2016). "p53 directly regulates the glycosidase FUCA1 to promote chemotherapy-induced cell death". In: *Cell Cycle* 15.17, pp. 2299–2308.

Bauer, Daniel E et al. (2005). "ATP citrate lyase is an important component of cell growth and transformation". In: *Oncogene* 24.41, p. 6314.

Baysal, Bora E et al. (2000). "Mutations in SDHD, a mitochondrial complex II gene, in hereditary paraganglioma". In: *Science* 287.5454, pp. 848–851.

Benz, Matthias R et al. (2011). "^{18}F-FDG PET/CT for monitoring treatment responses to the epidermal growth factor receptor inhibitor erlotinib". In: *Journal of Nuclear Medicine* 52.11, pp. 1684–1689.

Berwick, Daniel C et al. (2002). "The identification of ATP-citrate lyase as a protein kinase B (Akt) substrate in primary adipocytes". In: *Journal of Biological Chemistry* 277.37, pp. 33895–33900.

Bester, Assaf C et al. (2011). "Nucleotide deficiency promotes genomic instability in early stages of cancer development". In: *Cell* 145.3, pp. 435–446.

Birsoy, Kvanç et al. (2015). "An essential role of the mitochondrial electron transport chain in cell proliferation is to enable aspartate synthesis". In: *Cell* 162.3, pp. 540–551.

Bister, Klaus and Peter H Duesberg (1979). "Structure and specific sequences of avian erythroblastosis virus RNA: evidence for multiple classes of transforming genes among avian tumor viruses". In: *Proceedings of the National Academy of Sciences of the United States of America* 76.10, pp. 5023–5027.

Blacker, Thomas S and Michael R Duchen (2016). "Investigating mitochondrial redox state using NADH and NADPH autofluorescence". In: *Free Radical Biology and Medicine* 100, pp. 53–65.

Boidot, Romain et al. (2011). "Regulation of monocarboxylate transporter MCT1 expression by p53 mediates inward and outward lactate fluxes in tumors." In: *Cancer Research*, canres–2474.

Borger, Darrell R et al. (2014). "Circulating oncometabolite 2-hydroxyglutarate is a potential surrogate biomarker in patients with isocitrate dehydrogenase-mutant intrahepatic cholangiocarcinoma". In: *Clinical Cancer Research* 20.7, pp. 1884–1890.

Boroughs, Lindsey K and Ralph J DeBerardinis (2015). "Metabolic pathways promoting cancer cell survival and growth". In: *Nature Cell Biology* 17.4, p. 351.

Brigelius-Flohé, Regina and Helmut Sies (2015). *Diversity of selenium functions in health and disease*. Vol. 38. CRC Press.

Calabrese, Claudia et al. (2013). "Respiratory complex I is essential to induce a Warburg profile in mitochondria-defective tumor cells". In: *Cancer & Metabolism* 1.1, p. 11.

Cannino, Giuseppe et al. (2012). "Glucose modulates respiratory complex I activity in response to acute mitochondrial dysfunction". In: *Journal of Biological Chemistry* 287.46, pp. 38729–38740.

Cantó, Carles and Johan Auwerx (2010). "AMP-activated protein kinase and its downstream transcriptional pathways". In: *Cellular and Molecular Life Sciences* 67.20, pp. 3407–3423.

Cantor, Jason R and David M Sabatini (2012). "Cancer cell metabolism: one hallmark, many faces". In: *Cancer Discovery* 2.10, pp. 881–898.

Cardaci, Simone et al. (2015). "Pyruvate carboxylation enables growth of SDH-deficient cells by supporting aspartate biosynthesis". In: *Nature Cell Biology* 17.10, pp. 1317–1326.

Catanzaro, Daniela et al. (2015). "Inhibition of glucose-6-phosphate dehydrogenase sensitizes cisplatin-resistant cells to death". In: *Oncotarget* 6.30, p. 30102.

Cavalli, Luciane R, Marileila Varella-Garcia, Bertrand C Liang, et al. (1997). "Diminished tumorigenic phenotype after depletion of mitochondrial DNA". In: *Cell Growth and Differentiation* 8, pp. 1189–1198.

Cervera, Ana M et al. (2009). "Inhibition of succinate dehydrogenase dysregulates histone modification in mammalian cells". In: *Molecular Cancer* 8.1, p. 89.

Chajès, Véronique et al. (2006). "Acetyl-CoA carboxylase α is essential to breast cancer cell survival". In: *Cancer Research* 66.10, pp. 5287–5294.

Chang, Hwai Wen et al. (1997). "Transformation of chicken cells by the gene encoding the catalytic subunit of PI 3-kinase". In: *Science* 276.5320, pp. 1848–1850.

Chatterjee, A, E Mambo, and D Sidransky (2006). "Mitochondrial DNA mutations in human cancer". In: *Oncogene* 25.34, p. 4663.

Chen, Walter W, Kvanç Birsoy, et al. (2014). "Inhibition of ATPIF1 ameliorates severe mitochondrial respiratory chain dysfunction in mammalian cells". In: *Cell Reports* 7.1, pp. 27–34.

Chen, ZX and S Pervaiz (2010). "Involvement of cytochrome *c* oxidase subunits Va and Vb in the regulation of cancer cell metabolism by Bcl-2". In: *Cell Death and Differentiation* 17.3, p. 408.

Cheong, Heesun et al. (2012). "Therapeutic targets in cancer cell metabolism and autophagy". In: *Nature Biotechnology* 30.7, pp. 671–678.

Chouchani, Edward T et al. (2014). "Ischaemic accumulation of succinate controls reperfusion injury through mitochondrial ROS". In: *Nature* 515.7527, p. 431.

Chowdhury, Rasheduzzaman et al. (2011). "The oncometabolite 2-hydroxyglutarate inhibits histone lysine demethylases". In: *EMBO Reports* 12.5, pp. 463–469.

Comerford, Sarah A et al. (2014). "Acetate dependence of tumors". In: *Cell* 159.7, pp. 1591–1602.

Contractor, Tanupriya and Chris R Harris (2012). "p53 negatively regulates transcription of the pyruvate dehydrogenase kinase Pdk2". In: *Cancer Research* 72.2, pp. 560–567.

Cori, Carl F and Gerty T Cori (1925). "The carbohydrate metabolism of tumors II. Changes in the sugar, lactic acid, and CO_2-Combining Power of Blood Passing through a tumor". In: *Journal of Biological Chemistry* 65.2, pp. 397–405.

Cowley, Glenn S et al. (2014). "Parallel genome-scale loss of function screens in 216 cancer cell lines for the identification of context-specific genetic dependencies". In: *Scientific Data* 1, p. 140035.

Cunningham, John T et al. (2014). "Protein and nucleotide biosynthesis are coupled by a single rate-limiting enzyme, PRPS2, to drive cancer". In: *Cell* 157.5, pp. 1088–1103.

Dang, Lenny et al. (2009). "Cancer-associated IDH1 mutations produce 2-hydroxyglutarate". In: *Nature* 462.7274, p. 739.

Dasgupta, Santanu et al. (2008). "Mitochondrial cytochrome B gene mutation promotes tumor growth in bladder cancer". In: *Cancer Research* 68.3, pp. 700–706.

De Bock, Katrien et al. (2013). "Role of PFKFB3-driven glycolysis in vessel sprouting". In: *Cell* 154.3, pp. 651–663.

Denkert, Carsten et al. (2012). "Metabolomics of human breast cancer: new approaches for tumor typing and biomarker discovery". In: *Genome Medicine* 4.4, p. 37.

Deprez, Johan et al. (1997). "Phosphorylation and activation of heart 6-phosphofructo-2-kinase by protein kinase B and other protein kinases of the insulin signaling cascades". In: *Journal of Biological Chemistry* 272.28, pp. 17269–17275.

Desjardins, P, E Frost, and R Morais (1985). "Ethidium bromide-induced loss of mitochondrial DNA from primary chicken embryo fibroblasts." In: *Molecular and Cellular Biology* 5.5, pp. 1163–1169.

Dey, Souvik et al. (2015). "ATF4-dependent induction of heme oxygenase 1 prevents anoikis and promotes metastasis". In: *The Journal of Clinical Investigation* 125.7, p. 2592.

Ditta, G et al. (1976). "The selection of Chinese hamster cells deficient in oxidative energy metabolism". In: *Somatic Cell and Molecular Genetics* 2.4, pp. 331–344.

Dong, Lan-Feng et al. (2017). "Horizontal transfer of whole mitochondria restores tumorigenic potential in mitochondrial DNA-deficient cancer cells". In: *ELife* 6, e22187.

Döppler, Heike and Peter Storz (2015). "Differences in metabolic programming define the site of breast cancer cell metastasis". In: *Cell Metabolism* 22.4, pp. 536–537.

Duarte, Natalie C et al. (2007). "Global reconstruction of the human metabolic network based on genomic and bibliomic data". In: *Proceedings of the National Academy of Sciences of the United States of America* 104.6, pp. 1777–1782.

Duesberg, Peter H, Klaus Bister, and Peter K Vogt (1977). "The RNA of avian acute leukemia virus MC29." In: *Proceedings of the National Academy of Sciences of the United States of America* 74.10, pp. 4320–4324.

Dupuy, Fanny et al. (2015). "PDK1-dependent metabolic reprogramming dictates metastatic potential in breast cancer". In: *Cell Metabolism* 22.4, pp. 577–589.

Eberhardy, Scott R and Peggy J Farnham (2001). "c-Myc mediates activation of the cad promoter via a post-RNA polymerase II recruitment mechanism". In: *Journal of Biological Chemistry* 276.51, pp. 48562–48571.

Edmunds, Lia R et al. (2014). "c-Myc programs fatty acid metabolism and dictates acetyl-CoA abundance and fate". In: *Journal of Biological Chemistry* 289.36, pp. 25382–25392.

Farber, S, LK Diamond, et al. (1948). "Temporary remissions in acute leukemia in children produced by folk acid antagonist, 4-aminopteroylglutamic acid (aminopterin)". In: *New England Journal of Medicine*, pp. 787–93.

Farber, Sidney, Elliott C Cutler, et al. (1947). "The action of pteroylglutamic conjugates on man." In: *Science* 106, pp. 619–621.

Fendt, Sarah-Maria et al. (2013). "Reductive glutamine metabolism is a function of the α-ketoglutarate to citrate ratio in cells". In: *Nature Communications* 4, p. 2236.

Figueroa, Maria E et al. (2010). "Leukemic IDH1 and IDH2 mutations result in a hypermethylation phenotype, disrupt TET2 function, and impair hematopoietic differentiation". In: *Cancer Cell* 18.6, pp. 553–567.

Fliss, Makiko S et al. (2000). "Facile detection of mitochondrial DNA mutations in tumors and bodily fluids". In: *Science* 287.5460, pp. 2017–2019.

Frezza, Christian (2014). "The role of mitochondria in the oncogenic signal transduction". In: *The International Journal of Biochemistry & Cell Biology* 48, pp. 11–17.

Frezza, Christian, Liang Zheng, Ori Folger, et al. (2011). "Haem oxygenase is synthetically lethal with the tumour suppressor fumarate hydratase". In: *Nature* 477.7363, p. 225.

Frezza, Christian, Liang Zheng, Daniel A Tennant, et al. (2011). "Metabolic profiling of hypoxic cells revealed a catabolic signature required for cell survival". In: *PLoS one* 6.9, e24411.

Gammage, Payam A, Edoardo Gaude, et al. (2016). "Near-complete elimination of mutant mtDNA by iterative or dynamic dose-controlled treatment with mtZFNs". In: *Nucleic Acids Research* 44.16, pp. 7804–7816.

Gammage, Payam A, Joanna Rorbach, et al. (2014). "Mitochondrially targeted ZFNs for selective degradation of pathogenic mitochondrial genomes bearing large-scale deletions or point mutations". In: *EMBO Molecular Medicine*, e201303672.

Gao, Ping et al. (2009). "c-Myc suppression of miR-23 enhances mitochondrial glutaminase and glutamine metabolism". In: *Nature* 458.7239, p. 762.

Garcia-Cao, Isabel et al. (2012). "Systemic elevation of PTEN induces a tumor-suppressive metabolic state". In: *Cell* 149.1, pp. 49–62.

Gaude, Edoardo, Francesca Chignola, et al. (2013). "muma, An R package for metabolomics univariate and multivariate statistical analysis". In: *Current Metabolomics* 1.2, pp. 180–189.

Gaude, Edoardo and C. Frezza (2016). "Tissue-specific and convergent metabolic transformation of cancer correlates with metastatic potential and patient survival". In: *Nature Communications* 7.

Gaude, Edoardo and Christian Frezza (2014). "Defects in mitochondrial metabolism and cancer". In: *Cancer & Metabolism* 2.1, p. 10.

Gottlieb, Eyal and Ian PM Tomlinson (2005). "Mitochondrial tumour suppressors: a genetic and biochemical update". In: *Nature Reviews. Cancer* 5.11, p. 857.

Gottlob, Kathrin et al. (2001). "Inhibition of early apoptotic events by Akt/PKB is dependent on the first committed step of glycolysis and mitochondrial hexokinase". In: *Genes & Development* 15.11, pp. 1406–1418.

Gross, Andrew M, Jason F Kreisberg, and Trey Ideker (2015). "Analysis of matched tumor and normal profiles reveals common transcriptional and epigenetic signals shared across cancer types". In: *PLoS one* 10.11, e0142618.

Hakimi, A Ari et al. (2016). "An integrated metabolic atlas of clear cell renal cell carcinoma". In: *Cancer Cell* 29.1, pp. 104–116.

Hanahan, Douglas and Robert A Weinberg (2011). "Hallmarks of cancer: the next generation". In: *Cell* 144.5, pp. 646–674.

Hanse, EA et al. (2017). "Cytosolic malate dehydrogenase activity helps support glycolysis in actively proliferating cells and cancer". In: *Oncogene* 36.27, pp. 3915–3924.

Haq, Rizwan et al. (2013). "Oncogenic BRAF regulates oxidative metabolism via PGC1α and MITF". In: *Cancer Cell* 23.3, pp. 302–315.

Hatzivassiliou, Georgia et al. (2005). "ATP citrate lyase inhibition can suppress tumor cell growth". In: *Cancer Cell* 8.4, pp. 311–321.

He, Xuelian et al. (2013). "Suppression of mitochondrial complex I influences cell metastatic properties". In: *PLoS one* 8.4, e61677.

Hershey, Alfred D and Martha Chase (1952). "Independent functions of viral protein and nucleic acid in growth of bacteriophage". In: *The Journal of General Physiology* 36.1, pp. 39–56.

Hollander, M Christine, Gideon M Blumenthal, and Phillip A Dennis (2011). "PTEN loss in the continuum of common cancers, rare syndromes and mouse models". In: *Nature Reviews. Cancer* 11.4, p. 289.

Hopkins, Julia F. et al. (2017). "Mitochondrial mutations drive prostate cancer aggression". In: *Nature Communications* 8.1, p. 656.

Hu, Jie, Jason W Locasale, et al. (2013). "Heterogeneity of tumor-induced gene expression changes in the human metabolic network". In: *Nature Biotechnology* 31.6, pp. 522–529.

Hu, Wenwei, Cen Zhang, et al. (2010). "Glutaminase 2, a novel p53 target gene regulating energy metabolism and antioxidant function". In: *Proceedings of the National Academy of Sciences of the United States of America* 107.16, pp. 7455–7460.

Huber, Wolfgang et al. (2002). "Variance stabilization applied to microarray data calibration and to the quantification of differential expression". In: *Bioinformatics* 18.suppl_1, S96–S104.

Iba, Hideo et al. (1984). "Rous sarcoma virus variants that carry the cellular src gene instead of the viral src gene cannot transform chicken embryo fibroblasts". In: *Proceedings of the National Academy of Sciences of the United States of America* 81.14, pp. 4424–4428.

Iommarini, Luisa et al. (2013). "Different mtDNA mutations modify tumor progression in dependence of the degree of respiratory complex I impairment". In: *Human Molecular Genetics* 23.6, pp. 1453–1466.

Isaacs, Jennifer S et al. (2005). "HIF overexpression correlates with biallelic loss of fumarate hydratase in renal cancer: novel role of fumarate in regulation of HIF stability". In: *Cancer Cell* 8.2, pp. 143–153.

Ishikawa, Kaori et al. (2008). "ROS-generating mitochondrial DNA mutations can regulate tumor cell metastasis". In: *Science* 320.5876, pp. 661–664.

Itkonen, Harri M et al. (2013). "O-GlcNAc transferase integrates metabolic pathways to regulate the stability of c-MYC in human prostate cancer cells". In: *Cancer Research* 73.16, pp. 5277–5287.

Jain, Mohit et al. (2012). "Metabolite profiling identifies a key role for glycine in rapid cancer cell proliferation". In: *Science* 336.6084, pp. 1040–1044.

Jeon, Sang-Min, Navdeep S Chandel, and Nissim Hay (2012). "AMPK regulates NADPH homeostasis to promote tumour cell survival during energy stress". In: *Nature* 485.7400, p. 661.

Jiang, Lei, Alexander A Shestov, et al. (2016). "Reductive carboxylation supports redox homeostasis during anchorage-independent growth". In: *Nature* 532.7598, pp. 255–258.

Jiang, Peng, Wenjing Du, et al. (2011). "p53 regulates biosynthesis through direct inactivation of glucose-6-phosphate dehydrogenase". In: *Nature Cell Biology* 13.3, p. 310.

Jones, Jessa B et al. (2001). "Detection of mitochondrial DNA mutations in pancreatic cancer offers a mass-ive advantage over detection of nuclear DNA mutations". In: *Cancer Research* 61.4, pp. 1299–1304.

Ju, Young Seok et al. (2014). "Origins and functional consequences of somatic mitochondrial DNA mutations in human cancer". In: *Elife* 3, e02935.

Kadenbach, Bernhard, Rabia Ramzan, and Sebastian Vogt (2013). "High efficiency versus maximal performance - the cause of oxidative stress in eukaryotes: a hypothesis". In: *Mitochondrion* 13.1, pp. 1–6.

Kamarajugadda, S et al. (2013). "Manganese superoxide dismutase promotes anoikis resistance and tumor metastasis". In: *Cell death & disease* 4.2, e504.

Kang, Mi Ran et al. (2009). "Mutational analysis of IDH1 codon 132 in glioblastomas and other common cancers". In: *International Journal of Cancer* 125.2, pp. 353–355.

Kerr, Emma et al. (2016). "Mutant Kras copy number defines metabolic reprogramming and therapeutic susceptibilities". In: *Nature* 531.7592, p. 110.

Killian, J Keith et al. (2013). "Succinate dehydrogenase mutation underlies global epigenomic divergence in gastrointestinal stromal tumor". In: *Cancer Discovery* 3.6, pp. 648–657.

Kim, Jung-whan et al. (2006). "HIF-1-mediated expression of pyruvate dehydrogenase kinase: a metabolic switch required for cellular adaptation to hypoxia". In: *Cell Metabolism* 3.3, pp. 177–185.

King, Michael P and Giuseppe Attardi (1989). "Human cells lacking mtDNA: repopulation with exogenous mitochondria by complementation". In: *Science* 246.4929, pp. 500–503.

Knudson, Alfred G (1971). "Mutation and cancer: statistical study of retinoblastoma". In: *Proceedings of the National Academy of Sciences of the United States of America* 68.4, pp. 820–823.

Kohn, Aimee D et al. (1996). "Expression of a constitutively active Akt Ser/Thr kinase in 3T3-L1 adipocytes stimulates glucose uptake and glucose transporter 4 translocation". In: *Journal of Biological Chemistry* 271.49, pp. 31372–31378.

Kollareddy, Madhusudhan et al. (2015). "Regulation of nucleotide metabolism by mutant p53 contributes to its gain-of-function activities". In: *Nature Communications* 6, p. 7389.

Koonin, EV and L Aravind (2002). "Origin and evolution of eukaryotic apoptosis: the bacterial connection". In: *Cell Death and Differentiation* 9.4, p. 394.

Koppenol, Willem H, Patricia L Bounds, and Chi V Dang (2011). "Otto Warburg's contributions to current concepts of cancer metabolism." In: *Nature Reviews Cancer* 11.5.

Krebs, Hans Adolf and William Arthur Johnson (1937). "Metabolism of ketonic acids in animal tissues". In: *Biochemical Journal* 31.4, p. 645.

Lai, Michael MC, Sylvia SF Hu, and Peter K Vogt (1979). "Avian erythroblastosis virus: transformation-specific sequences form a contiguous segment of 3.25 kb located in the middle of the 6-kb genome". In: *Virology* 97.2, pp. 366–377.

Lane, DP and LV Crawford (1979). "T antigen is bound to a host protein in SY40-transformed cells". In: *Nature* 278.5701, pp. 261–263.

Lane, Nick and William Martin (2010). "The energetics of genome complexity". In: *Nature* 467.7318, p. 929.

LeBleu, Valerie S et al. (2014). "PGC-1α mediates mitochondrial biogenesis and oxidative phosphorylation in cancer cells to promote metastasis". In: *Nature Cell Biology* 16.10, pp. 992–1003.

Letouzé, Eric et al. (2013). "SDH mutations establish a hypermethylator phenotype in paraganglioma". In: *Cancer Cell* 23.6, pp. 739–752.

Lewis, Caroline A et al. (2014). "Tracing compartmentalized NADPH metabolism in the cytosol and mitochondria of mammalian cells". In: *Molecular Cell* 55.2, pp. 253–263.

Lheureux, Stéphanie et al. (2013). "FDG is a surrogate marker of therapy response and tumor recovery after drug withdrawal during treatment with a dual

PI3K/mTOR inhibitor in a preclinical model of cisplatinum-resistant ovarian cancer". In: *Journal of Nuclear Medicine* 54.supplement 2, pp. 503–503.

Linzer, Daniel IH and Arnold J Levine (1979). "Characterization of a 54K Dalton cellular SV40 tumor antigen present in SV40-transformed cells and uninfected embryonal carcinoma cells". In: *Cell* 17.1, pp. 43–52.

Liu, Vincent WS, Hong Hui Shi, et al. (2001). "High incidence of somatic mitochondrial DNA mutations in human ovarian carcinomas". In: *Cancer Research* 61.16, pp. 5998–6001.

Liu, Xing, Yukinari Kato, et al. (2013). "Isocitrate dehydrogenase 2 mutation is a frequent event in osteosarcoma detected by a multi-specific monoclonal antibody MsMab-1". In: *Cancer Medicine* 2.6, pp. 803–814.

Locasale, Jason W et al. (2011). "Phosphoglycerate dehydrogenase diverts glycolytic flux and contributes to oncogenesis". In: *Nature Genetics* 43.9, pp. 869–874.

Loriot, Céline et al. (2012). "Epithelial to mesenchymal transition is activated in metastatic pheochromocytomas and paragangliomas caused by SDHB gene mutations". In: *The Journal of Clinical Endocrinology & Metabolism* 97.6, E954–E962.

Love, Michael I, Wolfgang Huber, and Simon Anders (2014). "Moderated estimation of fold change and dispersion for RNA-seq data with DESeq2". In: *Genome Biology* 15.12, p. 550.

Lu, Chao, Patrick S Ward, et al. (2012). "IDH mutation impairs histone demethylation and results in a block to cell differentiation". In: *Nature* 483.7390, p. 474.

Lu, Ming, Lufang Zhou, et al. (2008). "Role of the malate–aspartate shuttle on the metabolic response to myocardial ischemia". In: *Journal of Theoretical Biology* 254.2, pp. 466–475.

Mackay, Gillian M et al. (2015). "Chapter Five-Analysis of Cell Metabolism Using LC-MS and Isotope Tracers". In: *Methods in Enzymology* 561, pp. 171–196.

Madiraju, Anila K et al. (2014). "Metformin suppresses gluconeogenesis by inhibiting mitochondrial glycerophosphate dehydrogenase". In: *Nature* 510.7506, p. 542.

Magda, Darren et al. (2008). "mtDNA depletion confers specific gene expression profiles in human cells grown in culture and in xenograft". In: *BMC Genomics* 9.1, p. 521.

Maki, Yoshio et al. (1987). "Avian sarcoma virus 17 carries the jun oncogene". In: *Proceedings of the National Academy of Sciences of the United States of America* 84.9, pp. 2848–2852.

Mannava, Sudha et al. (2008). "Direct role of nucleotide metabolism in C-MYC-dependent proliferation of melanoma cells". In: *Cell Cycle* 7.15, pp. 2392–2400.

Mardis, Elaine R et al. (2009). "Recurring mutations found by sequencing an acute myeloid leukemia genome". In: *New England Journal of Medicine* 361.11, pp. 1058–1066.

Marroquin, Lisa D et al. (2007). "Circumventing the Crabtree effect: replacing media glucose with galactose increases susceptibility of HepG2 cells to mitochondrial toxicants". In: *Toxicological Sciences* 97.2, pp. 539–547.

Martinez-Outschoorn, Ubaldo E et al. (2016). "Cancer metabolism: a therapeutic perspective". In: *Nature Reviews. Clinical Oncology* 14.1, pp. 11–31.

Martnez-Reyes, Inmaculada et al. (2016). "TCA cycle and mitochondrial membrane potential are necessary for diverse biological functions". In: *Molecular Cell* 61.2, pp. 199–209.

Mashimo, Tomoyuki et al. (2014). "Acetate is a bioenergetic substrate for human glioblastoma and brain metastases". In: *Cell* 159.7, pp. 1603–1614.

Matoba, Satoaki et al. (2006). "p53 regulates mitochondrial respiration". In: *Science* 312.5780, pp. 1650–1653.

Máximo, Valdemar et al. (2002). "Mitochondrial DNA somatic mutations (point mutations and large deletions) and mitochondrial DNA variants in human thyroid pathology: a study with emphasis on Hürthle cell tumors". In: *The American Journal of Pathology* 160.5, pp. 1857–1865.

Mayers, Jared R et al. (2016). "Tissue of origin dictates branched-chain amino acid metabolism in mutant Kras-driven cancers". In: *Science* 353.6304, pp. 1161–1165.

Meiser, Johannes et al. (2016). "Serine one-carbon catabolism with formate overflow". In: *Science Advances* 2.10, e1601273.

Menard, Lynda, David Maughan, and Jim Vigoreaux (2014). "The structural and functional coordination of glycolytic enzymes in muscle: evidence of a metabolon?" In: *Biology* 3.3, pp. 623–644.

Menendez, Javier A and Ruth Lupu (2007). "Fatty acid synthase and the lipogenic phenotype in cancer pathogenesis". In: *Nature Reviews. Cancer* 7.10, p. 763.

Metallo, Christian M et al. (2012). "Reductive glutamine metabolism by IDH1 mediates lipogenesis under hypoxia". In: *Nature* 481.7381, pp. 380–384.

Monod, Jacques (1971). *Chance and necessity: an essay on the natural philosophy of modern biology. Alfred A*.

Mookerjee, Shona A et al. (2017). "Quantifying intracellular rates of glycolytic and oxidative ATP production and consumption using extracellular flux measurements". In: *Journal of Biological Chemistry* 292.17, pp. 7189–7207.

Morais, Réjean et al. (1994). "Tumor-forming ability in athymic nude mice of human cell lines devoid of mitochondrial DNA". In: *Cancer Research* 54.14, pp. 3889–3896.

Morrish, Fionnuala et al. (2010). "Myc-dependent mitochondrial generation of acetyl-CoA contributes to fatty acid biosynthesis and histone acetylation during cell cycle entry". In: *Journal of Biological Chemistry* 285.47, pp. 36267–36274.

Mullen, Andrew R et al. (2012). "Reductive carboxylation supports growth in tumour cells with defective mitochondria". In: *Nature* 481.7381, pp. 385–388.

Müller, Johannes Peter (1838). *Ueber den feinern Bau und die Formen der krankhaften Geschwülste, von Dr. Johannes Müller*. G. Reimer.

Nicholson, Jeremy K and John C Lindon (2008). "Systems biology: metabonomics". In: *Nature* 455.7216, pp. 1054–1056.

Nicklin, Paul et al. (2009). "Bidirectional transport of amino acids regulates mTOR and autophagy". In: *Cell* 136.3, pp. 521–534.

Nikiforov, Mikhail A et al. (2002). "A functional screen for Myc-responsive genes reveals serine hydroxymethyltransferase, a major source of the one-carbon unit for cell metabolism". In: *Molecular and Cellular Biology* 22.16, pp. 5793–5800.

Nilsson, Roland et al. (2014). "Metabolic enzyme expression highlights a key role for MTHFD2 and the mitochondrial folate pathway in cancer". In: *Nature Communications* 5, p. 3128.

Oliveira-Ferrer, Leticia, Karen Legler, and Karin Milde-Langosch (2017). "Role of protein glycosylation in cancer metastasis". In: *Seminars in Cancer Biology*. Elsevier.

Ooi, Aikseng et al. (2011). "An antioxidant response phenotype shared between hereditary and sporadic type 2 papillary renal cell carcinoma". In: *Cancer Cell* 20.4, pp. 511–523.

Orth, Jeffrey D, Ines Thiele, and Bernhard Ø Palsson (2010). "What is flux balance analysis?" In: *Nature Biotechnology* 28.3, pp. 245–248.

Owen, Oliver E, Satish C Kalhan, and Richard W Hanson (2002). "The key role of anaplerosis and cataplerosis for citric acid cycle function". In: *Journal of Biological Chemistry* 277.34, pp. 30409–30412.

Owens, Kjerstin M et al. (2011). "Impaired OXPHOS complex III in breast cancer". In: *PLoS one* 6.8, e23846.

Pallotti, Francesco et al. (2004). "Biochemical analysis of respiratory function in cybrid cell lines harbouring mitochondrial DNA mutations". In: *Biochemical Journal* 384.2, pp. 287–293.

Papandreou, Ioanna et al. (2006). "HIF-1 mediates adaptation to hypoxia by actively downregulating mitochondrial oxygen consumption". In: *Cell Metabolism* 3.3, pp. 187–197.

Parker, Richard C, Harold E Varmus, and J Michael Bishop (1984). "Expression of v-src and chicken c-src in rat cells demonstrates qualitative differences between pp60v-src and pp60c-src". In: *Cell* 37.1, pp. 131–139.

Parsons, D Williams et al. (2008). "An integrated genomic analysis of human glioblastoma multiforme". In: *Science* 321.5897, pp. 1807–1812.

Pate, Kira T et al. (2014). "Wnt signaling directs a metabolic program of glycolysis and angiogenesis in colon cancer". In: *The EMBO Journal* 33.13, pp. 1454–1473.

Patra, Krushna C and Nissim Hay (2014). "The pentose phosphate pathway and cancer". In: *Trends in Biochemical Sciences* 39.8, pp. 347–354.

Pavlova, Natalya N and Craig B Thompson (2016). "The emerging hallmarks of cancer metabolism". In: *Cell Metabolism* 23.1, pp. 27–47.

Pearce, Erika L and Edward J Pearce (2013). "Metabolic pathways in immune cell activation and quiescence". In: *Immunity* 38.4, pp. 633–643.

Pearce, Erika L, Maya C Poffenberger, et al. (2013). "Fueling immunity: insights into metabolism and lymphocyte function". In: *Science* 342.6155, p. 1242454.

Permuth-Wey, Jennifer et al. (2011). "Inherited variants in mitochondrial biogenesis genes may influence epithelial ovarian cancer risk". In: *Cancer Epidemiology and Prevention Biomarkers*.

Pertega-Gomes, Nelma et al. (2015). "A glycolytic phenotype is associated with prostate cancer progression and aggressiveness: a role for monocarboxylate transporters as metabolic targets for therapy". In: *The Journal of Pathology* 236.4, pp. 517–530.

Petros, John A et al. (2005). "mtDNA mutations increase tumorigenicity in prostate cancer". In: *Proceedings of the National Academy of Sciences of the United States of America* 102.3, pp. 719–724.

Pinho, Salomé S and Celso A Reis (2015). "Glycosylation in cancer: mechanisms and clinical implications". In: *Nature Reviews. Cancer* 15.9, p. 540.

Piskounova, Elena et al. (2015). "Oxidative stress inhibits distant metastasis by human melanoma cells". In: *Nature* 527.7577, p. 186.

Polyak, Kornelia et al. (1998). "Somatic mutations of the mitochondrial genome in human colorectal tumours." In: *Nature Genetics* 20.3.

Porporato, Paolo E et al. (2014). "A mitochondrial switch promotes tumor metastasis". In: *Cell Reports* 8.3, pp. 754–766.

Possemato, Richard et al. (2011). "Functional genomics reveals serine synthesis is essential in PHGDH-amplified breast cancer". In: *Nature* 476.7360, p. 346.

Priolo, Carmen et al. (2014). "AKT1 and MYC induce distinctive metabolic fingerprints in human prostate cancer". In: *Cancer Research* 74.24, pp. 7198–7204.

Rathmell, Jeffrey C et al. (2003). "Akt-directed glucose metabolism can prevent Bax conformation change and promote growth factor-independent survival". In: *Molecular and Cellular Biology* 23.20, pp. 7315–7328.

Reczek, Colleen R and Navdeep S Chandel (2017). "The Two Faces of Reactive Oxygen Species in Cancer". In: *Annual Reviews*.

Reynolds, Miriam R et al. (2014). "Control of glutamine metabolism by the tumor suppressor Rb". In: *Oncogene* 33.5, p. 556.

Reznik, Ed, Martin L Miller, et al. (2016). "Mitochondrial DNA copy number variation across human cancers". In: *Elife* 5, e10769.

Reznik, Ed and Chris Sander (2015). "Extensive decoupling of metabolic genes in cancer". In: *PLoS Computational Biology* 11.5, e1004176.

Rizzuto, Rosario et al. (2012). "Mitochondria as sensors and regulators of calcium signalling". In: *Nature reviews. Molecular Cell Biology* 13.9, p. 566.

Rohle, Dan et al. (2013). "An inhibitor of mutant IDH1 delays growth and promotes differentiation of glioma cells". In: *Science* 340.6132, pp. 626–630.

Rous, Peyton (1910). "A transmissible avian neoplasm.(sarcoma of the common fowl.)" In: *Journal of Experimental Medicine* 12.5, pp. 696–705.

— (1911). "A sarcoma of the fowl transmissible by an agent separable from the tumor cells". In: *The Journal of Experimental Medicine* 13.4, p. 397.

Salabei, Joshua K, Andrew A Gibb, and Bradford G Hill (2014). "Comprehensive measurement of respiratory activity in permeabilized cells using extracellular flux analysis". In: *Nature Protocols* 9.2, p. 421.

Salway, Jack G (2016). *Metabolism at a Glance*. John Wiley & Sons.

Santidrian, Antonio F et al. (2013). "Mitochondrial complex I activity and NAD+ / NADH balance regulate breast cancer progression". In: *The Journal of Clinical Investigation* 123.3, p. 1068.

Schafer, Zachary T et al. (2009). "Antioxidant and oncogene rescue of metabolic defects caused by loss of matrix attachment". In: *Nature* 461.7260, p. 109.

Schug, Zachary T et al. (2015). "Acetyl-CoA synthetase 2 promotes acetate utilization and maintains cancer cell growth under metabolic stress". In: *Cancer Cell* 27.1, pp. 57–71.

Schwartzenberg-Bar-Yoseph, Fabiana, Michal Armoni, and Eddy Karnieli (2004). "The tumor suppressor p53 down-regulates glucose transporters GLUT1 and GLUT4 gene expression". In: *Cancer Research* 64.7, pp. 2627–2633.

Sciacovelli, Marco, Edoardo Gaude, et al. (2014). "The metabolic alterations of cancer cells". In: *Methods in Enzymology* 542, pp. 1–23.

Sciacovelli, Marco, Emanuel Gonçalves, et al. (2016). "Fumarate is an epigenetic modifier that elicits epithelial-to-mesenchymal transition." In: *Nature* 537.7621, pp. 544–547.

Selak, Mary A et al. (2005). "Succinate links TCA cycle dysfunction to oncogenesis by inhibiting HIF-α prolyl hydroxylase". In: *Cancer Cell* 7.1, pp. 77–85.

Seo, Byoung Boo et al. (1998). "Molecular remedy of complex I defects: rotenone-insensitive internal NADH-quinone oxidoreductase of Saccharomyces cerevisiae mitochondria restores the NADH oxidase activity of complex I-deficient mammalian cells". In: *Proceedings of the National Academy of Sciences of the United States of America* 95.16, pp. 9167–9171.

Shangary, Sanjeev and Shaomeng Wang (2009). "Small-molecule inhibitors of the MDM2-p53 protein-protein interaction to reactivate p53 function: a novel approach for cancer therapy". In: *Annual Review of Pharmacology and Toxicology* 49, pp. 223–241.

Shao, Diane D et al. (2013). "ATARiS: computational quantification of gene suppression phenotypes from multisample RNAi screens". In: *Genome Research* 23.4, pp. 665–678.

Sharma, Ashwini Kumar, Roland Eils, and Rainer König (2016). "Copy number alterations in enzyme-coding and cancer-causing genes reprogram tumor metabolism". In: *Cancer Research* 76.14, pp. 4058–4067.

Shaw, Reuben J and Lewis C Cantley (2006). "Ras, PI (3) K and mTOR signalling controls tumour cell growth". In: *Nature* 441.7092, p. 424.

Shidara, Yujiro et al. (2005). "Positive contribution of pathogenic mutations in the mitochondrial genome to the promotion of cancer by prevention from apoptosis". In: *Cancer Research* 65.5, pp. 1655–1663.

Shih, Thomas Y et al. (1979). "Identification of a sarcoma virus-coded phosphoprotein in nonproducer cells transformed by Kirsten or Harvey murine sarcoma virus". In: *Virology* 96.1, pp. 64–79.

Shim, Hyunsuk et al. (1997). "c-Myc transactivation of LDH-A: implications for tumor metabolism and growth". In: *Proceedings of the National Academy of Sciences of the United States of America* 94.13, pp. 6658–6663.

Sjöblom, Tobias et al. (2006). "The consensus coding sequences of human breast and colorectal cancers". In: *Science* 314.5797, pp. 268–274.

Smolková, Katarna et al. (2015). "Reductive carboxylation and 2-hydroxyglutarate formation by wild-type IDH2 in breast carcinoma cells". In: *The International Journal of Biochemistry & Cell Biology* 65, pp. 125–133.

Son, Jaekyoung et al. (2013). "Glutamine supports pancreatic cancer growth through a KRAS-regulated metabolic pathway". In: *Nature* 496.7443, p. 101.

Spriet, Lawrence L, Richard A Howlett, and George JF Heigenhauser (2000). "An enzymatic approach to lactate production in human skeletal muscle during exercise". In: *Medicine & Science in Sports & Exercise* 32.4, pp. 756–763.

Stambolsky, P et al. (2006). "Regulation of AIF expression by p53". In: *Cell Death and Differentiation* 13.12, p. 2140.

Stanley, William C et al. (1997). "Regulation of myocardial carbohydrate metabolism under normal and ischaemic conditions: potential for pharmacological interventions". In: *Cardiovascular Research* 33.2, pp. 243–257.

Stehelin, Dominique et al. (1976). "DNA related to the transforming genes of avian sarcoma viruses is present in normal avian DNA". In: *Nature* 260.5547, pp. 170–173.

Subramanian, Aravind et al. (2005). "Gene set enrichment analysis: a knowledge-based approach for interpreting genome-wide expression profiles". In: *Proceedings of the National Academy of Sciences of the United States of America* 102.43, pp. 15545–15550.

Sullivan, Lucas B, Dan Y Gui, et al. (2015). "Supporting aspartate biosynthesis is an essential function of respiration in proliferating cells". In: *Cell* 162.3, pp. 552–563.

Sullivan, Lucas B, Eva Martinez-Garcia, et al. (2013). "The proto-oncometabolite fumarate binds glutathione to amplify ROS-dependent signaling". In: *Molecular Cell* 51.2, pp. 236–248.

Suzuki, Sawako et al. (2010). "Phosphate-activated glutaminase (GLS2), a p53-inducible regulator of glutamine metabolism and reactive oxygen species". In: *Proceedings of the National Academy of Sciences of the United States of America* 107.16, pp. 7461–7466.

Svedrui, eljko M and H Olin Spivey (2006). "Interaction between mammalian glyceraldehyde 3-phosphate dehydrogenase and L-lactate dehydrogenase from heart and muscle". In: *PROTEINS: Structure, Function, and Bioinformatics* 63.3, pp. 501–511.

Tan, An S, James W Baty, et al. (2015). "Mitochondrial genome acquisition restores respiratory function and tumorigenic potential of cancer cells without mitochondrial DNA". In: *Cell Metabolism* 21.1, pp. 81–94.

Tan, Duan-Jun, Ren-Kui Bai, and Lee-Jun C Wong (2002). "Comprehensive scanning of somatic mitochondrial DNA mutations in breast cancer". In: *Cancer Research* 62.4, pp. 972–976.

Tarca, Adi Laurentiu et al. (2012). "Down-weighting overlapping genes improves gene set analysis". In: *BMC Bioinformatics* 13.1, p. 136.

Taylor, Ian W et al. (2009). "Dynamic modularity in protein interaction networks predicts breast cancer outcome". In: *Nature Biotechnology* 27.2, pp. 199–204.

Telang, Sucheta et al. (2012). "Cytochrome *c* oxidase is activated by the oncoprotein Ras and is required for A549 lung adenocarcinoma growth". In: *Molecular Cancer* 11.1, p. 60.

Tennant, Daniel A, Raúl V Durán, and Eyal Gottlieb (2010). "Targeting metabolic transformation for cancer therapy". In: *Nature Reviews. Cancer* 10.4, p. 267.

Ternette, Nicola et al. (2013). "Inhibition of mitochondrial aconitase by succination in fumarate hydratase deficiency". In: *Cell Reports* 3.3, pp. 689–700.

Terunuma, Atsushi et al. (2014). "MYC-driven accumulation of 2-hydroxyglutarate is associated with breast cancer prognosis". In: *The Journal of Clinical Investigation* 124.1, p. 398.

Thompson, CB (2011). "Rethinking the regulation of cellular metabolism". In: *Cold Spring Harbor Symposia on Quantitative Biology*. Vol. 76. Cold Spring Harbor Laboratory Press, pp. 23–29.

Tibshirani, Robert, Guenther Walther, and Trevor Hastie (2001). "Estimating the number of clusters in a data set via the gap statistic". In: *Journal of the Royal Statistical Society: Series B (Statistical Methodology)* 63.2, pp. 411–423.

Tomlinson, Ian PM et al. (2002). "Germline mutations in FH predispose to dominantly inherited uterine fibroids, skin leiomyomata and papillary renal cell cancer". In: *Nature Genetics* 30.4, p. 406.

Torrano, Veronica et al. (2016). "The metabolic co-regulator PGC1α suppresses prostate cancer metastasis". In: *Nature Cell Biology* 18.6, pp. 645–656.

Tsai, Jeff H and Jing Yang (2013). "Epithelial–mesenchymal plasticity in carcinoma metastasis". In: *Genes & Development* 27.20, pp. 2192–2206.

Tsugawa, Hiroshi et al. (2011). "Practical non-targeted gas chromatography/mass spectrometry-based metabolomics platform for metabolic phenotype analysis". In: *Journal of Bioscience and Bioengineering* 112.3, pp. 292–298.

Turcan, Sevin et al. (2012). "IDH1 mutation is sufficient to establish the glioma hypermethylator phenotype". In: *Nature* 483.7390, p. 479.

Vander Heiden, Matthew G, Lewis C Cantley, and Craig B Thompson (2009). "Understanding the Warburg effect: the metabolic requirements of cell proliferation". In: *Science* 324.5930, pp. 1029–1033.

Vanharanta, Sakari et al. (2013). "Epigenetic expansion of VHL-HIF signal output drives multiorgan metastasis in renal cancer". In: *Nature Medicine* 19.1, pp. 50–56.

Väremo, Leif, Jens Nielsen, and Intawat Nookaew (2013). "Enriching the gene set analysis of genome-wide data by incorporating directionality of gene expression and combining statistical hypotheses and methods". In: *Nucleic Acids Research* 41.8, pp. 4378–4391.

Vazquez, Francisca et al. (2013). "PGC1α expression defines a subset of human melanoma tumors with increased mitochondrial capacity and resistance to oxidative stress". In: *Cancer Cell* 23.3, pp. 287–301.

Viale, Andrea et al. (2014). "Oncogene ablation-resistant pancreatic cancer cells depend on mitochondrial function". In: *Nature* 514.7524, p. 628.

Vogelstein, Bert and Kenneth W Kinzler (1993). "The multistep nature of cancer". In: *Trends in Genetics* 9.4, pp. 138–141.

Vogelstein, Bert, Nickolas Papadopoulos, et al. (2013). "Cancer genome landscapes". In: *Science* 339.6127, pp. 1546–1558.

Vogt, Peter K (2012). "Retroviral oncogenes: a historical primer". In: *Nature Reviews. Cancer* 12.9, p. 639.

Wallace, Douglas C (2007). "Why do we still have a maternally inherited mitochondrial DNA? Insights from evolutionary medicine". In: *Annual Reviews in Biochemistry* 76, pp. 781–821.

— (2012). "Mitochondria and cancer". In: *Nature Reviews. Cancer* 12.10, p. 685.

Wallace, Douglas C and Weiwei Fan (2010). "Energetics, epigenetics, mitochondrial genetics". In: *Mitochondrion* 10.1, pp. 12–31.

Wang, Fang et al. (2013). "Targeted inhibition of mutant IDH2 in leukemia cells induces cellular differentiation". In: *Science* 340.6132, pp. 622–626.

Warburg, Otto (1924). "Über den stoffwechsel der carcinomzelle". In: *Naturwissenschaften* 12.50, pp. 1131–1137.

— (1956). "On the origin of cancer". In: *Science* 123.3191, pp. 309–314.

Ward, Patrick S, Jay Patel, et al. (2010). "The common feature of leukemia-associated IDH1 and IDH2 mutations is a neomorphic enzyme activity converting α-ketoglutarate to 2-hydroxyglutarate". In: *Cancer Cell* 17.3, pp. 225–234.

Ward, Patrick S and Craig B Thompson (2012). "Metabolic reprogramming: a cancer hallmark even Warburg did not anticipate". In: *Cancer Cell* 21.3, pp. 297–308.

Wassermann, A v, Franz Keysser, and Michael Wassermann (1911). "Beiträge zum Problem: Geschwülste von der Blutbahn aus therapeutisch zu beeinflussen". In: *DMW-Deutsche Medizinische Wochenschrift* 37.51, pp. 2389–2391.

Watson, James D, Francis HC Crick, et al. (1953). "Molecular structure of nucleic acids". In: *Nature* 171.4356, pp. 737–738.

Weinberg, Frank et al. (2010). "Mitochondrial metabolism and ROS generation are essential for Kras-mediated tumorigenicity". In: *Proceedings of the National Academy of Sciences of the United States of America* 107.19, pp. 8788–8793.

Wellen, Kathryn E et al. (2010). "The hexosamine biosynthetic pathway couples growth factor-induced glutamine uptake to glucose metabolism". In: *Genes & Development* 24.24, pp. 2784–2799.

Wieman, Heather L, Jessica A Wofford, and Jeffrey C Rathmell (2007). "Cytokine stimulation promotes glucose uptake via phosphatidylinositol-3 kinase/Akt regulation of Glut1 activity and trafficking". In: *Molecular Biology of the Cell* 18.4, pp. 1437–1446.

Wise, David R et al. (2011). "Hypoxia promotes isocitrate dehydrogenase-dependent carboxylation of α-ketoglutarate to citrate to support cell growth and viability". In: *Proceedings of the National Academy of Sciences of the United States of America* 108.49, pp. 19611–19616.

Xiao, Mengtao et al. (2012). "Inhibition of α-KG-dependent histone and DNA demethylases by fumarate and succinate that are accumulated in mutations of FH and SDH tumor suppressors". In: *Genes & Development* 26.12, pp. 1326–1338.

Xu, Wei et al. (2011). "Oncometabolite 2-hydroxyglutarate is a competitive inhibitor of α-ketoglutarate-dependent dioxygenases". In: *Cancer Cell* 19.1, pp. 17–30.

Yahagi, Naoya et al. (2003). "p53 Activation in adipocytes of obese mice". In: *Journal of Biological Chemistry* 278.28, pp. 25395–25400.

Yan, Hai et al. (2009). "IDH1 and IDH2 mutations in gliomas". In: *New England Journal of Medicine* 360.8, pp. 765–773.

Yanagida, Osamu et al. (2001). "Human L-type amino acid transporter 1 (LAT1): characterization of function and expression in tumor cell lines". In: *Biochimica et Biophysica Acta (BBA)-Biomembranes* 1514.2, pp. 291–302.

Yang, Ming and Patrick J Pollard (2013). "Succinate: a new epigenetic hacker". In: *Cancer Cell* 23.6, pp. 709–711.

Yang, Ming and Karen H Vousden (2016). "Serine and one-carbon metabolism in cancer". In: *Nature Reviews Cancer* 16.10, pp. 650–662.

Ye, Jiangbin et al. (2014). "Serine catabolism regulates mitochondrial redox control during hypoxia". In: *Cancer Discovery* 4.12, pp. 1406–1417.

Ying, Haoqiang et al. (2012). "Oncogenic Kras maintains pancreatic tumors through regulation of anabolic glucose metabolism". In: *Cell* 149.3, pp. 656–670.

Yizhak, Keren et al. (2014). "A computational study of the Warburg effect identifies metabolic targets inhibiting cancer migration". In: *Molecular Systems Biology* 10.8, p. 744.

You, Chun, Suwan Myung, and Y-H Percival Zhang (2012). "Facilitated substrate channeling in a self-assembled trifunctional enzyme complex". In: *Angewandte Chemie* 124.35, pp. 8917–8920.

Yuan, Yuan et al. (2017). "Comprehensive molecular characterization of mitochondrial genomes in human cancers". In: *bioRxiv*, p. 161356.

Yun, Jihye et al. (2009). "Glucose deprivation contributes to the development of KRAS pathway mutations in tumor cells". In: *Science* 325.5947, pp. 1555–1559.

Yuneva, Mariia O et al. (2012). "The metabolic profile of tumors depends on both the responsible genetic lesion and tissue type". In: *Cell Metabolism* 15.2, pp. 157–170.

Zhang, Aihua, Hui Sun, et al. (2012). "Modern analytical techniques in metabolomics analysis". In: *Analyst* 137.2, pp. 293–300.

Zhang, Bing, Jing Wang, et al. (2014). "Proteogenomic characterization of human colon and rectal cancer". In: *Nature* 513.7518, pp. 382–387.

Zhang, Cen, Meihua Lin, et al. (2011). "Parkin, a p53 target gene, mediates the role of p53 in glucose metabolism and the Warburg effect". In: *Proceedings of the National Academy of Sciences of the United States of America* 108.39, pp. 16259–16264.

Zhao, Shimin et al. (2009). "Glioma-derived mutations in IDH1 dominantly inhibit IDH1 catalytic activity and induce HIF-1α". In: *Science* 324.5924, pp. 261–265.

Zheng, Liang, Simone Cardaci, et al. (2015). "Fumarate induces redox-dependent senescence by modifying glutathione metabolism". In: *Nature Communications* 6.

Zheng, Xiaofeng, Julienne L Carstens, et al. (2015). "EMT program is dispensable for metastasis but induces chemoresistance in pancreatic cancer". In: *Nature* 527.7579, p. 525.

Zieliski, ukasz P et al. (2016). "Metabolic flexibility of mitochondrial respiratory chain disorders predicted by computer modelling". In: *Mitochondrion* 31, pp. 45–55.